AERO RESEARCH AVENUE

DISCOVERING THE WORLD

JUNE 2022

STUDENT CO-ORDINATOR'S
K RAM SAI
SURAJ

FACULTY CO-ORDINATOR
MR A SAI KUMAR

MLR INSTITUTE OF TECHNLOGY

DEPARTMENT OF AERONAUTICAL ENGINEERING

"AERO RESEARCH AVENUE"

2022

MARRI LAXMAN REDDY
GROUP OF INSTITUTIONS
MLR
Institute of Technology

Institute Vision:

Promote academic excellence, research, Innovation, and entrepreneurial skills to produce graduates with human values and leadership qualities to serve the nation

Institute Mission:

Provide student-centric education and training on cutting-edge technologies to make the students globally competitive and socially responsible citizens.

Create an environment to strengthen the research, innovation and entrepreneurship to solve societal problems.

Vision of the Department:

To be a centre of excellence in Aeronautical engineering with emphasis on Research & Innovation to serve the needs of industry with human values to build strong nation. The department's vision is derived from the institute vision and it vouches to help the institute in fulfilling its vision by becoming a center of excellence in Aeronautical Engineering.

Mission of the Department:

The mission statements are the action statements; the department intends to implement in fulfilling its vision. The key components are quality oriented technical education, multidisciplinary skills and Research & Innovation activities with human values.

M1. Provide quality oriented education, well-grounded in the fundamental principles of Aeronautical Engineering.

M2. Consistently produce top quality Aeronautical engineers with core and multidisciplinary skills, who can become ace leaders and successful entrepreneurs with human values.

M3. Continuously strive for knowledge; undertake Research and Innovation that will contribute to the industrial development of the nation.

Macro mechanical and water absorption properties of composite laminates with novolac resin and e-glass/sisal fibers

Cite as: AIP Conference Proceedings **2446**, 040012 (2022); https://doi.org/10.1063/5.0109433
Published Online: 29 November 2022

A. Vivek Anand, P. Velmurugan, R. Arvind Singh, et al.

Macro Mechanical and Water Absorption Properties of Composite Laminates with Novolac Resin and E-Glass/Sisal Fibers

A. Vivek Anand[1,a)], P. Velmurugan[2], R. Arvind Singh[3], S. Jayalakshmi[3], K. Srinivas Rao[4] and P. S. Prem Kumar[5]

[1]*Department of Aeronautical Engineering, MLR Institute of Technology, Hyderabad, India*
[2]*Department of Mechanical Engineering, Shri Ram Murti Smarak College of Engineering, UP, India*
[3]*School of Mechanical and Electrical Engineering, Wenzhou University, China*
[4]*Department of Computer Science and Engineering, MLR Institute of Technology, Hyderabad, India*
[5]*Department of Aeronautical Engineering, Kumaraguru College of Technology, Coimbatore, India*

Corresponding author: a) vivekanand7adr@gmail.com

Abstract. Natural fiber- reinforced composites are currently being researched for their selection and use in the industries spanning aerospace, automotive, ground transportation, and several other high- performance-critical end products. Two of the key reasons in favor for the selection and use of natural fibers are, their biodegradability coupled with an overall ease of availability that makes the production of engineered composites not only cost effective but also economically viable. However, the selection and use of natural fibers/matrix is curtailed primarily because of three competing drawbacks, namely (i) high moisture absorption, (ii) inferior mechanical properties, and (iii) poor interfacial bonding strength between fiber and matrix, when compared one-on-one with the synthetic fibers/matrix. Due to these reasons, natural fibers are often used in combination with synthetic fibers for engineering composites, so as to achieve a material that offers the possibility of improved performance at the desired level. In this research study, composite laminates with novolac resin and sisal/coir/E-glass fiber reinforcement (60:40) were fabricated using the hand lay-up method. The fabricated composite laminates were characterized for macromechanical properties, namely, tensile strength and water absorption test was conducted to explore the moisture absorption characteristics of composite laminates. Test results revealed the composite laminates with natural fibers/resins to possess many attributes in favor of their selection and use in structural components.

Keywords: Natural fiber/resin; Sisal; E-Glass; Novolac; Composite laminate

INTRODUCTION

Natural fiber-reinforced composite materials are well known for their excellent environmentally friendly characteristics, which makes them suitable for a wide range of applications in the industries spanning automobile, aerospace, ground transportation and several commercial end products to include both the performance-critical and non-performance-critical. To meet the current market needs and to concurrently protect the environment, several of the researchers scattered through the different nations are working towards replacing the polymer composites containing synthetic fibers with polymer composites containing natural fibers, and a combination of natural fibers and synthetic fibers. In industrial sectors, a 10 percent growth in the use of natural fiber-reinforced composite materials has been reported [1-3]. Glass fiber (GF) is a synthetic fiber, which is widely chosen for use as a reinforcement for polymer matrices due to an ease in availability and better mechanical properties. Among the natural fibers, the sisal and coir fiber is a promising option. The sisal and coir fiber are widely cultivated in Asian countries like India, and available in abundance. The sisal/coir fibre has low density, biodegradability, low cost and

International Conference on Materials Research in Science and Engineering
AIP Conf. Proc. 2446, 040012-1–040012-5; https://doi.org/10.1063/5.0109433
Published by AIP Publishing. 978-0-7354-4208-5/$30.00

excellent abrasion resistance characteristics [4,5]. From literature it is observed that sisal/coir fiber can easily bond with thermoset matrices and thermoplastic matrices [6,7]. The sisal/coir fiber is hydrophilic in nature and by proper surface treatment the interfacial bonding between the reinforcing fiber and polymer matrix can be improved. Hence, for the sisal/coir fibers can effectively replace glass fiber as a potentially viable and economically affordable reinforcement for polymer composites [8-11]. The physical properties and mechanical properties of natural/synthetic fibre-reinforced composite materials can vary depending on the following: (i) the selection of matrix, (ii) geometrical dimensions of the reinforcing fiber, (iii) manufacturing technique used, and (iv) fiber orientation. In this research study, a combination of coir fibre, sisal fibre and E-glass fiber has been used to prepare polymer composite laminates. The fabricated composites were tested for their tensile strength and water absorption behavior and briefly discussed.

EXPERIMENTAL PROCEDURE

Fabrication Process and Specimen Preparation

Hand lay-up molding process was used to fabricate hybrid (Sisal and E-glass) fiber composites. Phenol-formaldehyde based novolac resin with molar ratio less than one was used as matrix due to its outstanding bonding efficiency and cost effectiveness [12]. The raw sisal and coir fibre were treated with 5% sodium hydroxide solution at room temperature for 6 hours to improve the surface roughness for better chemical bonding. Before fabrication of laminate, Novolac resin was coated on all natural fibers at room temperature and were cured for 24 hours at room temperature. Composites of thickness 4 mm were fabricated in the form of laminates. To obtain 4-mm thickness, 14 layers of angle ply laminate were precision stacked upon each other with in a steel mold of 350mm X 150mm. The volume fraction Vf is kept constant for all the composite laminate. The releasing agent (wax) was coated on the surface of the mold. The chopped (short) fibers approximately 0.4 mm were randomly sprinkled over the mold layer by layer. Meanwhile Novolac resin were pored over the reinforcement gently without any formation of micro air bubbles. A hand roller was used to ensure the removal of air bubbles and uniform impregnation of resin all over the surface of the fiber for perfect interfacial bonding and to augment the interfacial strength between the fibre and matrix. The solidification was done under closed environment within the mold itself, placed in universal testing machine (hydraulic pressure =10 bar). After curing specimens were cut as per the ASTM standards using precision diamond saw cutter. The fabricated specimens were shown in figure 1.

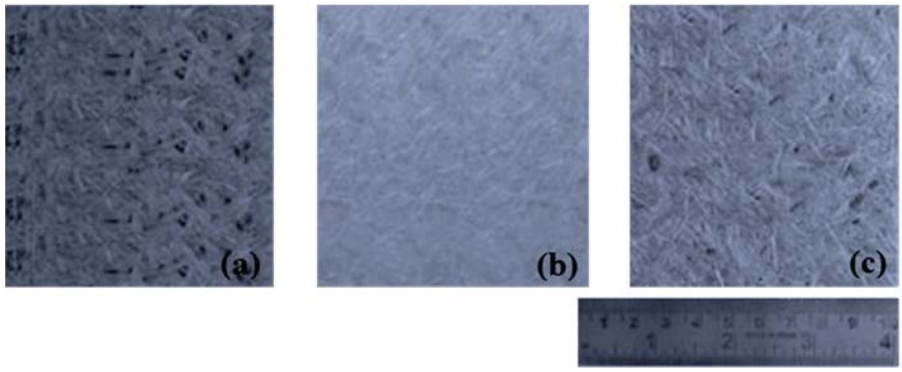

FIGURE 1. Fabricated composite laminates with reinforcements: (a) coir/glass (CG), (b) sisal/glass (SG) and (c) coir/sisal (CS).

Macromechanical and Micromechanical Property (Tensile Strength)

Macromechanical property - tensile strength of the fabricated composite laminates were explored by conducting tensile tests using Universal Testing Machine (UTM) at a displacement velocity of 2 mm/minute. In conformance with specifications detailed in the standard ASTM D3039, the composite samples were cut to the dimension 120 mm x 25 mm x 4 mm. Prior to initiation of the experiment, geometrical dimension (thickness and width) of the specimens were noted and cross sectional area of the test specimen was calculated.

Water Absorption Test

Water absorption test was conducted on the fabricated composite laminates as per ASTM 570 standard. Microbalance was used to measure the initial weight of the samples before dipping in the medium. The deionized water (230C) was used as medium to conduct water absorption test and weight of the samples were measured at the interval of 24 hours and continued up to the specimen reaches the saturation point [13]. Equation 2 was used to calculate the water absorption of the samples.

$$Water\ Absorption\ (\%) = \frac{Weight\ of\ the\ Wet\ Specimen - Intial\ Weight\ of\ the\ Specimen}{Intial\ Weight\ of\ the\ Specimen} X\ 100 \quad (1)$$

RESULTS AND DISCUSSION

Tensile Strength

The major constituents of the composite materials are fibre and matrix. Fibre is the major load carrying member (normal stress), both in longitudinal and transverse direction. The purpose of matrix is to transfer the load to fibre by a shearing mechanism and to carry minimal amount of load (shear stress). Hence, the tensile strength of the composite material is majorly depending upon the individual strength of the fibre followed by interfacial bonding between fiber and matrix [14]. The results obtained (table 1) are in line with the above statement, tensile strength of the tested composite laminates (SG>CG>CS) are also same order as individual fibre: sisal fiber 530-640 MPa, coir 175 MPa and E glass 3400 MPa [15]. The micro structure of the coir fibre comprising lot of porosity when compare to other natural fibres [16] which in turn directly affects the tensile strength of the composite laminates.

TABLE 1. Macromechanical (tensile) properties of composite laminates

Sample	Tensile Strength (N/mm^2)	Elongation (%)
CS	295	2.9
CG	379	4.5
SG	495	5.3

The failure of the composite laminate imitates once the peak load is reached, fiber pull out is favored to occur, which leads to damage due to interfacial bonding. The matrix is having low modulus when compare to the reinforcement which will produce higher longitudinal strain in the matrix when compare to the reinforcement [17]. This eventually results in the load being suddenly transferred to the matrix. However, the matrix being the minor load carrying member, it is unable to carry the transferred load, which eventually results in conditions that are conducive for failure of the composite laminate. The alkali treatment increases the surface roughness of the fibre which leads in strengthening the interfacial bonding between the fibre and matrix [18]. In mean time for coir fibre alkali treatment triggers the water absorption due to lackage of lignin pigment [19]. The reaction of Novolac resin with sisal increases the interfacial bonding [20] whereas in coir fibre it is not that much effective due to the removal of lignin pigment.

Water Absorption

Water absorption of natural fibre was shown in figure 2. The specimen with pure natural fibre combination (Coir/Sisal CS) absorbs more moisture than synthetic/natural fibre combination. Lignin, cellulose, hemicellulose, pectin and was are the major content in natural fibers and its composition will lead to vary from one fibre to another fiber. Cellulose and hemicellulose content in the natural fibre are responsible for the natural fibre to absorb more moisture content when compare to synthetic fibres [21] that's the reason CS combination specimen absorbs more moisture than other specimens. The lignin content decreases the water absorption characteristics of the fibre [19], alkaline treatment in sisal fibre forms an insulating layer over the sisal fibre and locks its lignin content without losing. In turn sisal fibre combination specimen SG shows less water absorption when compare to CG specimen.

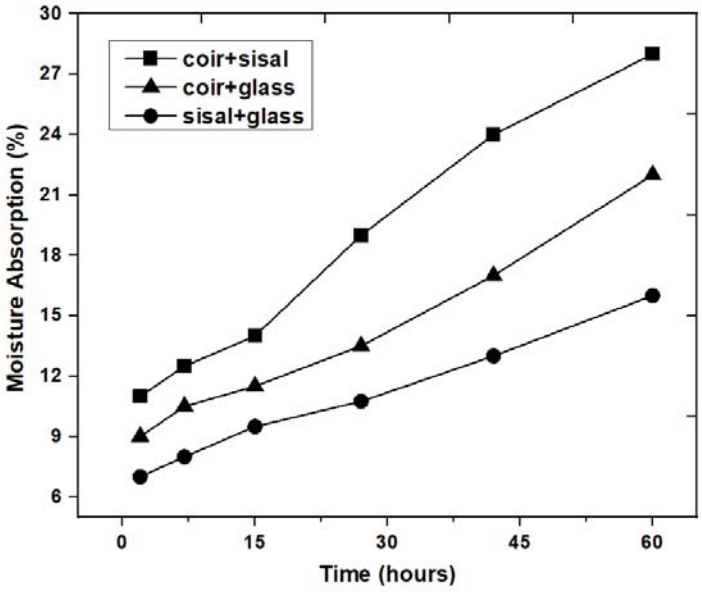

FIGURE 2. Moisture absorption characteristics of fabricated composite laminates

CONCLUSION

The following are the conclusions that can be drawn from this research study.

- Water Absorption: The SG specimen shows excellent less water absorption characteristics when compare to CG and CS specimens. The reason behind is alkali treatment in sisal fibre removes the hydrophilic content – cellulose and hemicellulose and protects the lignin content which reduces its moisture absorption.
- Tensile Strength: Tensile strength of the composite laminate was majorly depends upon the individual strength of the fibre since it is a major load carrying member and interfacial bonding between fibre and matrix. The SG specimen shows better tensile strength when compare to other specimens. Higher porosity in the coir fibre reduces the tensile strength of the laminates.
- Novolac resin is an optimum candidate for matrix in sisal fibre which augments its tensile strength by providing better interfacial bonding when compare to other fibers coir and glass.

REFERENCES

1. A. May-Pat, A. Valadez-González and P.J. Herrera-Franco, “Effect of fiber surface treatments on the essential work of fracture of HDPE-continuous henequen fiber-reinforced composites”, Polymer Testing, 32 (6) (2013), pp. 1114–1122.
2. N. Uddin, Developments in Fiber-Reinforced Polymer (FRP) Composites for Civil Engineering (UK: Woodhead Publishing Limited) (2013).
3. V. Fiore, T. Scalici, G. Di Bella and A. Valenza, “A review on basalt fibre and its composites”. Composites Part B: Engineering, (2015) pp.74-94.
4. D. Verma, P.C. Gope, A. Shandiya, A. Gupta and M.K Maheshwari, “Coir fibre reinforcement and application in polymer composites: A review”, J. Mater. Environ. Sci., 4 (2) (2013), pp. 263-276.
5. Laxmikanta Nayak, D. Nag, S. Das, Deb Prasad Ray and Lakshmanan Ammayappan, “Utilization of sisal fibre (Agave Sisalana L.) – A review”, Agri. Review, (32) (2) (2011), pp. 150-152.
6. Camila Cruz da Silva, Raimundo Carlos Silverio Freire Júnior, Elmo Thiago Lins Cöuras Ford, Camilla Medeiros Dantas, Jayna Kátia Dionisio dos Santos and Eve Maria Freire de Aquino, “Mechanical behavior and water absorption in sisal/glass hybrid composites” Revistamateria, (23) (4) (2018), Issn 1517-7016 artigo e012246.

7. M.Z Rong, M.Q Zhang and Y. Liu, “The effect of fiber treatment on the mechanical properties of unidirectional sisal-reinforced epoxy composites”, Composites Science and Technology, (61) (2001), pp. 1437–1447.
8. L.P Nhlapo and A.S. Luyt, “Thermal and Mechanical Properties of LDPE/Sisal Fiber Composites Compatibilized with Functionalized Paraffin Waxes”, Journal of Applied Polymer Science (123) (2012), pp. 3627–3634.
9. R.S Rana, Ashish Kumre, Sarawati Rana and Rajesh Purohit, “Characterization of properties of epoxy sisal/glass fiber reinforced hybrid composite”, Materials Today Proceedings Part D, 4 (4) (2017), pp. 5445-5451.
10. A. Vivek Anand, V. Hariprasad, S. Jayalakshmi, R. Arvind Singh, V.R. Ravivarma and S. Gollakota, “Sisal/coir/glass fiber based hybrid composite laminate structure”, International Journal of Mechanical and Production Engineering Research and Development”, 8 (7) (2019), ISSN: 2249-6890.
11. Muhammed Anaz Khan, A. Vivek Anand, Lokasani Bhanuprakash, A. Ravindra and V. Hariprasad, “Mechanical Properties of E-Glass Fiber- Basalt Fiber Reinforced Polymer Matrix Composite”, International Journal of Recent Technology and Engineering, 9 (2) (2020), pp. 1019-1022.
12. M.G. Longley and D.H. Solomon, “The chemistry of Novolac resin. A review on the use of models”, Australian Journal of Chemistry, 48 (2) (1995), pp. 323-331.
13. L. Bhanuprakash, S. Parasuram and S. Varghese, “Experimental investigation on graphene oxides coated carbon fibre/epoxy hybrid composites: Mechanical and electrical properties”, Composites Science and Technology, 179 (2019), pp. 134-144.
14. S. Shyam Kumar, “Evaluation of mechanical properties of PEEK HAp bio-composite used in load bearing bone implants”, Material science forum, 909 (2017), pp.193- 198.
15. Emad Omrani, Pradeep L. Menezes and Pradeep K. Rohatgi, “State of the art on tribological behavior of polymer resin composites reinforced with natural fibers in the green materials world”, Engineering Science and Technology an International Journal, 19 (2) (2016), pp. 717-736.
16. L.Q.N Tran, T. Nguyen Minh, C.A. Fuentes, T. Truong Chi, A.W. Van Vuure, and I. Verpoest, “Investigation of microstructure and tensile properties of porous natural coir fibre for use in composite materials”, Industrial Crops and Products, 65 (2015), pp. 437-445.
17. N. Prabhu Kishore, “Performance Comparison of GFRP Composite I Section With An Aluminium I section”, International Journal of Civil Engineering and Technology, 8 (4) (2017) ,pp. 278–286.
18. P.A. Udaya Kumar, Ramalingaiah, B. Suresha and R. Hemanth, “Mechanical and Tribological Behavior of Vinyl Ester Hybrid Composites”, Tribology in Industry, 40 (2) (2018), pp. 283-299.
19. Mohit Mittal and Rajiv Chaudhary, “Experimental Study on the Water Absorption and Surface Characteristics of Alkali Treated Pineapple Leaf Fibre and Coconut Husk Fibre”, International Journal of Applied Engineering Research, 13 (15) (2018) pp. 12237-12243.
20. M. Das, V.S. Prasad and D. Chakrabarty, “Thermogravimetric and weathering study of novolac resin composites reinforced with mercerized bamboo fiber”, Polymer Composites, 30 (10) (2009), pp 1408 – 1416.
21. Alvin Devadas, Umar Nirmal and J. Hossen, “Investigation into mechanical & tribological performance of kenaf fibre particle reinforced composite”, Cogent Engineering, 1 (2018) 1479210.

Numerical investigation of supersonic flow past circular cross-section bodies

Cite as: AIP Conference Proceedings **2446**, 180029 (2022); https://doi.org/10.1063/5.0108443
Published Online: 29 November 2022

Nirmith Kumar Mishra, M. B. Naveed, D. Shivam, et al.

Numerical Investigation of Supersonic Flow Past Circular Cross-Section Bodies

Nirmith Kumar Mishra[1,a)], M. B. Naveed[1], D. Shivam[1], S. Chandrashekhar[1], P. Hrithik[1] and P. S. Prem Kumar[2]

[1]*Department of Aeronautical Engineering, MLR Institute of Technology, Laxman Reddy Avenue, Dundigal, Hyderabad-500 043, Telangana, India*
[2]*Department of Aeronautical Engineering, Kumaraguru college of technology, Coimbatore, Tamil Nadu, 641049, India*

[a]Corresponding author: nirmithmishra@gmail.com

Abstract. With the intend to study the flow behavior over cruise missiles and rockets, we aim to perform numerical simulations over circular cross-section models in supersonic flow regime specifically Mach 2 at different angles of attack. These simulations and investigations would provide us with axial and normal forces and moment coefficients which would further be used for obtaining aerodynamic forces. The models are to be created in CATIA v5 and then exported to ANSYS Fluent for analysis and calculations. With accordance to iterations and numerical solutions these models will be verified and validated with special considerations on formation of shockwaves. In conclusion, the computational fluid dynamics (CFD) results will be compared and analyzed with the experimental data. In future, the project has the scope to develop additional structures like fins or other control surfaces on the configurations to improve the performance and further compare them with each other. It could further lead to a step-by-step process of designing a complete aerodynamically efficient rocket or missile depending upon the prosperity requirement.

Keywords: Circular cross-section, Supersonic flow, Aerodynamic forces, Computational fluid dynamics, Shockwaves

INTRODUCTION

It has been observed that from past few decades' supersonic flow analysis over a body has become a prominent criterion for analysis of aerodynamic characteristics of a body. The term aerodynamic characteristic refers how high the speed of flow is affecting the body in the sense of forces and moments generated over the body it encounters. There are lot of researches debating about the efficient cross-section of a body that takes a projectile in supersonic flow, typically around Mach 2. The primary cross-sections for research include circular, elliptical and square bodies. Various authors came up with significance of each of the cross-sectional bodies but only at an expense of some other parameter. A deep research investigation was carried out bySigal and Lapidot[1], in which different types of cross-sections were used – rectangular and square with rounded edges and a normal circular. On analysing the different parameters, they came to conclusion that though the coefficient of normal force for rectangular cross-section was maximum compared to rest but it was not aerodynamically efficient and stable compared to circular cross-section. This was due to rolling nature of the rocket/missile which would be stable when circular cross-section is used. Nielsen, J.N[2] described about the problems occurring in such shapes was solely due to the irregularity in the separation of flow in these non-circular cross-sections. And makes us understand the significance of utilizing the circular models. The research on the analysis of flow behaviour of such cross-sections are not many and hence creating a novelty to this particular article. The research presented in this paper focuses on the effects of varying the length of the missile's leading cone and body on the normal, axial forces and moment coefficients with studying the

International Conference on Materials Research in Science and Engineering
AIP Conf. Proc. 2446, 180029-1–180029-4; https://doi.org/10.1063/5.0108443
Published by AIP Publishing. 978-0-7354-4208-5/$30.00

flow behaviour. For different angle of attacks but same Mach number i.e.2, analysis is performed experimentally and computationally. They are further compared and validated for the accuracy of the results obtained.

COMPUTATIONAL ANALYSIS

In this section, the specifications of the computational simulation and solution is described with brief analysis of the key parameters. The CFD software used here is ANSYS Fluent as the processor is fast and user friendly for such analysis. The further sections are the details of the inputs like geometry, meshing, set-up etc. entered for performing the analysis.

Geometry

There are four circular cross-sections of the bodies which are compared to study the effects on and are created in the geometry part in the ANSYS Workbench. The fig 1 shows the drawing of these models. It is to be noted that the dimensions are in "mm".

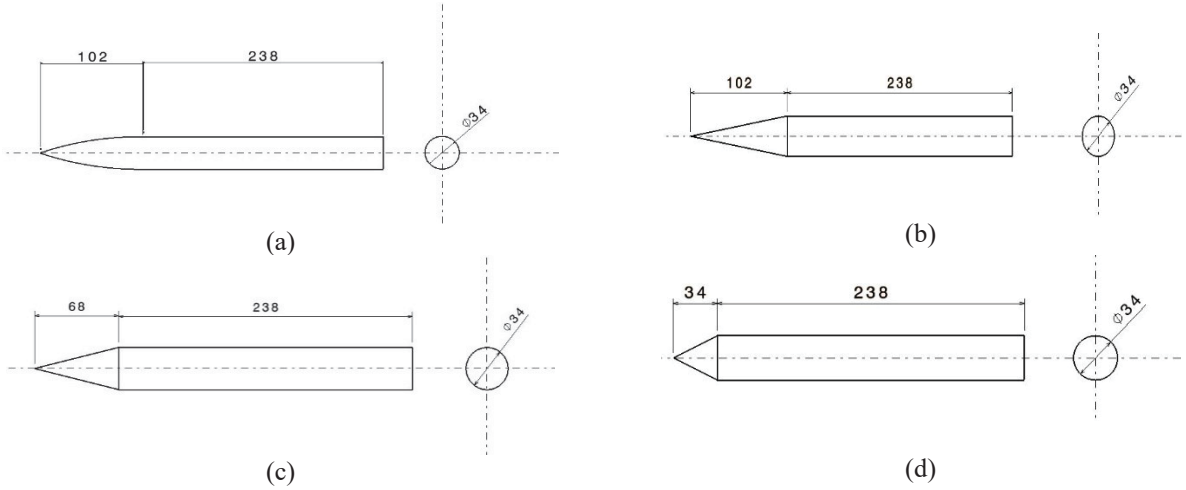

FIGURE 1. (a), (b), (c), (d) Four circular cross-section bodies with varying geometric properties

It is also to be noted that fig. (a) and fig. (b) are not similar and the difference is of the sharpness and bluntness of the leading nose cone. This selection of model provides the study of detachment of shockwaves and thereby studying the aerodynamic characteristics.

Meshing and Set-up

For meshing, the solver uses finite element method (FEM) to discretize the complete flow domain into sub domains to obtain precise solution of the equation over the given geometry. This is the most important part in the analysis since if the fluid domain is not properly meshed the results that we desire and the solution may diverge. Our main importance is to get a stable solution with a proper convergence.As it is a 2D model, the face meshing is performed with an additional edge meshing provided at the bow shock angle calculated theoretically on the leading section. This is done so as to obtain a clear visual of the shockwave.

Further in set-up section, the solution method used here along with the boundary conditions is the K-Omega SST method which is a turbulence based model and provides better result for the 2D analysis. As it is a supersonic flow, it is an obvious fact the flow is supposed to get turbulent and hence the selection of this equation*. The density based solver is selected since it is a compressible flow and there are density changes. The boundary conditions for the same are described below in a tabular form.

$$\frac{\partial k}{\partial t} + U_J \frac{\partial k}{\partial x_j} = P_k - \beta * k\omega + \frac{\partial}{\partial x_j}[(\vartheta + \sigma_k \vartheta_T)\frac{\partial k}{\partial x_j}] \quad (1)$$

TABLE 1. Boundary Conditions

Domain name	Boundary condition
Inlet	Velocity inlet velocity : 694.37m/s Pressure farfield
Far field	Gauge pressure :101325N/m2 Mach Number:2
Outlet	Pressure outlet

Solution and Results

The solution uses second order upwind to get accurate for the given flow domain results. The residual values are set to 1e-7 and the iterations are set to 5000. The desired values and plots are obtained for different angle of attacks after analyzing all the four models and hence results are presented in contours. The different contours shown are for the first model (a) shown in fig. 2 which has turned out to be the most aerodynamically efficient by reducing of shockwaves due to curvy leading edge cone. All the obtained data are put in the form of graphs to study the parameters. The plots are of L/D vs angle of attack are shown in the fig. 3 which is evident for the high values of aerodynamic efficiency for the model (a) as shown in fig 1. The CFD simulations also provide the study of shockwave formations and the results are validated with the theoretical concepts of oblique shockwaves. The nose area shape influences the stream design assuming we use nose shape to be gruff, at supersonic speed it's anything but a bow shock (or) segregated shock wave since obtuse shape has higher range of nose, the title is identified with our work as we have determined diagonal properties at Mach 2 by hand a then did the examination of stream on the model by utilizing these properties as limit conditions and discovered the power coefficients esteems.

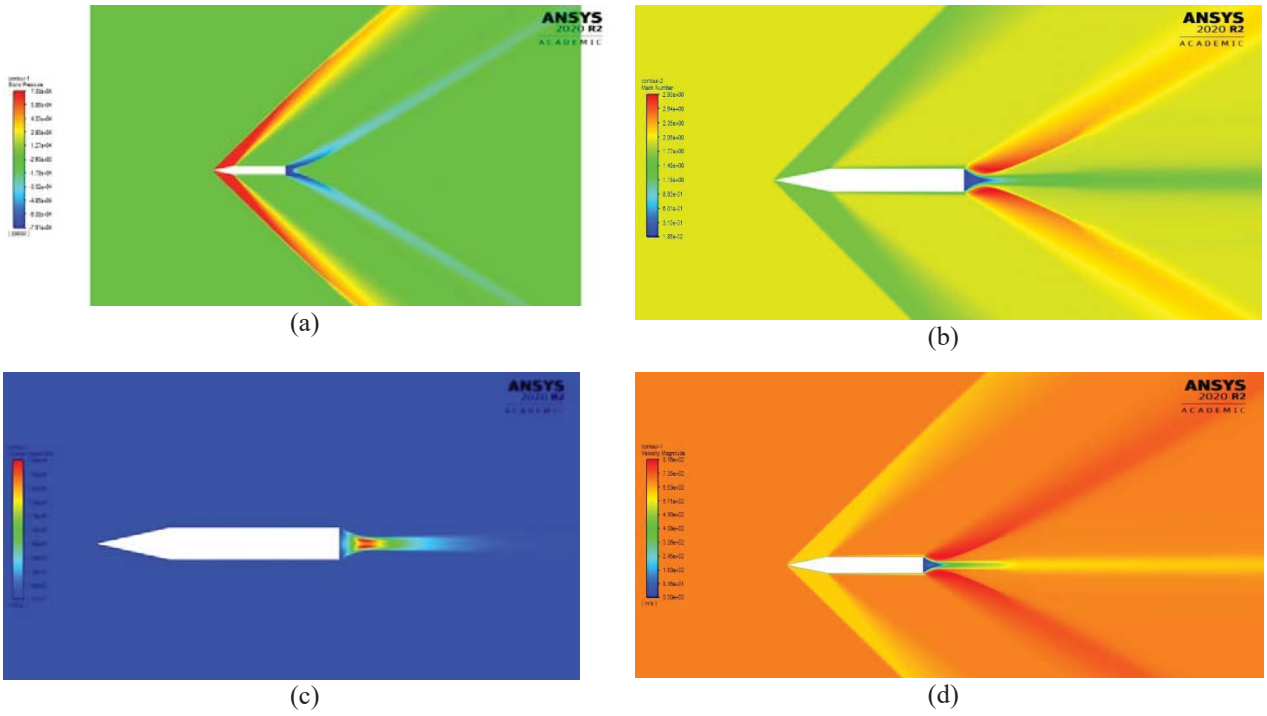

FIGURE 2. (a) Static contour, (b) Mach Number contour, (c) Turbulence contour, (d) Velocity contour

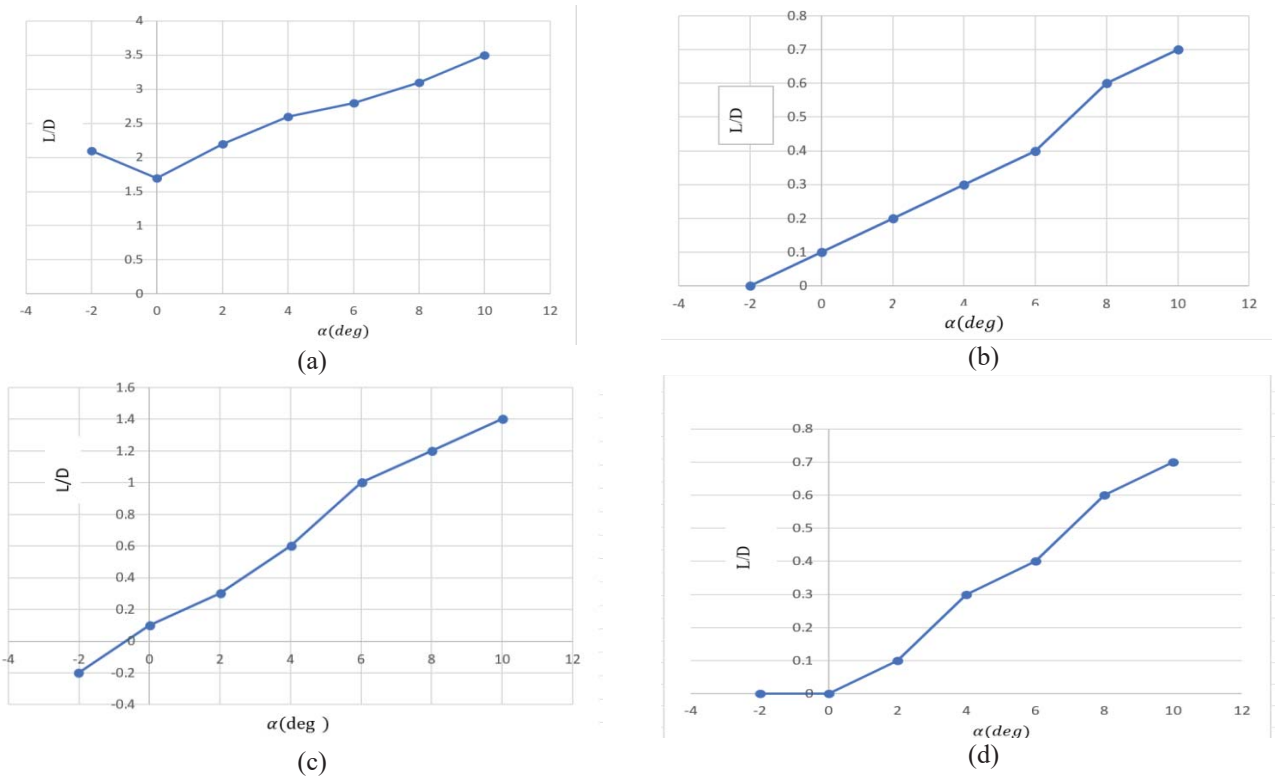

FIGURE 3. L/D vs Angle of attack plots for the 4 models (a), (b), (c) and (d) respectively.

REFERENCES

1. Eppakayala Naresh, Pinnamaneni Dileep Kumar, Anil Kumar.N, B. Nagaraj goud, "Drag reduction over A circular cylinder", International Journal of Civil Engineering and Technology (IJCIET) ISSN Print: 0976-6308 and ISSN Online: 0976-6316, Volume 8, Issue 8, August 2017, pp. 1334–1345.
2. Suddala Abhishek , B.Nagaraj Goud, "Compressor Design optimization for a High speed Jetengine", IOP Conference Series: Materials Science and Engineering, 2018, 455(1), 012036.
3. A. Sai Kumara), M. Shivaleela, L. Srilekha, and B. Sruthi, " Flow field analysis of rudder in CFD", AIP Conference Proceedings 2317, 040011 (2021).
4. Sigal, A. and Lapidot, E., “The Aerodynamic Characteristics of Configurations Having Bodies with Square, Rectangular, and Circular Cross-Sections at a Mach Number of 0.75”, AIAA, Inc., 1987.
5. Nielsen, J.N., “Problems Associated with the Aerodynamic Design of Missile Shapes”, Proceedings of the Second Symposium on Numerical and Physical Aspects of Aerodynamic Flows, Long Beach, CA, Jan. 1983.
6. Jackson, C.M. and Sawyer, W.C., “Bodies with Non-Circular Cross-Sections and Bank-to-Turn Missiles”, Progress in Astronautics and Aeronautics, Vol. 141, pp. 365-389, 1991.
7. Schneider, W., “Experimental Investigation of Bodies with Non-Circular Cross-Section in Compressible Flow”, AGARD-CP-336, Symposium on Missile Aerodynamics, Trondheim, Norway, pp. 19-1-19-15, Sept. 1982.
8. Zipfel, P. H.: Modeling and Simulation of Aerospace Vehicle Dynamics, 2nd ed., AIAA Education Series, 2007.

Static analysis of conventional aircraft fuselage with different materials

Cite as: AIP Conference Proceedings **2446**, 180044 (2022); https://doi.org/10.1063/5.0109231
Published Online: 29 November 2022

K. Veeranjaneyulu, G. Sravanthi, K. Surya Kiran, et al.

Static Analysis of Conventional Aircraft Fuselage with Different Materials

K. Veeranjaneyulu[1, a)], G. Sravanthi[1, b)], K. Surya Kiran[2,c)], K. Khushal[1, d)] and G. Raj Kumar[3, e)]

[1]*Department of Aeronautical Engineering, MLR Institute of Technology, Hyderabad, India*
[2]*Department of Mechanical and Mechatronics Engineering, University of Waterloo, Ontario, Canada*
[3]*Department of Aeronautical Engineering, Kumaraguru College of Technology, Coimbatore, Tamil Nadu, India*

Corresponding author:[a)]veerak2k@gmail.com
[b)]grandhamalasravanthi@gmail.com
[c)]suryakk58k@gmail.com
[d)]kul.knight@outlook.com
[e)]rajkumar.g.aeu@kct.ac.in

Abstract. The fuselage structure is one of the important subassemblies of an airplane. It is used to house the passengers, baggage and cargo and subjected to many loads in the flight and during the ground roll. The significance of this research paper is to compare the stresses induced in the fuselage under various flight and loading conditions. The structural analysis is carried out for two different materials that is Aluminium, Al-7075 and Titanium alloys. The deformation of the fuselage structure at the various loading conditions and for different materials is analysed using ANSYS-Static Structural, and the Modelling of the fuselage structure is performed by using CREO 4.0. The stresses induced in the aluminium fuselage are more than that developed in the titanium alloy fuselage. The deformation at different places of the aluminium fuselage structure is also more than the titanium alloy fuselage**.**

Keywords: Static stresses, Deformation, Aluminum-6060, CREO 4.0, ANSYS

INTRODUCTION

The fuselage is one of the important structures of the aircraft. Fuselage houses the payload i.e passengers, cargo, controls, accessories and other equipment. In some aircrafts, the engine is buried in the fuselage and in some airplanes; engines are attached to the rear fuselage. The size of the fuselage depends on the passenger capacity and volume of the cargo to be transported. They are also divided into different compartments. Figure 1.1 depicts the construction details of different types of fuselage structures used in the airplane [1-8]. Aircraft fuselage is also made up of different materials. In this work, Aluminum, Al-6061 and Titanium alloys are considered for the design and analysis of the fuselage.

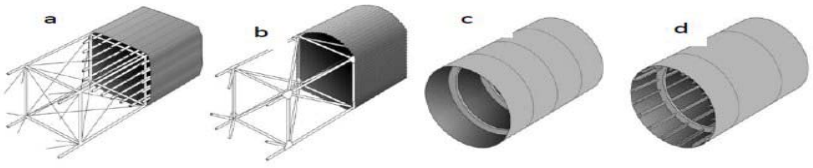

FIGURE 1. Fuselage structure a. Truss with canvas b. Truss with corrugate plate c. Monocoque fuselage d. Semi-Monocoque fuselage

International Conference on Materials Research in Science and Engineering
AIP Conf. Proc. 2446, 180044-1–180044-4; https://doi.org/10.1063/5.0109231
Published by AIP Publishing. 978-0-7354-4208-5/$30.00

This paper encompasses static analysis of fuselage frame under different loading conditions and with Aluminum-6061 and Titanium alloys. The aircraft fuselage structural components are modeled and assembled in the CAD software CREO 4.0. The static structural analysis of the fuselage structure is performed using Ansys work bench. The finite element used in the structural analysis is hexahedral element. The Pressure loads during the flight are applied on the structure and the stresses and the deformation on the structure are analyzed. The stresses in the aluminum fuselage are more than the stresses induced in the titanium fuselage. The deformation in the deformation in the aluminum fuselage is also more than the titanium alloy fuselage.

LITERATURE REVIEW

A large body of literature is available on the structural analysis of aircraft fuselages. “Finite Element Analysis of Composite Aircraft Fuselage Frame. “Finite Element Analysis of Composite Aircraft Fuselage Frame” Frames also ensure fail-safe design against skin crack propagation due to hoops stress. Ideal fuselage frames cross section is often circular ring shape with a frame cap of Z section.. A high strength to weight ratio materials results in a lighter aircraft structure [9-16].

FUSELAGE GEOMETRY AND MODELLING

Airframe models are made using one of the CAD packages CREO 4.0. After the modeling, the geometry is imported to the ANSYS Workbench. The complete model assembly is illustrated in the figure 2.

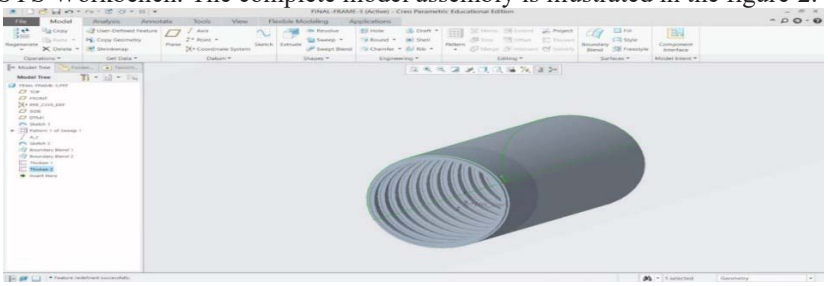

FIGURE 2. Final model of the fuselage structure

STATIC ANALYSIS OF THE FUSELAGE

Static analysis is performed on the fuselage structure to evaluate the displacement, stresses and strains induced in structures or components due to the external loads. A linear static analysis is used in the present work. The materials used in the construction of the fuselage are

1. Aluminum 6061
2. Titanium alloy (TI-6AL-2NB-1TA10.80MO)

Al-6061 is magnesium and silicon based hardened aluminum alloy. The major elements in the alloy are magnesium and silicon. In its alloy form, exhibits excellent mechanical properties and good welding properties. It is the most common alloys of aluminum which is used for general-purpose.

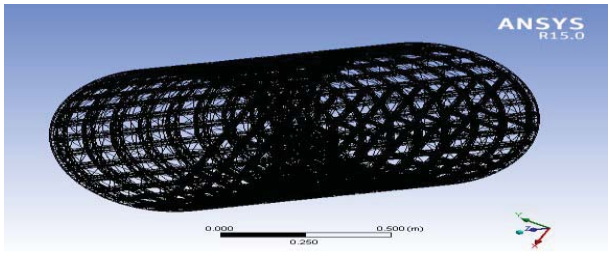

FIGURE 3. Meshed Semi Monocoque

Fig. 3 shows a meshed fuselage with hexahedral elements. The are performing structural analysis in internal skin of fuselage structure, so we need to consider pressure load that is -62466 negative sign for outward direction. Here

only a concentrated force at the centre at symmetric and done the analysis by varying the skin material. In this work two different new materials models are considered.

RESULTS AND DISCUSSION

The static analysis of the circular fuselage is performed by using the Ansys workbench. The results which are obtained from the static structural analysis are tabulated below in the table 2. The deformation for both fuselages increase with increase in the force applied on the structure. The maximum deformation for the aluminum fuselage is 0.0014m and the minimum displacement 7.64E-06m.The maximum and minimum deformations for the titanium alloy fuselage are 0.001029m and 5.94E-06m respectively. The maximum displacements are within the available limits [12] when compared with the other aluminum alloys.

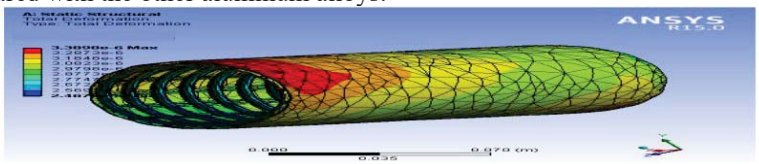

FIGURE 4. Total deformation of Aluminium alloy

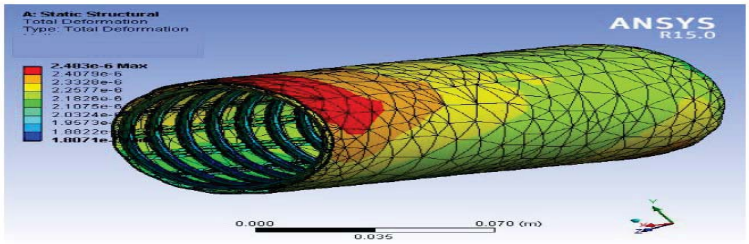

FIGURE 5. Total deformation of Titanium alloy

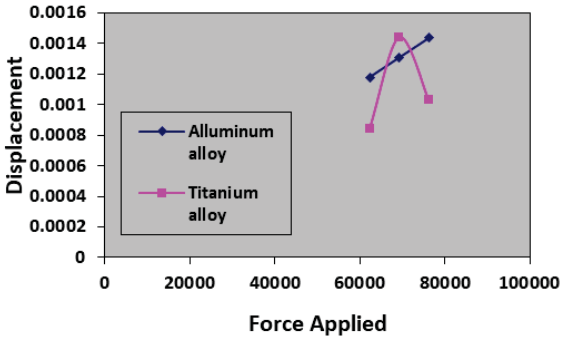

FIGURE 6. Force-Maximum displacement

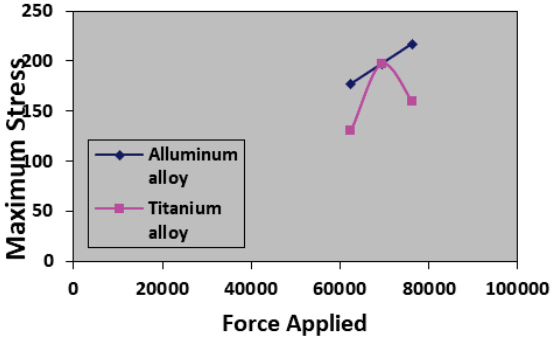

FIGURE 7. Force-Maximum Stress

CONCLUSION

The static analysis is carried out on fuselage by using ANSYS. The materials considered for the fuselage structure are aluminum alloy and titanium alloy. The results are tabulated in the table2 and the conclusions derived from the results are

- Titanium alloy is preferable compared to aluminum 6061 when the stress in the fuselage is considered.
- Titanium alloy fuselage displays good resistance to deformation compared to the aluminum alloy fuselage.

REFERENCES

1. Airframe and Aircraft Components, 1st edition, prepared by School of Aeronautics and Approved by the DGCA, Govt., of India
2. Florence Graves and Sara K. Goo (Apr 17, 2006). "Boeing Parts and Rules Bent, Whistle-Blowers Say". Washington Post. Retrieved April 23, 2010.
3. Todd Curtis (2002). "*Investigation of the Crash of American Airlines Flight 587". AirSafe.com.*
4. James H. Williams, Jr. (2002). "Flight 587". *Massachusetts Institute of Technology*.
5. Sara Kehaulani Goo (Oct 27, 2004). "*NTSB Cites Pilot Error in 2001 N.Y. Crash*". Washington Post. Retrieved April 23, 2010.
6. A Thesis Submitted to the Graduate School of Natural & Applied Sciences of the Middle East Technical University
7. A Thesis submitted to University of Texas
8. Static Analysis of Airframe Structure and Optimization, *International Journal on Theoretical and Applied Research in Mechanical Engineering (IJTARME)* V-5 No.2
9. Analysis of Stiffeners in a Semi Monocoque System of an Air Craft, *International Journal of Engineering Science Invention ISSN (Online):* 2319 – 6734, ISSN (Print): 2319 – 6726
10. E.F. Rybicki and M.F. Kanninen, 1997, "A finite element calculation of stress intensityfactor by a modified crack closure integral." *Engineering fracture mechanics,* vol. 9, pp.931-938.
11. Amy L. Cowan **"**Crack path bifurcation at a tear strap in a pressurized stiffened cylindrical Shell" in August 24,1999.
12. AndrzejLeski,2006,"Implementation of the virtual crack closure technique in engineering FE calculations". *Finite element analysis and design* 43, 2003,261-268.
13. A. Vivek Anand, V. Arumugam, R. Kannan, 2017, "Static wetting characteristics of micro-textured stainless steel surfaces under uniaxial loading condition", *Int. J. Surface Science and Engineering,* vol. 11, No. 2, pp. 174-190
14. K Veeranjaneyulu, Udaya Deepika A, Buckling Analysis of Stiffened Panel for Aircraft Fuselage, *International Journal of Mechanical and Production Engineering Research and Development*, ISSN(P): 2249-6890; ISSN(E): 2249 ,Dec2017
15. Dr. M SatyanarayanaGupta, Prof & HOD K Veeranjaneyulu, Associate Professor, Fabrication and Analysis of Adhesive joints Used in Aircraft Structures Pg. No:Volume 4, Issue 8, Pages 7155-9346 2017*International Conference on Advancements in Aeromechanical Materials for Manufacturing (ICAAMM-2016International MLRIT, Hyderabad* July 9-11, 2016
16. D. Mahesh Kumar ,N.Madhavi, Muttangi Sushma, Thin walled C-Sectional Beam under Axial Load, *International Journal of Innovative Technology and Exploring Engineering (IJITEE)* ISSN: 2278-3075, Volume-9 Issue-3, January 2020.

Interpretive structural modelling approach: Implementation of sustainability concept and lean in aerospace sectors

Cite as: AIP Conference Proceedings **2446**, 170014 (2022); https://doi.org/10.1063/5.0109432
Published Online: 29 November 2022

A. Vivek Anand, G. Sivaraj, P. Velmurugan, et al.

Interpretive Structural Modelling Approach: Implementation of Sustainability Concept and Lean in Aerospace Sectors

A. Vivek Anand[1,a], G. Sivaraj[2], P. Velmurugan[3], K. Srinivas Rao[4], Muhammed Anaz Khan[5,] and P. S. Prem Kumar[6]

[1]*Department of Aeronautical Engineering, MLR Institute of Technology, Hyderabad, India*
[2]*Department of Aeronautical Engineering, Bannari Amman Institute of Technology, Sathyamangalam, India*
[3]*Department of Mechanical Engineering, Shri Ram Murti Smarak College of Engineering, UP, India*
[4]*Department of Computer Science and Engineering, MLR Institute of Technology, Hyderabad, India*
[5]*Department of Mechanical Engineering, MLR Institute of Technology, Hyderabad, India*
[6]*Department of Aeronautical Engineering, Kumaraguru College of Technology, Coimbatore, India*

[a]Corresponding author: vivekanand7adr@gmail.com

Abstract. Interpretive Structural Modelling (ISM) is applied for interpolating the factors dictating the implementation of lean and sustainability concepts in aerospace sector. Modern aerospace component manufacturers are expected to be lean and sustainable to sustain in the competitive market scenario. Lean and sustainable strategies offers benefits such as waste elimination and minimal environmental impact. ISM has been preferred to create the structural model to explore the interrelationship between factors. 15 major factors are identified from prior art and further validated based on expert opinion. Based on computation, the influential factors are being identified and the structural model developed, management infrastructure and customer pressure factors are found to have top priority. The study has been conducted with inputs from expert and practitioners and the study is focused on aerospace sector. Hence, the outcomes are practically valid based on case study.

Keywords: Lean manufacturing; Interpretive Structural Modelling; Sustainable manufacturing

INTRODUCTION

Aerospace component manufacturing sector face intensive competition during the recent years [1]. Aerospace component manufacturers are forced to adopt both lean and sustainability concepts in their design and manufacturing practices [2]. Lean principles ensure streamlined process and waste elimination [3]. Sustainable concepts enable the development of environmentally friendlier products/processes [4]. A structural model is required to identify the interrelation between lean and sustainability concepts. In this context, this article reports a study in developing the structural model based upon Interpretive Structural Modelling (ISM). Digraph has been developed. 15 factors are being analysed and the structural model has been created. Based on the study, the influential factors are being determined.

Lean principles are applied in manufacturing and operational process and its application in aerospace sector is categorized into three levels namely process design strategy level, hierarchy level and project management level [5]. The studies proves that lean principles can be applied in real case small and large scale companies and are achieved by implementing support management tools and technology in aerospace sector. Sustainability concept is applied for aircraft manufacturing process to minimize energy consumption. The literature review [6] was performed on various aircraft manufacturers and the results showed that the absence of systematic approach was considered as the main

International Conference on Materials Research in Science and Engineering
AIP Conf. Proc. 2446, 170014-1–170014-5; https://doi.org/10.1063/5.0109432
Published by AIP Publishing. 978-0-7354-4208-5/$30.00

factor for implementing sustainability concept in aerospace sector. They concluded that, energy consumption was reduced over 70% by successful implementation of sustainability concepts in aerospace sector. In recent days, researchers explored the potential for developing green transport system by manufacturing green aircrafts [7]. This includes introduction of noval technologies, aircraft design, augmenting operational efficiencies, air traffic control and reducing emissions from aviation. The results showed that most of the emissions occur at higher altitudes and it can be reduced by engine design and improvement in fuel use efficiency.

ISM can be applied to analyze the difficulties in implementing lean techniques [8]. A Hierarchical Relationship Model (HRM) was developed based on ISM approach to explain relationship between lean implementation challenges. Based on the study, they found the major business parameters and non-linear behaviors as the most predominant challenges. ISM structural model can be developed based on variables that influence lean techniques in Indian automobile industry [9]. From literature survey and discussion with experts, the authors concluded 18 variables influence lean techniques in Indian automobile industry. They formulated an ISM model which showed nine variables as dependent and nine variables as drivers and none of them are linkage and autonomous variables. Based on the prior art search it has been found that no concrete research has been done on the structural model development to analyze the factors influencing lean and sustainability concepts in aerospace sector. In this context, this study has been conducted.

INTERPRETIVE STRUCTURAL MODELLING (ISM) METHODOLOGY

Interpretive Structural Modeling (ISM) is a systematic method for establishing relationship among set of variables which addresses the problems in process/system. In some system or process, there may be difficulty on arriving at a solution due to complex issues/problems in the system and also there may be difficulty in establishing relation among those complex variables. Defining proper structure to variables is a key factor in problem solving. Therefore, it is important to develop a methodology that can sort complex variables. In this methodology, a structural model is created by establishing directly and indirectly establishing relation among variables.

Structural Self-Interaction Matrix (SSIM)

Structural Self-Interaction Matrix (SSIM) establishes the indirect and direct relation within the factors. SSIM forms the basic structure of ISM methodology. Their relationship between factors is expressed by four symbols and listed in table 1. Cell (1,14) is designated as symbol B because factor 1 (mindset and behaviour) influences factor 14 (product design with minimal environmental impact). Cell (1,15) is designated to symbol ‘P’ because factor 15 (compliance of legal environmental regulations) influences factor 1 (mindset and behaviour).

Cell (2,12) is designated to symbol ‘X’ because both factor 2 (operations standardization) and factor 12 (government support) influences each other. Cell (2,14) is designated to symbol ‘O’ since both factor 2 (operations standardization) and factor 14 (product design with minimal environmental impact) does not have any influence each other. SSIM is formed by using these symbols in each cell of the matrix. The conceptual relationship between factors has been assigned by domain experts from industry, research laboratories and academics. The expert team consists of two academicians and five practitioners with rich knowledge in lean and sustainability concepts.

Initial Reachability Matrix

After forming SSIM, initial reachability matrix is framed with binary transition of SSIM. Each relationship in SSIM is converted into binary digits 0. Cell (1,14) is ‘V’ in SSIM, then cell (1,14) is assigned as 1 and cell (14,1) is assigned as 0 in initial reachability matrix. Cell (1,15) is ‘A’ in SSIM, then cell (15,1) is assigned as 1 and cell (1,15) is assigned as 0 in initial reachability matrix. Cell (2,12) is ‘X’ in SSIM, then cell (2,12) is assigned as 1 and cell (12,2) is also assigned as 1 in initial reachability matrix. Cell (2,14) is ‘O’ in SSIM, then cell (2,14) is assigned as 0 and cell (14,2) is also assigned as 0.

TABLE 1. Structural Self-Interaction Matrix.

Factor	F_{15}	F_{14}	F_{13}	F_{12}	F_{11}	F_{10}	F_9	F_8	F_7	F_6	F_5	F_4	F_3	F_2	F_1
F_1	P	B	B	X	P	B	P	B	B	B	X	P	P	P	-
F_2	B	O	P	X	P	P	P	B	P	B	X	X	P	-	-
F_3	P	B	B	X	P	P	B	B	B	B	X	B	-	-	-
F_4	O	O	O	O	P	P	X	B	P	P	B	-	-	-	-
F_5	O	B	B	O	O	P	P	B	X	B	-	-	-	-	-
F_6	P	P	P	P	P	P	X	B	X	-	-	-	-	-	-
F_7	P	B	B	P	X	P	P	B	-	-	-	-	-	-	-
F_8	P	P	P	P	P	B	P	-	-	-	-	-	-	-	-
F_9	B	B	B	O	P	X	-	-	-	-	-	-	-	-	-
F_{10}	O	V	B	O	P	-	-	-	-	-	-	-	-	-	-
F_{11}	B	B	B	O	-	-	-	-	-	-	-	-	-	-	-
F_{12}	X	X	X	-	-	-	-	-	-	-	-	-	-	-	-
F_{13}	X	X	-	-	-	-	-	-	-	-	-	-	-	-	-
F_{14}	X	-	-	-	-	-	-	-	-	-	-	-	-	-	-
F_{15}	-	-	-	-	-	-	-	-	-	-	-	-	-	-	-

Final Reachability Matrix (FRM)

FRM is framed by applying transitivity principles in initial reachability matrix. Transitivity principle states that when ‘i’ is linked to ‘j’ and when ‘j’ is linked to ‘k’, ‘i’ and ‘j’ are also linked. In SSIM, cell (1,15) is assigned as X and cell (5,7) is assigned as X. Then, the cell (1,7) must be assigned as X in final reachability matrix. Likewise transitivity is checked for each cell and final reachability matrix is formed. Dependence and driving power are obtained and levels are assigned to each factor. Factor 3 had maximum driving power and assigned level I. Similarly, factors 13 and 14 had maximum dependence power and are assigned level I. Likewise each factor are assigned levels according to their dependence and driving power and shown in table 2.

ISM Based Model

Management infrastructure and customer pressure are key factors which are at base level. Market trends and government support are at next level. Group problem solving enables the generation of approximate solution to problems and occupies next level. Operations standardization, pull system and compliance with legal environmental regulations occupy next level. This is followed by mindset and behaviour, worker empowerment, training, continuous improvement and competition at subsequent levels. Adoption of clean technologies and product design with minimal environmental impact form the top level factor in the model. ISM-based models are represented as chart in figure 1 in the order of influencing factors. ISM models are formed based on conical matrix and level partitions. Factors at least level form base of the model. They are the most dominant factors influencing lean and sustainable concepts in aerospace sector. Similarly, factors having higher levels are placed on top of ISM model. They are the least influencing factor. Likewise, other factors are placed based on their levels. From Figure 1, it is observed that factor 3 (management infrastructure) and factor 11 (customer pressure) forms the base for ISM model and they are most dominant factors. These factors will influence all other factors due to its stronger driving power. Similarly, factor 13 (adoption of clean technologies) and factor 14 (product design with minimal environment impact) are on the top of ISM model and they are the least dominant factors. These factors are least influencing and have least driving power.

TABLE 2. Final Reachability Matrix

Factor	F_1	F_2	F_3	F_4	F_5	F_6	F_7	F_8	F_9	F_{10}	F_{11}	F_{12}	F_{13}	F_{14}	F_{15}	Driving power	Rank
F_1	1	0	0	0	1	1	1	1	0	1	$1^\dagger$	1	1	1	0	10	IV
F_2	1	1	0	1	1	1	0	1	$1^\dagger$	$1^\dagger$	0	1	$1^\dagger$	$1^\dagger$	1	12	III
F_3	1	1	1	1	1	1	1	1	1	$1^\dagger$	$1^\dagger$	1	1	1	$1^\dagger$	15	I
F_4	1	1	0	1	1	$1^\dagger$	0	1	1	$1^\dagger$	0	0	$1^\dagger$	$1^\dagger$	0	10	IV
F_5	1	1	1	0	1	1	1	1	0	$1^\dagger$	0	0	1	1	0	10	IV
F_6	0	0	0	1	0	1	1	1	1	$1^\dagger$	$1^\dagger$	0	$1^\dagger$	$1^\dagger$	0	9	V
F_7	$1^\dagger$	1	$1^\dagger$	1	1	1	1	1	0	$1^\dagger$	1	0	1	1	$1^\dagger$	13	II
F_8	0	0	0	0	0	0	0	1	0	1	0	0	$1^\dagger$	$1^\dagger$	0	4	VI
F_9	1	1	0	1	1	1	1	1	1	1	0	0	1	1	1	12	II
F_{10}	0	1	1	1	1	1	1	0	1	1	0	0	1	1	0	10	IV
F_{11}	1	1	1	1	0	1	1	1	1	1	1	0	1	1	1	13	II
F_{12}	1	1	1	0	0	1	1	1	0	0	0	1	1	1	1	10	IV
F_{13}	0	1	$1^\dagger$	$1^\dagger$	0	1	0	1	0	0	0	1	1	1	1	9	V
F_{14}	0	$1^\dagger$	$1^\dagger$	$1^\dagger$	0	1	0	1	0	0	0	1	1	1	1	9	V
F_{15}	1	$1^\dagger$	1	0	0	1	1	1	0	0	0	1	1	1	1	10	IV
Dependence power	10	12	9	10	8	14	10	14	7	11	5	7	15	15	9		
Rank	VII	IV	VII	VI	VIII	III	VII	II	VIII	V	IX	VIII	I	I	VII		

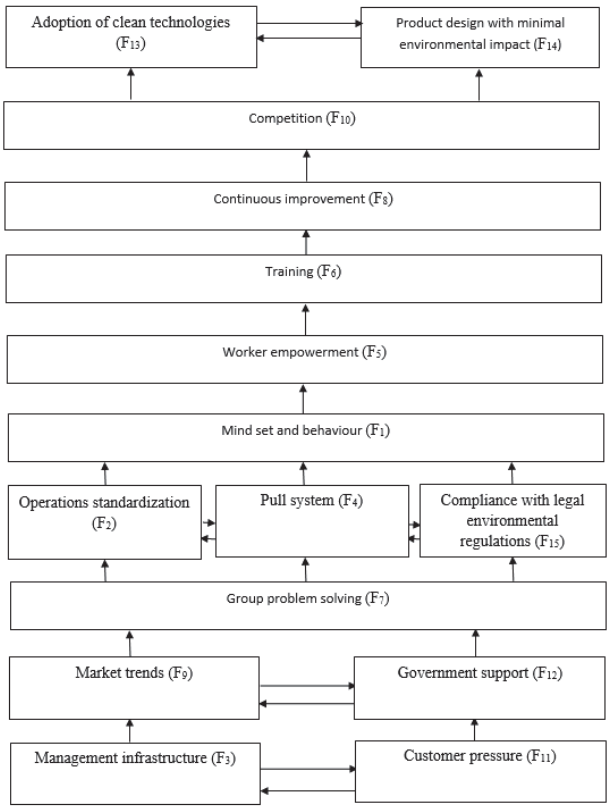

FIGURE 1. ISM- Model

CONCLUSION

Lean and sustainable strategies are needed for attaining competitiveness by aerospace component manufacturers. Combined lean and sustainable strategies provide benefits such as waste elimination and environmental impact reduction. 15 factors are being identified from prior art and expert opinion. ISM has been used for developing the structural model. Based on computation are found to be most significant factors. The conduct of the study would enable the practitioners to systematically analyse the factors influencing lean and sustainable concepts implementation in aerospace sector. In future, the approach could be used for studying the interrelationship among factors/barriers in the context of other manufacturing paradigms

REFERENCES

1. E. Cudney and C. Elrold, "A comparative analysis of integrating lean concepts into supply chain management in manufacturing and service industries", International Journal of Lean Six Sigma, 2 (1) (2011), pp. 5 – 22.
2. L.M.J Michaels, "The making of a lean aerospace supply chain supply chain management in manufacturing and service industries", International Journal of Lean Six Sigma, 2 (1) (1999), pp. 5 – 22.
3. J.R. Jadhav, S.S. Mantha and S.B. Rane, "Development of Framework for Sustainable Lean Implementation: An ISM Approach", Journal of Industrial Engineering International, 10 (2014), p. 72.
4. Y. Romaniw and B. Bras,"Survey of Common Practices in Sustainable Aerospace Manufacturing for the Purpose of Driving Future Research", Leverage Technology for a Sustainable World, 1 (2012) pp. 485-490.
5. S. Womack and M. Jones, "Proceedings of the Institution of Mechanical Engineers Part B-Journal of Engineering Manufacture", Professional Engineering Publishing Ltd, 217 (10) (2003), pp. 1409-1420.
6. P. Lunt and A. Levers, "Reducing Energy Use in Aircraft Component Manufacture -Applying Best Practice in Sustainable Manufacturing", SAE International, 2011-01-2739.
7. A.N. Sarkar, "Evolving Green Aviation Transport System: A Hoilistic Approach to Sustainable Green Market Development", American Journal of Climate Change, 1 (2012), pp. 164-180.
8. J.R. Jadhav, S.S. Mantha and S.B. Rane, "Roadmap for Lean Implementation in Indian Automotive Component Manufacturing Industry: Comparative Study of UNIDO Model and ISM Model", Journal of Industrial Engineering International, 11 (2015), pp. 179–198.
9. A. Kumar, "A Qualitative Study on the Barriers of Lean Manufacturing Implementation: An Indian Context", International Journal of Engineering and Science, 3 (4) (2014), pp. 21-28.

A conceptual design of tailless minicopter

Cite as: AIP Conference Proceedings **2446**, 180042 (2022); https://doi.org/10.1063/5.0109212
Published Online: 29 November 2022

N. Madhavi, K. Harsha Vardhan, Siddhanth Thakuri, et al.

A Conceptual Design of Tailless Minicopter

N. Madhavi[1,a)], K. Harsha Vardhan[1], Siddhanth Thakuri[1], B. Akhil Goud[1], Shivam Dubey[1], U. Rajendar[1] and R. Vijayanandh[2]

[1]*Department of Aeronautical Engineering, MLR Institute of Technology, Hyderabad, India*
[2] *Department of Aeronautical Engineering, Kumaraguru College of Technology, Coimbatore, Tamil Nadu, India*

Corresponding author mail: [a)] madhunagireddy@gmail.com

Abstract. This paper describes the design process of a tailless mini copter having surveillance capability by integrating it with Internet of Things. The microprocessor controls different sensors of the tailless mini copter, where python programming language acts as an interface for the raspberry pi microprocessor. The major challenge is to overcome is the inertial rotation of the copter due to the absence of a tail rotor. The inertial rotation can be cancelled out by implementing the co-axial mechanism with contra-rotating propellers. The copter would make its place where other UAVs cannot reach, because of its compact design and low self-weight. Integrating more sensors would open a wide range of applications in different fields.

Keywords: Tailless copter, Internet of Things, Co-Axial Mechanism, Contra Rotating Propeller, Raspberry Pi.

INTRODUCTION

Back in 1745, Mikhail Lomonosov from Czarist Russia proposed the single-rotor configuration, pioneers knew about the fundamentals of coaxial design mechanism. The first coaxial mechanism in Spain (1920-26), Raoul Pescara designed and built a helicopter with coaxial rotors consisting of four blades with each diameter of six meters. In 1928's, D'Ascanio from Italy constructed a helicopter with two sets of coaxial rotors and the helicopter reached a height of 18 meters.[1] Tailless mini-copter mainly focuses on the surveillance part and design simplicity. The UAV is integrated with software system which uses raspberry pi coupled with the Internet of things (IoT) by using programming language called Python, which acts as an interface. It consists of raspberry pi (microprocessor), LDR (light dependent resistor) sensor which indicates the presence and absence of light, ultrasonic sensors that measures the distance of target object by emitting ultrasonic sound waves and reflect sound into electrical signals, camera sensor that identifies and transmits information. The role of UAV is to monitor the climatic changes, carry out research operations after natural disasters, photography, filming and delivering goods. They are specially known for the reconnaissance, surveillances and target attacks.

DESIGN OF TAILLESS COPTER

Co-Axial Mechanism

The tailless helicopter has two contra-rotating rotors which rotate using coaxial mechanism. In this work, the lower rotor works by the downwash of upper rotor as shown in Fig-1. It overcomes the disadvantages of the conventional single rotor helicopter [Coleman, 1997], which works on lower maneuverability and here we used bevel gear mechanism to obtain the rotation of rotors in opposite direction. The coaxial design had already proposed on coaxial rotor machine in 1754 by Mikahail Lomonosov from Czarist Russia. In 1992, a helicopter with two sets of coaxial rotors constructed by D'Ascanio, who is belongs from Italy, in which a helicopter reached a major

International Conference on Materials Research in Science and Engineering
AIP Conf. Proc. 2446, 180042-1–180042-6; https://doi.org/10.1063/5.0109212
Published by AIP Publishing. 978-0-7354-4208-5/$30.00

altitude of 18 meters. There were many papers attempting to construct a tailless contra-rotating helicopter in early days of helicopter development [Heatley, 1985]. The tailless helicopter has advantage of having contra-rotating rotors to recompense each other's torque. The power efficiency of a tailless helicopter is better and it will allow all the power in developing lift without a tail rotor. When compared with the single rotor helicopter, the size of the tailless helicopter reduces by 35-40% and by this the moment of inertia of tailless helicopter decreases there by controllability and maneuverability of the helicopter increases. The main disadvantage of conventional helicopter is its dissymmetry of lift in forward flight. Theoretically tailless helicopter solves this problem by cancelling lift difference using two rotors.

Contra-rotating Propellers

Torque is force acting in the opposite direction of the spinning propeller. Contra-rotating propellers are the ideal solution to cancel torque, here with the help of two propellers toques will cancel each other by compensating perfectly.

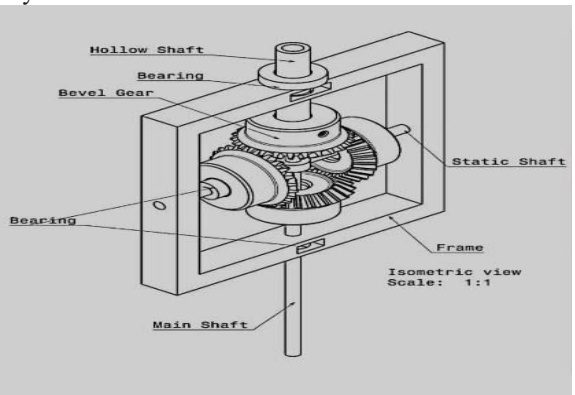

FIGURE 1. Co-Axial Mechanism

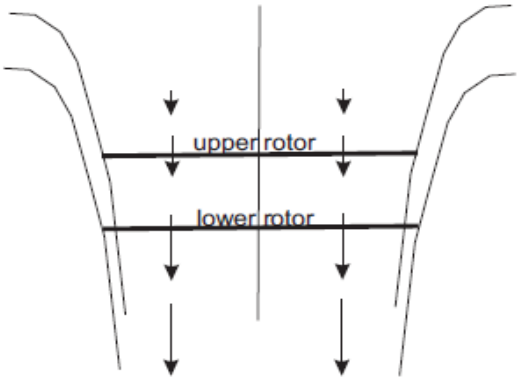

FIGURE 2. Contra-rotating Propeller

The two propellers produce high thrust, the top rotor is not linked to any servos and the bottom propeller is connected with two servos which connect to the rotor by a swash plate. The relative pitch between two propellers is stationary because both propellers cannot vary their collective pitch, when the pitches of one blade increases then the pitch of other blade decreases by keeping a continual average pitch [2].

Fuselage

Fuselage is one of the main components in the tailless mini copter because major components which are going to control the copter are placed inside the fuselage. It is divided into three parts. First part (top) consists of electric motor with damper and servos. Second part (middle) consist of lithium ion battery, electronic speed control (ESC) and receiver. Third part (bottom) consist raspberry Pi, LDR (light dependent resistor) sensor, camera, bread board and ultrasonic module sensor. The fuselage is made-up of plywood which is very strong, light in weight and it is going to take all the weight of co-axial mechanism, blades, rotor heads and swash plate. The weight is equally distributed to all the landing gears. Landing gears are connected to the top corner's portions of the fuselage. The third part is more important in the fuselage because it is going to perform aim of this paper i.e., surveillance.

FIGURE 3. Fuselage CAD assembly

Electronic Circuit System

There are two circuit systems, in which first circuit system will be present in top and middle parts. In this the motor is connected to the ESC, which is connected to battery and receiver. In this circuit system receiver place a major role, this is revealed in Figure 4. Second circuit system will be present in bottom part. In this system raspberry pi is connected to power- bank, camera, ultrasonic sensor module and LDR sensor. The circuit diagram of this system is shown in Figure 5.

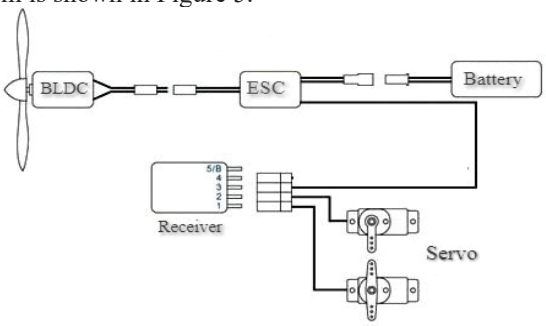

FIGURE 4. Motor circuit system

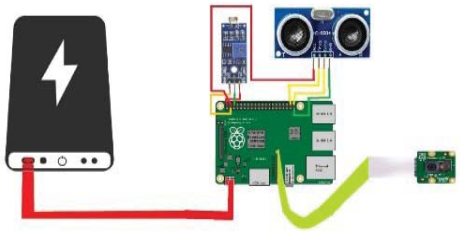

FIGURE 5. Sensor circuit system

Landing Gear

The purpose of landing gear is that it is going to take the load from the fuselage and give good support while on the ground and perform safe landing. The material used for landing gear is Aluminum (2024) and shape is T-section, which is having better properties compared with all different sections. In this landing gear we used Aluminum damper to avoid vibration while landing. In this we used rubber foot for better support. The purpose choosing Aluminum for landing gear is that it is having high strength, good workability and it is also having damping capability.

TABLE 1. Aluminum 2024 Composition

S.NO	Material	Composition
1	Copper	3.8%
2	Manganese	0.5%
3	Magnesium	1.2%

DIRECTIONAL CONTROL

It is possible to control six degrees of freedom using six inputs but that would be very difficult for humans. So, using the coupling method, the number of control input can be minimized. This concludes that single input can result in multiple outputs. Basically, there are four controls in a helicopter.

I. Vertical control: it refers to a simple up and down motion or change in altitude. This can be achieved by collective pitch input i.e., varying the pitch angle of all blades collectively changes the angle of attack and leads to a subsequent change in lift, which results in a vertical motion. **II. Longitudinal control:** it is also called forwarding motion. This is defined as a pitching moment that accompanies the force to move forward on giving the control input. The forward motion of the copter achieved by tilting the main rotor disc in forward direction and thus thrust vectoring can be achieved. The thrust vector has two components one is a vertical component which supports the weight, and the horizontal components equalize the forward force. **III. Lateral control:** it is a sideward motion. Here rolling moment goes with the force to move sideward by applying control input. This can be achieved by tilting the rotor disc to the left or right. **IV. Directional control:** It refers to changing the direction of helicopter's yaw degree of freedom. This can be achieved by changing the pitch angle of the tail rotor, where as in tailless mini copter we are replacing the tail part to a co-axial rotor mechanism which will work the same as tail rotor and cancels the torque acting on the axis of the body frame [3, 4].

Coupling Method

The lateral and longitudinal control is coupled with the moments which will generate force, this is because of tilting the rotor disc. The center of gravity is no longer aligned with the thrust vector and the moments are generated. So, here the balance of forces and moments should be achieved, this might not be possible in all cases, this is the reason why copters cannot fly at very high speeds. The rotor disc can be tilted in all the desired directions (360°), this is one of the main advantages of the helicopter. The tilting mechanism can be achieved by two methods; one is by tilting the main shaft which is connected to rotor disc and the other method by tilting the rotor disc. This can be achieved by cyclic pitch control. The tailless mini-copter follows the directional control and coupling method, with the help of a device called swash plate.

Swash Plate Mechanism

A swash-plate is a device that translates input via flight control into the motion of main rotor blades. Swash-plate consists of two rotating parts one is a stationary swash-plate and the other is a rotating swash-plate. The stationary swash-plate is fixed on the main rotor and it is coupled to cyclic and collective controls, by a series of pilot inputs. It has the benefit of tilting in all directions and move vertically. The inner or rotating swash-plate is fixed to the stationary swash-plate with the help of bearing and gives access to rotate the main rotor blade. The collective servo will give the command to the entire swash plate unit as a whole, up and down. Thus, the pitch angle of all the blades can be changed by the same angle called collective pitch. The next is the cyclic pitch which concludes the tilting of the swash plate in the longitudinal plane about the lateral axis when the swash-plate is tilted on varying blade pitch angle. The pitch bearing is fixed with the control rod for changing the pitch angle. When the servo moves up and down to change the pitch angle, the control rod attached to the swash plate will be tilted in the longitudinal plane. Here the throttle is used to maintain the co-axial mechanism's RPM depending upon the payload conditions. Hence, throttle control can be varied depending upon the requirements.

Microcontroller

A raspberry pi is a credit-card sized micro-processor which uses peripherals like keyboard, mouse, display system and acts as a mini personal computer. It uses Debian based Raspbian OS which is an official operating system for raspberry pi. It is widely used to explore computing, learn programming, applying programming languages like python in real world applications. Raspberry pi is popularly used for real time world applications like image processing, video processing, IoT (Internet of Things) and robotic based applications.

Implementation of Raspberry Pi in Tailless Minicopter

For a mini copter to perform the following tasks like: Live video streaming, Obstacle avoidance, light detection, and Distance measurement, etc. Micro-processors and sensors play a major role. Therefore, raspberry pi (micro-processor) is used in this mini copter. The Raspberry pi helps in accessing controls over sensors present in the mini-copter, to which we can give the respective commands and acquire required results. Light detection and distance measurement can be achieved by any micro-controllers and micro-processors, and requires not much instruction to perform tasks. Live video streaming and object detection requires sensor like pi camera which then requires processors like raspberry pi to handle the functioning.

Integrating Raspberry pi with IoT

To obtain the results/outputs from the raspberry pi to the display screens wirelessly it needs to be integrated with IoT (Internet of Things), which is a system of interrelated, internet-connected objects which helps in data transmission wirelessly anywhere around the world without human intervention. For the IoT to work we must have a processor that connects with the internet, and that processor is raspberry pi. Hence, the output from the raspberry pi is transmitted wirelessly through IoT to our display screens, i.e., required data can be collected and required information/tasks can be assigned to the mini-copter.

Sensors

The authors can use multiple sensors, depending on the applications. The few sensors used in this mini copter are: PI Camera Module, LDR Module, and Ultrasonic Sensor Module

PI Camera Module

PI Camera is a mini camera specially designed for raspberry pi. It contains variety of variants, as for this mini copter, camera module v_1 is sufficient, which gives the following: 1] Resolution of 5 mega pixels, 2] Video modes of 1090p03, 720p60 and 640x480p60/90, and 3] weighs around 3 gm. The main purpose of this in the mini copter is for video live streaming and obstacle avoidance.

LDR Module

LDR is a light dependent resistor which is used to detect the presence and absence of light and perform tasks accordingly. To achieve night flight of mini-copter we use lights which are attached to the mini-copter, turns it “on” when it is dark and turns it “off” when it is not dark using the light sensor, hence achieving the proper night flight.

Ultrasonic Sensor Module

The purpose of Ultrasonic sensor Module is to measure the distance between object and the mini-copter, also using it for different tasks like measuring the landing distance, sending information, obstacle avoidance, etc.

FIGURE 6. A Tailless mini-copter CAD model

CONCLUSION

A Tailless mini-copter is compact UAV which can be used for surveillance, vaccine delivery, policing etc. Wide range of applications can be achieved by integrating raspberry pi with the internet of things. This paper briefly describes about working coaxial mechanism, counter rotating propellers and how these technologies can be used to design a tailless mini copter.

REFERENCES

1. L.Chen, Phillip J. McKerrow, Modeling of the lama(2007).
2. Dario Martin Schafroth,Aerodynamics, Modeling and Control of an Autonomous Micro Helicopter(2010).
3. Prof. C Venkatesan, Introduction to helicopter aerodynamics and Dynamics, NPTEL Lectures.
4. Daniel P.Raymer, Aircraft Design: A Conceptual Approach, Fourth Edition, AIAA, 2006.
5. John D Anderson Jr, Introduction to Flight, Fifth Edition, Tata Mc Graw Hill, 2007.
6. Pascual Marque's, Fight Stability and Control of Tailless Lambda Unmanned Aircraft, (2003).
7. S. Senthil Kumar, R. Vijayanandh and S. Mano. 2018. Mathematical Modelling and Attitude Control of Quadcopter based on Classical Controller, Int. J. Vehicle Structures & Systems, 10(5), pp. 318-323. doi:10.4273/ijvss.10.5.02.
8. J. Darshan Kumar, Rani Thottungal, & Vijayanandh, R. (2021). Effective Monitoring By Drone Using Advanced Deep Machine Learning Strategies With IoT, Journal of Environmental Protection and Ecology, Vol. 22, Issue No 3, pp. 1246–1258.
9. Vijayanandh. R, Ramesh. M, Senthil Kumar. S, Raj Kumar. G, Senthil Kumar. M & Naveen Kumar. R, The Conceptual Design of the Tilt-Copter Based On the Speech Control (A Theoretical Approach), International Journal of Mechanical and Production Engineering Research and Development, ISSN (E): 2249-8001, Vol. 8, Issue 7, 423-439, 2018.
10. S. Senthil Kumar & R. Vijayanandh, A Dynamic Response And Stability Analysis Of Hybrid UAV With The Linear Controllers, International Journal of Mechanical and Production Engineering Research and Development, ISSN(E): 2249-8001, Vol. 8, Issue 7, 330-342, 2018.

Determination of stacking fault energy for a Nitinol based shape memory alloys by molecular dynamics simulation

Cite as: AIP Conference Proceedings **2446**, 180055 (2022); https://doi.org/10.1063/5.0109530
Published Online: 29 November 2022

M. N. V. S. Swetha Bala, N. Uday Ranjan Goud, Dheeraj Kumar Gara, et al.

Determination of Stacking Fault Energy for a Nitinol Based Shape Memory Alloys by Molecular Dynamics Simulation

M. N. V. S. Swetha Bala[1, a)], N. Uday Ranjan Goud [1], Dheeraj Kumar Gara [2] and R. Kannan[3]

[1]*Department of Aeronautical Engineering, MLR Institute of technology, Hyderabad, India – 500043*
[2]*Department of Aeronautical Engineering, Malla Reddy College of Engineering and Technology, Hyderabad, India – 500100*
[3]*Department of Physics, School of Foundational Sciences, Kumaraguru College of Technology, Coimbatore – 641 049, Tamil Nadu, India.*

[a)]Corresponding author: swethabalamlr@gmail.com

Abstract. Shape memory alloys exhibit interesting phenomena termed as shape memory effect, which occurs at a specific composition for a class of materials when alloyed together. In current work, we consider Nickel and Titanium (nitinol) which exhibits this interesting phenomena at near equiatomic composition. In a quest to develop a structure-property correlation, it is expected that among other parameters, defects in the materials also contribute towards the properties of material developed. As a result, stacking fault energy is one such defect which decides the properties of materials. The current work estimates the staking fault energy of nitinol based alloy system from second nearest neighbor embedded atomic model using molecular dynamics simulation that allows to establish a structure-property correlation.

Keywords: Nitinol, shape memory, staking fault energy, 2NNEAM

INTRODUCTION

Nitinol being bio compatible cannot be directly integrated to aerospace and automotive industry since, aerospace and automotive industry demands high strength to weight ratio, thermal resistance etc. As a result, it involves different processing techniques, different composition to attain sustainability of these alloys for aerospace and automotive domain hence our present study emphasizes it by developing an analytical model to estimate the macroscopic behavior from the crystallographic defects at microscopic level. The microscopic defects will be configured from the series of numerical simulations to find out the requisite parametric data to validate the analytical model. This enables user friendly environment to understand the processing parameters by estimating the SFE and test for macroscopic properties.

The preset motivation is enveloped for the shape memory alloys as it indicates different behavior at varying compositions, stacking fault energy becomes an important phenomenon. In connection to this however there are few literatures being cited in the scientific community emphasizes very little on analytical work but ample work on experimental environments. Hence it is difficult for the engineers to process a suitable composition with specific properties. Therefore, there is need for an in-situ which forms the novelty of the present work. The current context is to model the Stacking fault energy from the microscopic principals using statistical mechanics approach at varying composition of alloys (Ni% in Nitinol). The governing equations used in [1] are used to calculate the stacking fault energy at various composition of Ni in Ni-Ti SMA.

It is imperative to discuss the parameters that are associated with SFE since it is the only parameter that predicts the behavior of the SME at microscopic and macroscopic level. An extensive research is already available in literature about the stacking fault defects, but for different materials such as steels and magnesium, zinc etc. It is to

International Conference on Materials Research in Science and Engineering
AIP Conf. Proc. 2446, 180055-1–180055-8; https://doi.org/10.1063/5.0109530
Published by AIP Publishing. 978-0-7354-4208-5/$30.00

be noted that SFE depends strictly on the composition and processing environment. As a result, in line with our present research work, we intend to constrain only for alloy composition but not the processing parameters. However, an emphasize will be made on the selected processing route considered for the development of as received product.

Mostly Face Centered Cubic (FCC) structures undergo twining which is primarily due to SFE. The effect of SFE on the mechanical properties can be studied by changing the temperature during the tensile test which is readily available in [2] and [3]. Whilst with a decreasing value of the SFE, plasticity is achieved by:

1. Partial and perfect dislocations gliding,
2. Gliding and mechanical twinning, which increases the elongation to fracture and provides the best hardening rate and
3. Gliding and Strain (ε) martensitic transformations which give the best yield strength and a good hardening rate. [3]

According to [4] the SFE is considered as a specific case of a Gibbs interface because SFE is anisotropic with respect to orientation of the surface in a crystal.

$$\Gamma = 2\rho\Delta G^{\gamma\rightarrow\varepsilon}\sigma \tag{1}$$

Where , SFE Γ is the Gibbs Energy

ρ Is molar surface density and is obtained by $= \frac{4}{\sqrt{3}}\frac{1}{a^2 N}$, N is Avogadro's number, a is the lattice parameter

Following Gibbs, we consider a system composed of a matrix phase, denoted by a superscript m and a planar interface, the stacking fault, separating two regions of the matrix and denoted by a superscript s. Differentially and reversibly displacing the system and summing the various reversible work terms, we find for the variation in internal energy of the system, from the first law of thermodynamics,

$$dE = Tds - Pdv + \mu_i\, dn_i + \gamma dA + d\omega \tag{2}$$

Where, T is temperature, S is entropy, P is pressure, V is volume, μ_i and n_i are the chemical potential and number of molecules, A is area and *dw* represents other possible work terms which we set equal to zero at present. From [5] it is evident that the stacking fault can be segregated into twin boundaries or other types of two dimensional faults satisfying certain conditions. The expression is derived for the concentration difference at equilibrium and for the fault energy as a function of the concentration difference.

$$\gamma(x_s, x_a) = \omega(x_s) + \varepsilon(x_s, x_a) + G_m(x_s) - x_s\overline{G_B}(x_a) - (l - x_s)\overline{G_A}(x_a) \tag{3}$$

Where, G_A and G_B are the chemical potentials of elements A and B. γ is the surface energy at equilibrium. ε is energy per mole. x_a is the homogeneous composition of matrix, x_s is the atomic fraction of element B and G_m is the molar free energy as shown in **Figure 1** [6].

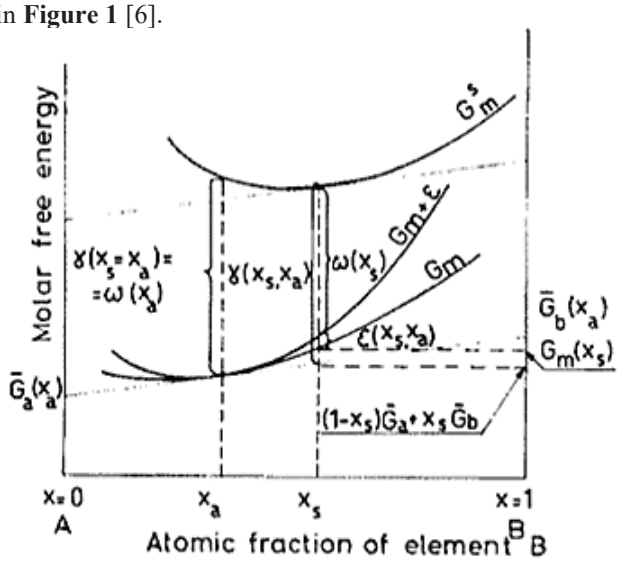

FIGURE 1. Free energy Diagram

From [7] we obtain the general conditions for equilibrium between a stacking fault and a phase for any binary solid solution alloy.

$$\left(\frac{d\Delta F\{m_b,T\}}{dm_b}\right)_{atm_b} - \left(\frac{d\Delta F\{m_b,T\}}{dm_b}\right)_{atfm_b} = \frac{V}{t}\frac{d\gamma\{fm_b,T\}}{dfm_b} \quad (4)$$

Where, $\Delta F\{m_b,T\}$ is the free energy of mixing one mole of the alloy. $\gamma\{fm_b,T\}$ is the free energy per unit area of the fault. T is the temperature. $\frac{V}{t}$ is volume rate. All the above relations are in terms of thermal and Gibbs free energy equation. Now by using electron microscopy the SFE can be determined by measuring the dissociation width of edge dislocations. The SFE is also related with the iconicity of the bond. The plasticity in the ionic bond can be traced back to the dislocation velocities. [8]

Since we are dealing with NiTi alloy and our paper emphasizes on different composition of Ni in NiTi, we ought to know the stacking fault energy of the Ni as shown in **TABLE 1**. The stacking fault energy of nickel ranges from 79 mJ m^2 to 415 mJ m^2 [9].

TABLE 1. Previous determinations of the SFE of nickel

$\gamma\ mJm^{-2}$	Method
90	τ_3
95	Creep data
410	τ_3
150	Extrapolated (Ni-Co) node data
300	Extrapolated (Ni-Co) node data
300	τ_3
345	Reinterpretation of Howie and Swann result
450	Rolling Texture
$\leq 180 \pm 55$	Faulted dipole
≥ 375	Absence of tetrahedral data
$\leq 160 \pm 16$	Extrapolated (Ni-Co) tetrahedral data
≤ 160	Extrapolated (Ni-Co) tetrahedral data
240	Rolling Texture
79	Dissociated edge dipole
250	Comparison of previous data
415	τ_3
140	τ_3
234	Flow stress analysis

In FCC metals the stacking fault takes place at extended dislocations. If there is a complete dislocation in these materials, there is chance of energy being lost by splitting into two Shockley partial dislocations connected by a ribbon of stacking fault this is known as extended dislocations.

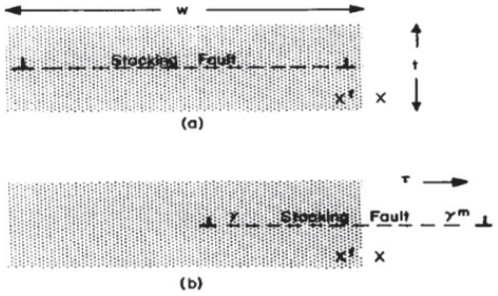

FIGURE 2. (a) Schematic representation of an extended dislocation in a segregated alloy. (b) Motion of the extended dislocation to free it form its segregated solute atmosphere.

From the **Figure.2** we can see the dislocations has a width 'w' determined by balancing the repulsive force of the particle against the attractive force equivalent to a positive SFE. It is known that SFE usually decreases with increasing solute concentration in FCC binary alloys.

$$G_t' = G'(n_A, n_B) + G'\left(n_A^f, n_B^f\right) + G_d' \quad (5)$$

In this the first term is the free energy of the matrix and the last two are the energy of the faulted region. The quantitiesn_B, n_A, n_B^f, n_A^f are total number moles of component A and B in the matrix and faulted region respectively [10].

$$G_d' = (\gamma\omega - C\ln\omega + D)l \tag{5}$$

Where G_d' is the energy of the extended dislocations, the first term is the energy of the stacking faults and the second is the repulsive interaction of the partial dislocation pairs, γ is the stacking fault, w is stacking fault width, C and D are functions of the Burgers vector and the elastic constants and l is the total length of the dislocations in the alloy [11].

It can be now conferred that, processing parameters and alloy compositions play a major role in introducing shape memory effect and on Superelasticity range. But, it is important to note that only few parameters will vary the shape recovery range when the composition changes. So prediction of that parameter was deduced from the literature. It is one of the defects during processing parameter, termed as stacking fault sequence which is addressed in the current context. Atomistic energy/strain energy is used to model the stacking fault energy which never an attempt made ever in the literature. A microscopic model is developed to estimate the strain energy of the alloy with stacking fault energy as a variant. Since stacking fault can be different in different planes, an analytical model amenable to solve the stacking fault energy for various planes is also an area of interest and hence the current work will emphasize on simulation results and have been discoursed in the present work. A dataset on the potential of stacking fault energy will be calculated using an embedded atomic model (EAM) by a suitable molecular dynamics simulation.

METHODOLOGY

The stress at an atomic level for a homogeneous system can be written as

$$\tau_{ij} = \frac{1}{\Omega}\sum_{k\epsilon\Omega}(-m^{(k)}(u_i^{(k)} - \bar{u}_i)\left(u_j^{(k)} - \bar{u_j}\right) + \frac{1}{2}\sum_{l\in\Omega}(x_i^{(l)} - x_i^{(k)})f_j^{(kl)}) \tag{6}$$

And also proven for its compatibility for short range interactions using ensemble average method.

Where,

k and l are atoms in the domain,

Ω is he volume of the domain,

$m^{(k)}$ is mass of the atom k,

$u_i^{(k)}$ is the i[th] component of the velocity of atom k,

$\overline{u_j}$ is the j[th] component of the average velocity of atoms in the volume,

$x_i^{(k)}$ is the i[th] component of the position of atom k, and

$f_j^{(kl)}$ is the i[th] component of the force applied on the atom k by atom l,

Interatomic potential:

$$\text{Morse potential } \{v(\mathrm{r})\} = \mathrm{D_e}\left[\mathrm{e}^{-2\mathrm{a}(\mathrm{r}-\mathrm{r_e})} - 2\mathrm{e}^{-\mathrm{a}(\mathrm{r}-\mathrm{r_e})}\right] \tag{7}$$

We know that,

$$\frac{\partial v(\mathrm{r})}{\partial r} = f \tag{8}$$

f - Interatomic force

$$f = \sqrt{2k_eD_e}\left[\mathrm{e}^{-\mathrm{a}(\mathrm{r}-\mathrm{r_e})} - \mathrm{e}^{-2\mathrm{a}(\mathrm{r}-\mathrm{r_e})}\right] \tag{9}$$

$$\sigma = \frac{f * \mathrm{r}}{\Omega}$$

The above equations are simulated in the LAMMPS package followed by OVITO visualization software. The total number of neighbors were 391880, average number of neighbour per atom were 108.56 and expected wall time of 127 seconds with a single MPI thread produced a stacking fault energy of -29485.0566955018 mJ/m^2. The initial and final energy of atoms are -13496.4826291891 eV and -15471.2118355838 eV.

RESULTS AND DISCUSSION

The output file from the LAMMPS has been loaded to Ovito MD simulation tool to analyze actual stacking fault sequence and their gradients as they change their stacking faults based on the different lattice planes. Each lattice plane has its own lattice parameter and hence stacking fault results different in different planes. The initial loaded case of lattice input is as shown in the **Figure.3** below.

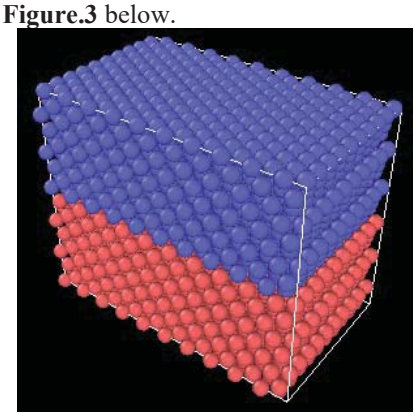

FIGURE 3. Arrangement of atoms with stacking fault sequence

It can be seen from the above **Figure.3**, the stacking has been initiated at centrosymmetric and thus symmetry of stacking is followed on top half and bottom half respectively. The below **Figure.4** displays the top view of the above specimen explaining the stacking fault sequences about centrosymmetric.

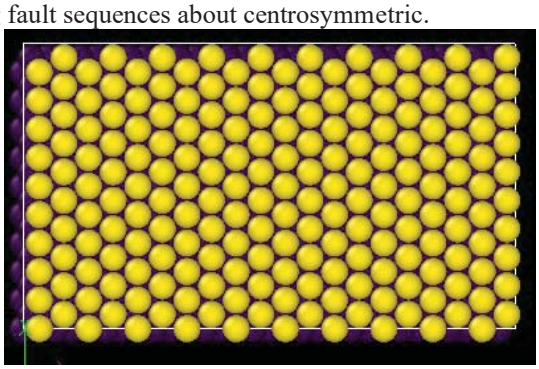

FIGURE 4. stacking fault sequences about Centrosymmetric

The variation of lattice sequence along the X direction can be seen in the **Figure.5** below. The figure also indicates the perfect alignment of the sequence of the stacking fault.

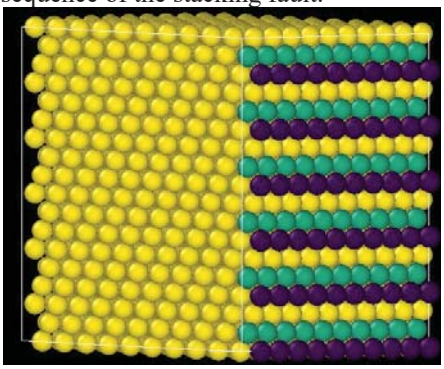

FIGURE 5. Stacking Fault in X direction

The variation of lattice sequence along the Y direction can be seen in the **Figure.6** below. The figure also indicates the perfect alignment of the sequence of the stacking fault but only one stacking fault sequence whereas in X direction we have two stacking fault sequences.

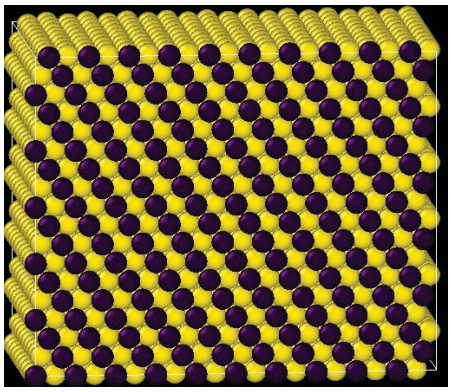

FIGURE 6. Stacking Fault in Y direction

The variation of lattice sequence along the Z direction can be seen in the **Figure.7** below. The figure also indicates the perfect alignment of the sequence of the stacking fault.

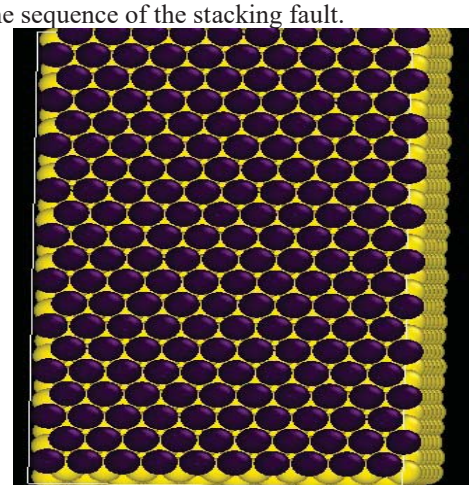

FIGURE 7. Stacking Fault in Z direction

The scattered plot in the **Figure.8** below indicates the variation of shear strains per atom to the stress per atom during uniaxial loading is performed to find out the stacking fault energy of the specimen. However, the curve shows the applied load about the symmetric axis reflects the internal shear stress initiated along the two half excluding the center of symmetry from where the stacking sequence has been traced/initiated.

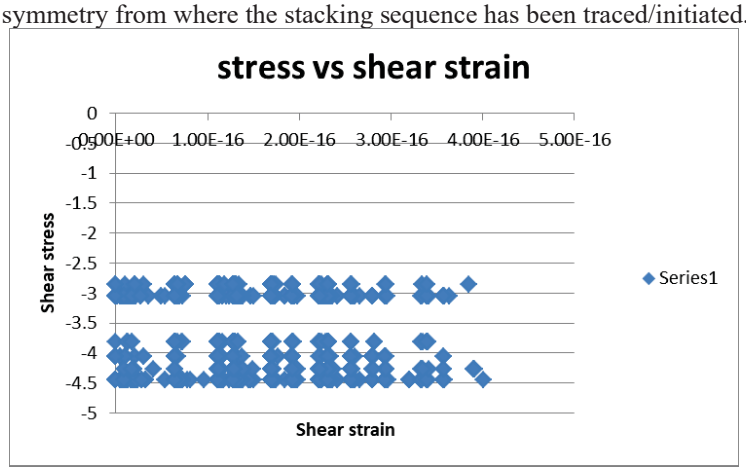

FIGURE 8. Shear stress vs shear strain

The input code being the same, the value of the lattice parameter upon the increase in the concentration of nickel in nitinol, one can clearly observe that there is decrement in the stacking fault energy, however the assumed

processes for the compositions of alloy is performed in the same environment. The stacking fault energies for different compositions in different planes are calculated and are discussed below.
The following key observations are noted during the simulation and found to be in good argument with analytical equations and available literature.

1. The stacking fault energy for each individual composition is plotted in the Figure.9 below. The stacking fault sequence has been very hierarchal as it involves stacking defect in different planes for different compositions. There is a rapid decrease in the stacking fault energy as the percentage of the nickel increases. Keeping the processing constant and increasing the Ni content allows settling the atoms without missing sequencing reducing the number of stacking defects. But as the stacking faults decreases, the total stacking fault energy of the system decreases and the range of pseudoelasticity also reduce.
2. One more important observation is stacking fault sequence is one of the crucial processing parameter which relates the shear stress and strain rate dependent factor in the Arrhenius equation to determine different parameters. It is also important in determining the range of transition temperature required for shape memory during austenite.
3. We require vast number of iterations to be performed for the solution to be converged, however in the present proposal we intended to used Embedded Atomistic model was used as a pair potential function and the large set of data was developed for the future research.

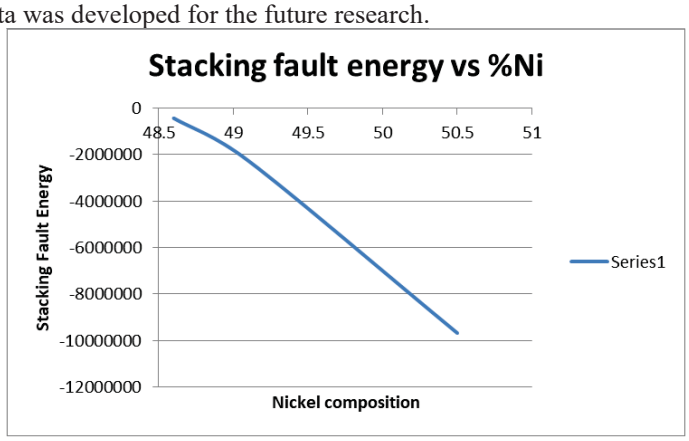

FIGURE 9. Stacking Fault Energy against percentage of Nickel in Nitinol

1. Among the constitutive models developed so far, there is no such viable model which involves composition in the model to realize the importance of shape memory in terms of stacking fault energy.
2. The present model perfumed its test for three different compositions 48.6, 49.1, 50.5 percent

CONCLUSION

1. The analytical model developed is tested in molecular dynamic simulations followed by the lammps editor to test the hypothesis generated by the stacking faults behaviors for different compositions in different planes.
2. It is found to be in agreement that from literature as the composition of the nickel increases, following the same process, for different compositions the stacking fault energy may decrease. As we can observe this from the above figure.
3. The data for atomistic strains, stretch tensor and strain tensors followed by deformation gradients have been analyzed so that these microstructural parameters can be related to solid specimen via Cauchy-Borne hypothesis.
4. From the literature a scope for involving different processing parameters influencing stacking fault energy and shape memory effect needs to be addressed which establishes a good relation between the type of processing and requisite shape memory. That means, we can develop specimen on the basis of our requirement and process accordingly.
5. These data sets enable readers and researchers to validate their data for various experiments. Alongside, a provision in the constitutive model developed has an advantage of integrating as many parameters as one can making the model more suitable to the research in the area among the scientific community.

ACKNOWLEDGMENTS

We sincerely thank the faculty of the Department of Aeronautical Engineering of MLR Institute of Technology for allowing us to carry out the research.

REFERENCES

1. T. E. Mitchell & P. B. Hirsch P. R. Thornton, "The dependence of cross-slip on stacking-fault energy in facecentred cubic metals and alloys ," The philosophical magazine, vol. 7, no. 80, pp. 1349-1369, June 1962.
2. J.-P. Chateau, S. Allain, S. Migot, O. Bouaziz A. Dumay, "Influence of addition elements on the stacking-fault energy and mechanical properties of an austenitic Fe–Mn–C steel," Elsevier, vol. 483-484, pp. 184-187, june 2008.
3. J.-P. Chateau, O. Bouaziz, S. Migot, N. Guelton S. Allain, "Correlations between the calculated stacking fault energy and the plasticity mechanisms in Fe–Mn–C alloys," Elsevier, vol. 387-389, pp. 158-162, december 2004.
4. J. P. HIRTH, "Thermodynamics of Stacking Faults," Springer, september 1970.
5. T Ericsson, "On the suzuki effect and spinodal decomposition," Elsevier, vol. 14, no. 9, pp. 1073-1084, september 1966.
6. T Ericsson, "On the suzuki effect and spinodal decomposition," Elsevier, vol. 14, no. 9, pp. 1073-1084, september 1966.
7. John E. Dorn, "THERMODYNAMICS OF STACKING FAULTS IN BINARY ALLOYS ," university of California, september 1962.
8. P.A Flinn, "Solute hardening of close-packed solid solutions," Elsevier, vol. 6, no. 10, pp. 631-635, october 1958.
9. G. Patzer, H. Alexander H. Gottschalk, "Stacking fault energy and ionicity of cubic III–V compounds," PSS, vol. 45, no. 1, pp. 207-217, january 1978.
10. C. B. CARTER and S. &I. HOLMES, "The stacking-fault energy of nickel ," PHILOSOPHICAL MAGAZINE, vol. 35 , no. 5, pp. 1161-1 172 , november 1976.
11. R.E Howard R deWit, "Relation of the stacking fault energy to segregation at stacking faults and to the occurrence of phase boundaries in f.c.c. binary alloys," Elsevier, vol. 13, no. 6, pp. 665-661, june 1965.

Design and fabrication of semi-automatic child retraction mechanism from bore well

Cite as: AIP Conference Proceedings **2446**, 180031 (2022); https://doi.org/10.1063/5.0108329
Published Online: 29 November 2022

K. Arunkumar, T. Kumaran, G. Sravanthi, et al.

Design and Fabrication of Semi-Automatic Child Retraction Mechanism from Bore Well

K. Arunkumar[1, a)], T. Kumaran[2,b)], G. Sravanthi[1, c)] and R. Vijayanandh[3, d)]

[1]*Department of Aeronautical Engineering, MLR Institute of Technology, Hyderabad, India*
[2] *Department of Aeronautical Engineering, Vel Tech Rangarajan Dr.Sagunthala R&D Institute of Science and Technology, Chennai, India*
[3]*Department of Aeronautical Engineering, Kumaraguru College of Technology, Coimbatore, Tamil Nadu, India*

Corresponding Author: a) arunssksamy@gmail.com
b)tkumaran@veltech.edu.in
c)grandhamalasravanthi@gmail.com
d) vijayanandh.raja@gmail.com

Abstract. The scenario of child falling into a bore well has become more and more common as the bore wells are dug in numerous counts in search of water all over our country. There is no proper method for retraction of the fallen child safely and quickly. Many mechanisms were proposed in the resent times but failing to make up to the task when required due to one or the other reason. The paper deals with the design of a semi-automatic mechanism for retraction of the fallen child from the bore well. Existing designs were studied and their limitations were found with which new design is developed in a way to overcome all hurdles faced. Dimensions are based on the ergonomic data collected for children of various age groups. The mechanism involves dual hold system with vacuum and robotic arm employed. Vacuum pressure is selected based on medical reports in such a way that it doesn't harm the child on lifting.
Keywords: Semi-Automatic Mechanism, Bore Well Rescue, Ergonomic data, Structural Simulation

INTRODUCTION

Forty five deaths of children have been reported in the country since September 2001. From that we have only nineteen with the proof of newspapers. Their deaths are caused due to uncovered dry bore wells. When the casing pipes costing hardly Rs.2000-3000/- are removed, even a six inch bore became wider and trap an unwary child [1]. A basic survey was carried out to study the physical parameters involved in these occurrences and to quantify the details so that they provide the guide line and requirements for a safe design. The survey covers some occurrences out of many that occurred. Some of the details are tabulated in table.1.

TABLE 1. Survey Details

S.No	Age	Depth	Place	Time	Status
1	1.5	47ft	Tamil Nadu	26	Dead
2	4	50ft	Haryana	48	Saved
3	5	70ft	Haryana	48	Dead
4	9	100ft	Rajasthan	72	Dead
5	6	160ft	Karnataka	50	Dead
6	4	26ft	Karnataka	50	Dead
7	3	60ft	Tamil Nadu	19	Dead
8	5	12ft	Tamil Nadu	15	Dead
9	5	20ft	Tamil Nadu	10	Dead
10	4	75ft	Karnataka	52	Dead

International Conference on Materials Research in Science and Engineering
AIP Conf. Proc. 2446, 180031-1–180031-7; https://doi.org/10.1063/5.0108329
Published by AIP Publishing. 978-0-7354-4208-5/$30.00

Nithin, Gowtham, Venkatachalam & S. Narayanan details the rescue of the sufferer from the bore well. A virtual model is built and the model is tested for structural integrity. A virtual simulation of the rescue is attempted to prove its effectiveness in the time of need. The robot is expected to be fabricated in such a way that the trained operator opens the stand and fixes over the bore well and give the input regarding depth and diameter of the bore well. The robot self-operating system starts with the given input into the well. The rescue robot is going to sense the position of the person or child and it is going to send a long assisting pipe so that child can mount on them. Then with the help of motors, the child or person mounted on the three legs of rescue robot is pulled upward safely in fastest possible time [4]. Manish Raj, P.Chakraborty and G.C.Nand detailed a technique for rescue task in bore well environment has been proposed. Here we are proposing a robotic system which will attach a harness to the child using pneumatic arms for picking up. A teleconferencing system will also be attached to the robot for communicating with the child. The design consists of two robotic arms and a harness. The arms are manipulated to fit the harness around the child and the child is retracted from the well. Additional systems such as oxygen supply and lighting are also included [5].

DESIGN AND ASSEMBLY

The conceptual design initiates with finalizing the method of extraction of the child, based on all the collected case study and literature we can finalize the extraction methodology. The procedure needs a appropriate equipment for the task, the equipment design starts with ergonomic study, then the data are used to design a mechanism which fits the child who is in need.

The word ergonomics comes from two Greek words: ERGO meaning work; NOMOS meaning laws. Ergonomics is a science focused on the study of human fit, and decreased fatigue and discomfort through product design. When Ergonomics applied to office furniture design requires that we take into consideration how the products we design fit the people that are using them. At work, at school, or at home, when products fit the user, the result can be more comfort, higher productivity, and less stress [2]. Here we apply the study to get the dimensional constrains for the children.

The data got from the study gives the minimum diameter at which the child will get struck in the bore well. The waist dimension will be the largest in a human body which will get struck at some point if the hole is conical [1]. The child will get disoriented at some position to get struck.

The ergonomic detail of a 2-3 year old child is considered as nominal value for design, but the minimum value is to be considered for the worst possible case and thus a 6 months old baby dimensions are considered as equipment maximum size constrains [3].

FIGURE 1. Equipment model

FIGURE 2. Retraction position

After detail study of these two models, first model was considered as a better option over the second as the volume is high and the needed stability can be achieved easily when compared to canard. The mechanism is designed in a modular design. The mechanism is divided into the following sub systems.

- Vacuum Cup System
- Holding Arm Assembly System
- Central Support Assembly System
- Electrical Control& Monitoring System
- Oxygen Feed System
- Rope Feed System.

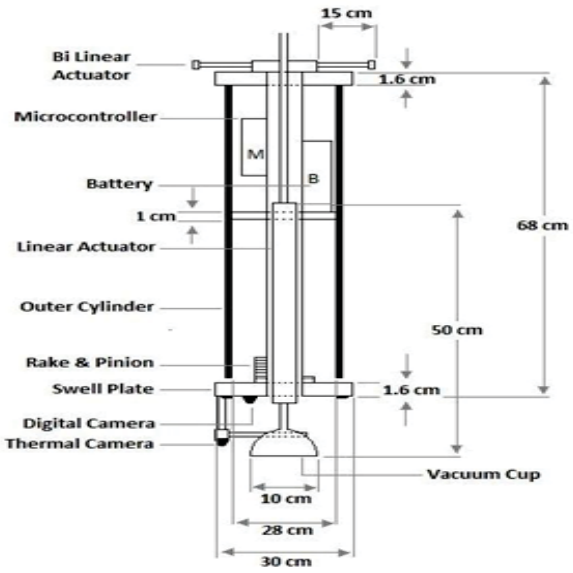

FIGURE 3. Detailed view

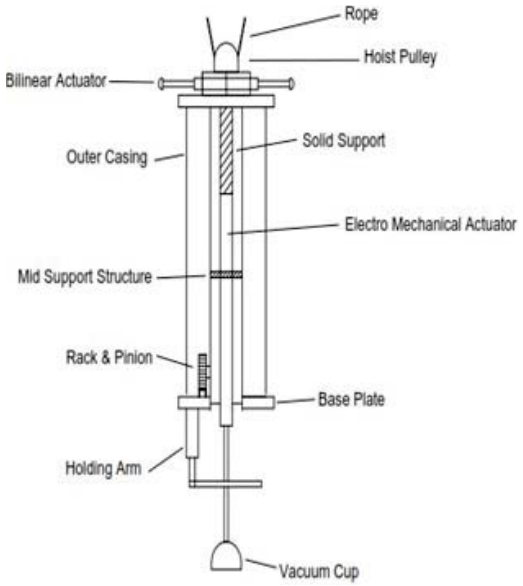

FIGURE 4. Front view

The modular design is adopted for the ease of maintenance and assembly. The cross section shown elaborates the modular arrangement of the mechanism. A solid mushroom cup is used in the vacuum system for holding the child as the particular component is used in the medical field for the very same purpose. It is used in pulling out the child in a vacuum assisted delivery [6]. The detailed specifications of the major components are tabulated as follows in Table 2

TABLE 2. List of Components

Sl. No	Components	Dimensions
1	Linear Actuator	Length 50cm, Weight 4kg
2	Cylinder	Diameter 28cm, Length 68 Cm
3	Rope	Diameter 25mm UIAA Standard
4	Pulley	Diameter 100mm
5	Bi Linear Actuator	Stroke 15cm
6	Rake And Pinion	Inner Diameter 15cm
7	Vacuum Cup	Solid Mushroom Cup
8	Swell Plate	Diameter 30cm, Thickness 2cm
9	Oxygen Supply Line	Diameter 1.27 cm
10	Flow Control Valve	Quick Return Valve
11	Microcontroller	8086
12	Battery	12V
13	Camera	Digital
14	Thermal Camera	
15	Vacuum Pump	
16	LED Light Source	
17	Mike And Speaker	

SKULL ANALYSIS

Failure Mode Effect Analysis was conducted to evaluate the failure probability and to identify the possible causes [7]. With the evaluation alternatives were added up in the system. Structural analysis was also done on the head of a 2 year old child model generated in CATIA, to evaluate the risk of applying suction pressure to lift the child [8, 9]. The vacuum pressure was applied on the head and the maximum stress, strain and deformation patterns were studied.

The boundary conditions for the analysis on skull are as follows,

- Skin thickness: 1cm
- Vacuum pressure applied: 0.01 bar
- Simulated weight: 15 kg
- Density: 1000 kg/m3
- Young's Modulus: 16.7 MPa
- Poisson's Ratio: 0.42

The structural details used for the modeling of the skin and skull structures are shown in the tabulation above. The modeling of the skull is carried out using CATIA and the analysis is carried out using ANSYS. The bottom the skull is fixed to simulate the neck joint [10,11]. It is evident from the stress and deformation pattern that the maximum deformation is less and not harmful for the child. It won't cause any permanent injuries to the child on any sort. Thus the vacuum system proves to be non-hazardous of any sort [12].

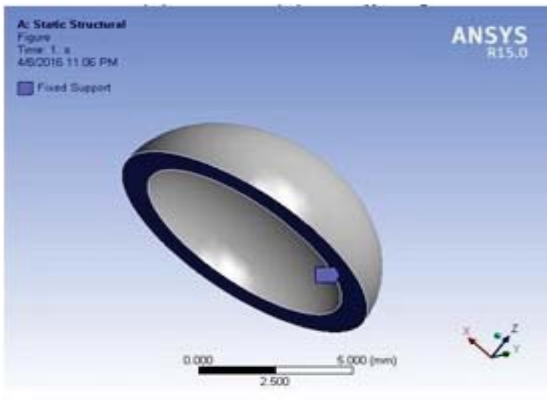

FIGURE 5. Fixed Point

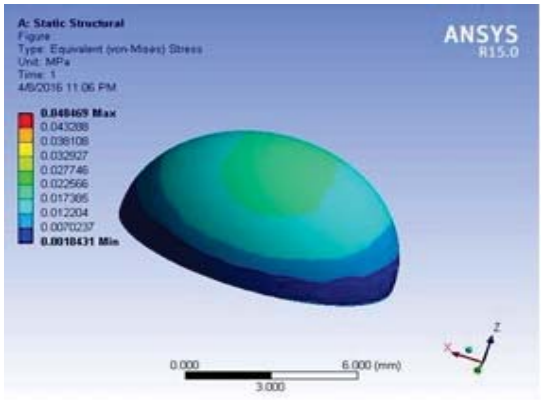

FIGURE 6. Von-Misses Stress Pattern

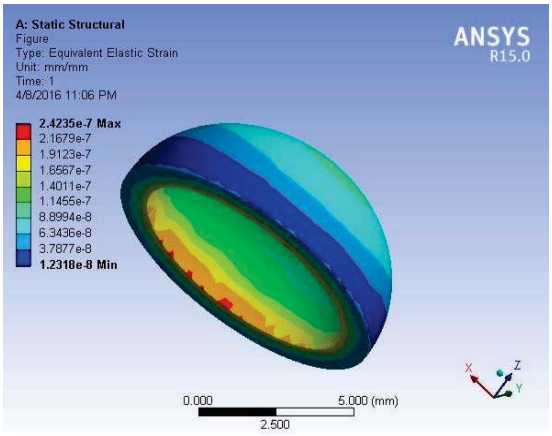

FIGURE 7. Elastic Strain Pattern

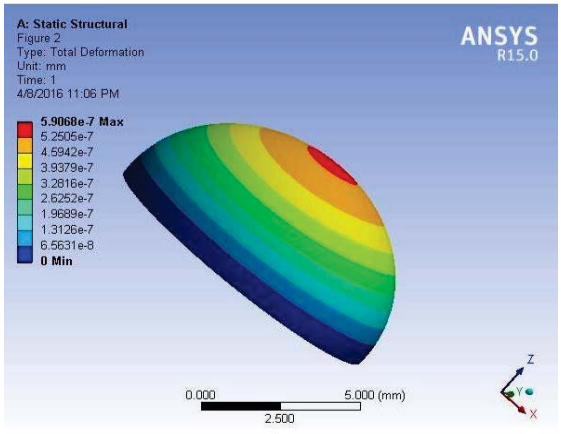

FIGURE 8. Total Deformation Pattern

FABRICATION AND TESTING

The fabricated setup is shown as below. The major functionalities of the design are modeled out for evaluation under simulated environment.

FIGURE 9. Experimental Set up

The setup fabricated was a functional prototype; it is developed to evaluate the major systems of the mechanisms in real time. The setup was used to carry out some basic functionality tests such as vacuum system functioning, mechanical arm setup and hold on the child. Basic dimensions are given in table 3.

TABLE 3. Specification experimental setup

S.NO	Description	Specification
1	Length	68 cm
2	Diameter of Protective case	28 cm
3	Diameter of Base plate	30 cm
4	Vacuum pump stroke	40 cm
5	Vacuum system actuator travel	100cm/min
6	Vacuum system actuator Load	20 kg
7	Bi linear actuator stroke	20 cm
8	Total weight	10kg
9	Base plate revolution	4 RPM
10	Holding arm max weight	25 kg

TEST UNDER SIMULATED ENVIRONMENT

The designed setup is tested under simulated environment with the following conditions.

- Dummy weight : 10kg
- Depth : 80ft
- Bore well diameter : 60cm

The total time taken for the retraction procedure with the mechanism developed is within 2 hours. The average time it would take for the extraction procedure is around 10 hours.

A comparative chart for the processes involved with time as shown.

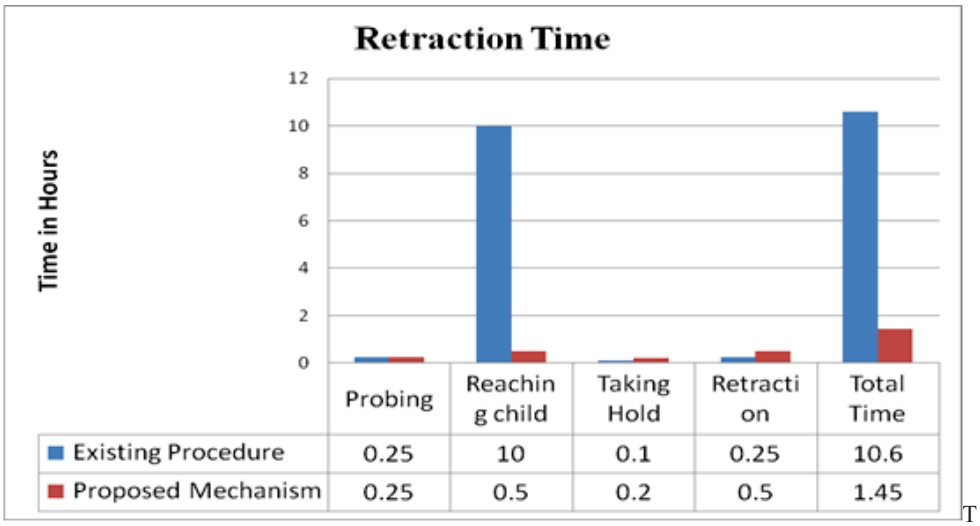

T

FIGURE 10. Retraction time plot

RESULTS AND DISCUSSION

A static force analysis was carried out sing ANSYS. This was mandatory to prove the safety of the vacuum cup system attached. The vacuum cup is one of the highlights of the mechanism but at the same time it was risky as it could inflict permanent physical damage to the child.

If excessive suction is to be employed, it can cause a pull out of skin from the skull. The static force analysis was done considering a lift of child of 10kg. An appropriate pressure of 0.2 bar was applied as the load with bottom of the skull is fixed, resembling the neck joint.

The deformation in excess of 0.2cm will prove fatal for the child. The density of the skin used in the analysis is 1000kg/m3, young's modulus employed will be16.7 MPa and the Poisson's ratio as 0.42. The deformation achieved by the vacuum suction cup was 0.02mm which is very much safe. Thus proving to be non harmful.

An experimental validation involved the setup to be tested under simulated conditions. The testing was carried out with the help of Fire and rescue team, Vaniyambadi Vellore district. A dummy weight of 10Kg was used and the simulated depth was safe. A 12 inch bore well was the simulated fall zone. The overall retraction was divided into three steps for the monitoring - reaching the child, taking hold and retraction.

Our extraction process was as follows,

- A probe has been sent in to the bore well.
- An air bag was inflated over the child to stop debris falling.
- The depth of the child struck was detected.
- The setup was inserted into the bore well.
- A vacuum was generated to remove the debris.
- The air bag was deflated.
- The setup was supported by the arms which extend to the wall.
- The vacuum cup was extended to hold the child's head.
- The child was pulled up.
- At a few centimeters the child was supported with mechanical clamping.
- Vacuum pressure has been reduced.
- The child has been pulled out safely.

By the data collected from the Fire rescue team, a total time of about 11 hours would have been spent if the existing retraction procedure is to be employed. The mechanism on use proved to be quick.

Step Time taken

- Reaching the child : 0.75 hours
- Taking child : 0.20 hours
- Retraction : 0.60 hours

A total time of two hours was taken for safe retraction. It proves to be 80% reduction in time taken for the rescue.

CONCLUSION

The Semi-Automatic Mechanism developed for child retraction is done based on the study involving the requirements, existing complications and time saving. The design thus proposed is also fabricated as prototype and tested under simulated environment is found to perform better than the existing designs and extraction methodology. It not only saved time on retraction it also had an active child health monitoring system that keeps us aware of the child state and the time constrain for the rescue. The design is done so as to probe through small bore well which are otherwise difficult to reach.

REFERENCES

1. T. Serre, L. Lalys And S. Lecoz, Anthropometric data of the 3 and 6 year-old child regarding the position of the safety belt
2. Rani Lueder, Valerie J. Berg Rice, Ergonomics for Children Designing products and places for toddlers to teens
3. Bor-Shong Liu and Ching-Wen Lien, Incorporating Anthropometry into Design of Products
4. G. Nithin, G. Gowtham, G. Venkatachalam, S. Narayanan, Design And Simulation Of Bore Well Rescue Robot
5. Manish Raj, P.Chakraborty and G.C.Nandi, Rescue Robotics in Bore well Environment
6. Michael D. Gilchrist, ―Modelling and Accident Reconstruction of Head Impact Injuries‖, Key Engineering Materials Vols. 245-246 (2003) pp. 417429, http://www.scientific.net
7. J.S. Ruan, T. Khalil, A.I. King, Dynamic response of the human head to impact by three-dimensional finite element analysis, J Biomech Eng 116 (1) (1994)4450
8. Zhang, L., Hardy, W., Omori, K., Yang, K.H.,King, A.I. 2001. ―Recent advances in brain injury research: a new model and new experimental data, Bioengineering Center, Wayne State University
9. A.M. Nahum, R. Smith, C.C. Ward, ―Intracranial pressure dynamics during head impact‖, Proceedings of the 21st Stapp Car Crash Conference, Vol.SAE Paper No. 770922, 1977.
10. Voo K, Kumaresan S, Printar FA et al. Finite element models of the human head J. Med Biol Eng Comput, 1996, 34(5): 375-381.
11. K. Sreelakshmi, N Madhavi, M Satyanarayana Gupta," Analysis of Interlaminar Stresses in a Composite Material with A Circular Hole by Using Finite Element Method", IJCIET, Volume 8, May2017.
12. N Madhavi, B Niharika M Satyanarayana Gupta "Evaluation of ply orientation on failure of Kevlar Epoxy149" IJCIET, Volume 8, May2017.

Numerical investigation of a finite wing section with a bleed hole allowing boundary layer suction

Cite as: AIP Conference Proceedings **2446**, 180054 (2022); https://doi.org/10.1063/5.0108446
Published Online: 29 November 2022

Nirmith Kumar Mishra, A. Sai Kumar, B. Shashank, et al.

Numerical Investigation of a Finite Wing Section with a Bleed Hole Allowing Boundary Layer Suction

Nirmith Kumar Mishra[1,a)], A. Sai Kumar[1, b)], B. Shashank[1,c)], K. Sai Vamsi[1,d)], Suhas Annem[1,e)], B. Dileshwar Rao[1,f)] and K. Sundararaj[2,g)]

[1]*Department of Aeronautical Engineering, MLR Institute of Technology, Hyderabad, India*
[2]*Department of Aeronautical Engineering, Kumaraguru College of Technology, Coimbatore, India*

Corresponding Author: [a)]nirmithmishra@gmail.com
[b)] ask.mraj@gmail.com
[c)] shashankb2011@gmail.com
[d)]saivamc500@gmail.com
[e)]annemsuhas@gmail.com
[f)]dileshwarrao0209@gmail.com
[g)]sundararaj.k.aeu@kct.ac.in

Abstract. The aim of the study is to optimize a wing section which can have an ability to operate at higher aerodynamic efficiency and function as a high lifting device. The computational study is carried over a finite wing segment in an effort to enhance the aerodynamic performance by controlling the boundary layer flow to minimize the separation region and delaying the boundary layer flow separation. A boundary layer suction flow control mechanism is used to allow the free stream flow to pass through the duct from leading edge to arbitrary point on the surface at various points respectively. This study is carried out on the wing section with a constant inlet duct area, varying areas and locations of duct outlets. The arbitrary points of exit are considered at 0.70c, 0.50c, 0.25c at 0o, 5o ,10o angles of attack respectively. These points are selected by studying the transition point on the airfoil where the laminar boundary layer starts to transform into turbulent. These ducts are shaped as converging, diverging and constant area ducts to study the varying momentum transfer into the boundary layer and their effects on aerodynamic efficiency. The study is carried in Ansys tool and analyzed.

Keywords: Boundary layer suction, flow separation , laminar bubbles.

INTRODUCTION

Flow control over airfoils is directed at increasing the lift and decreasing the drag produced by airfoil. This is usually achieved by manipulating the boundary and shear flows in order to minimize the separation region. The low-energy limit layer stream super surface of the airfoil is the guilty party, in blend with the unfriendly pressing factor inclination which causes stream division and in this way slows down. Via consequently adding energy to the limit layer by means of little openings or spaces on the upper surface of the airfoil, stream division can be deferred. This can prompt considerable expansions in CL max. Dynamic limit layer attractions has not been utilized at this point on standard assembling of planes. It stays in the class of a convoluted innovation thing.

Boundary Layer Association with Drag

As the fluid streams over the material, the particles closest to the surface tie to it. As atoms simply over the surface crash into particles that hold fast to the surface, they delayed down. These atoms, thus, cause the stream

International Conference on Materials Research in Science and Engineering
AIP Conf. Proc. 2446, 180054-1–180054-7; https://doi.org/10.1063/5.0108446
Published by AIP Publishing. 978-0-7354-4208-5/$30.00

simply above them to back off. The farther one is away from the article's surface, the less impacts it causes. The limit layer is a slight layer of liquid at the surface where the speed differs from zero at the surface to the free stream esteem away from the surface.

Contingent upon the Reynolds number, limit layers might be either laminar (layered) or violent (confused). The limit layer is laminar at lower Reynolds numbers, and the streamwise speed differs. Consistently as one moves from the divider. The limit layer gets fierce at higher Reynolds numbers, and the stream-wise speed is characterized by flimsy (changing after some time) twirling streams inside the limit layer. The outward stream reacts to the limit layer's edge similarly it never really article's actual surface. As an outcome, the limit layer gives any item an effective shape that fluctuates somewhat from its actual shape. To add to the disarray, the limit layer can take off or "independent" from the body, bringing about a successful shape that varies essentially from the genuine shape. This happens in light of the fact that the limit stream has low energy (as opposed to the free stream) and is hence more handily determined by changes in pressure. At high approaches, wing slow down is brought about by stream partition. The lift coefficient contains the impacts of the limit layer on lift, while the drag coefficient contains the impacts of the limit layer on drag.

Consider an airfoil at different approaches to perceive how contact drag (otherwise called gooey drag) and pressing factor drag (otherwise called shape drag or profile drag) communicate. The limit layers on the top and base surfaces experience just slight pressing factor slopes at little approaches, and they stay connected for practically the whole harmony length. The drag is overwhelmed by gooey contact inside the limit layers, and the wake is little. Regardless, The pressing factor inclinations on the airfoil ascend in extent as the approach increments. The unfavorable pressing factor slope on the top back bit of the airfoil, specifically, can turn out to be sufficiently high to make an isolated stream. The size of the wake will grow as a result of the separation, as will the pressure losses in the wake due to eddy formation. As a consequence, pressure drag increases. When a significant portion of the flow over the top surface of the airfoil is isolated at a higher angle of attack, the airfoil is said to be stalled. The pressure drag is much greater than the viscous drag at this stage [1-16].

Methods to delay Flow Separation

Much exertion and examination has gone into the plan of streamlined surface forms and added highlights that defer stream division and keep the stream appended as far as might be feasible. They incorporate. -

- Creating a more streamlined body shape.
- Using surface roughness to transition the limit layer from laminar to fierce.
- Vacuuming up the reduced stream.
- Using a high-velocity fluid to inject into the boundary layer
- Having spaces near the main edge.
- Flow control in a confined space.
- Installing a revolving cylinder close to the leading edge.
- Adding the correct amount of swirl to the incoming flow to energize it

METHODOLOGY

Airfoil Study

Before attempting a boundary layer control, boundary characteristics of low Reynolds number airfoil NACA 2412 are investigated. The airfoil is analyzed from 0o to 15o. The non-dimensional numbers (Cl, Cd, Cm, CP) and transition locations on upper and lower surfaces (Top Xtr, Bot Xtr) of airfoil is analyzed. The data is tabulated from the analysis performed on NACA 2412 airfoil with chord length 100mm, velocity 30m/s and Reynolds number 211,164.

TABLE 1. Airfoil Plot Data

Alpha	Cl	Cd	Cm	Top-Xtr	Bot-Xtr	XCp
0	0.2723	0.00964	-0.0585	0.8272	0.9744	0.4636
0.5	0.3729	0.00959	-0.0673	0.7939	0.9987	0.4288
1	0.4228	0.00956	-0.0662	0.7582	1	0.4041
1.5	0.4695	0.00966	-0.0643	0.7212	1	0.3841
2	0.5168	0.00986	-0.0624	0.6866	1	0.3675
2.5	0.5639	0.01012	-0.0606	0.6521	1	0.3536
3	0.6113	0.01043	-0.0587	0.6194	1	0.3418
3.5	0.6587	0.0108	-0.0568	0.5877	1	0.3316
4	0.7058	0.01119	-0.0549	0.5555	1	0.3226
4.5	0.7527	0.01158	-0.053	0.5214	1	0.3148
5	0.7995	0.01203	-0.0511	0.4865	1	0.3077
5.5	0.8459	0.01249	-0.0491	0.4483	1	0.3014
6	0.8915	0.01301	-0.0471	0.4062	1	0.2957
6.5	0.9356	0.01365	-0.045	0.3564	1	0.2903
7	0.9767	0.01455	-0.0425	0.2963	1	0.2852
7.5	1.014	0.01583	-0.0396	0.2263	1	0.2802
8	1.0473	0.01751	-0.0364	0.1597	1	0.2752
8.5	1.0775	0.01945	-0.0327	0.1177	1	0.2703
9	1.1066	0.02136	-0.029	0.0939	1	0.2654
9.5	1.1332	0.02329	-0.0249	0.0794	1	0.2606
10	1.1554	0.02539	-0.0204	0.0698	1	0.2555
10.5	1.179	0.02757	-0.0164	0.0622	1	0.2511
11	1.2032	0.03005	-0.013	0.0566	1	0.2472
11.5	1.2292	0.03266	-0.0101	0.0517	1	0.2439
12	1.2521	0.03526	-0.0071	0.0477	1	0.2406
12.5	1.2781	0.03845	-0.0046	0.0446	1	0.2377
13	1.2987	0.04159	-0.0021	0.0418	1	0.2349
13.5	1.313	0.04562	0.0004	0.0395	1	0.2322
14	1.3201	0.05001	0.0027	0.0376	1	0.2295
14.5	1.3325	0.05442	0.0043	0.0362	1	0.2275
15	1.3233	0.06115	0.0056	0.0353	1	0.2255

Design of Boundary Layer Suction Mechanism

NACA 2412 is selected with a chord length of 100mm, span of 30mm.The airfoil is modelled without the bleed holes and with bleed holes having suction positions at 25%c, 50%c and 75%c with a suction angle 90o (perpendicular to the local surface) from the leading edge as suction control parameters. These suction points are chosen soon after the transition point. The contours of converging, diverging a uniform duct sections are chosen for the study.

Uniform duct- The inlet diameter of 3.5 mm (3.5% of chord) and outlet diameter of 3.5mm (3.5% of chord) is selected. Converging duct- The inlet diameter of 3.5 mm (3.5% of chord) and outlet diameter of 2mm (2% of chord) is selected. Diverging duct- The inlet diameter of 3.5 mm (3.5% of chord) and outlet diameter of 6mm (6% of chord) is selected.

All the wing sections with following parameters are modelled at angles of attack 0o, 5o,10o with the suction locations at 0.75%C, 0.50%C, 0.25%C respectively.

Computational Study

Spalart-Allamars turbulence model, A one condition model that tackles a demonstrated vehicle condition for kinematic whirlpool tempestuous thickness is utilized for the computational investigation. Ansys familiar is utilized for playing out the investigation. The model is considered viable for the low Reynolds number streams.

Rectangular domain dimensions 1200mm*30mm*1000mm are chosen and discretization is performed using a Curvature mesh function with a minimum edge length of 3e-5 m and max edge length of 1e-3m. Speed channel limit conditions and pressing factor outlet limit conditions are received for the outer limit of the computational space. Non-slip strong divider condition is utilized for the airfoil surface and mass stream rate condition is embraced for the attractions opening. The tempestuous force is 5% and the violent thickness proportion is 10 on the bay., are the least dominant factors.

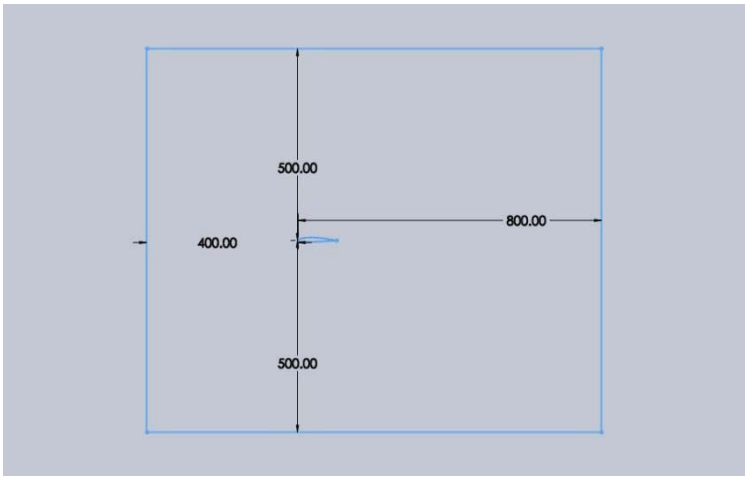

FIGURE 1. 2D domain dimensions involving finite wing section

RESULTS

Changes In Relative Pressures

The computational pressure contours are illustrated showing drastic changes in the reduction of pressures before the quarter chord on the upper surface of airfoil. Changes in relative pressures and generation of favorable pressure gradients are evident in the contours. Changes in relative minimum pressures are tabulated as follows

TABLE 2. Changes in relative pressure

Angle of attack	No duct	Converging duct	Uniform duct	Diverging duct
0	2.121 e+002	- 2.32 e+002	-2.19 e+002	-1.56 e +002
5	-1.291 e+002	-7.296 e+002	-6.043 e+002	-4.302 e+002
10	-9.468 e+002	-2.404 e+003	-2.465 e+003	-2.278 e+003

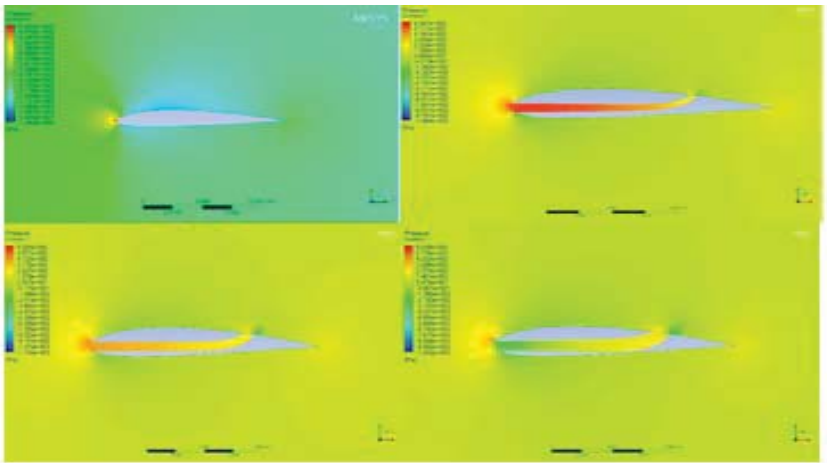

FIGURE 2. Pressure contours of NACA 2412 without bleed hole, with bleed hole exit diameters 2mm, 3.5mm, 6mm and inlet diameter 3.5mm at angle of attack 0.

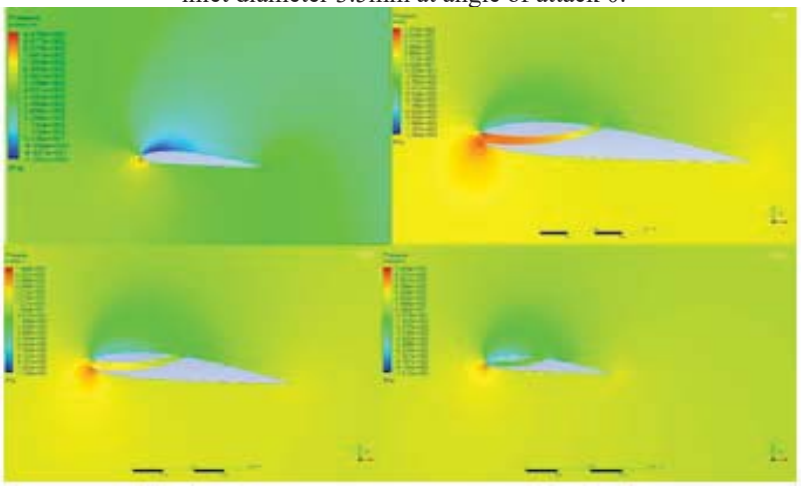

FIGURE 3. Pressure contours of NACA 2412 without bleed hole, with bleed hole exit diameters 2mm, 3.5mm, 6mm and inlet diameter 3.5mm at angle of attack 5

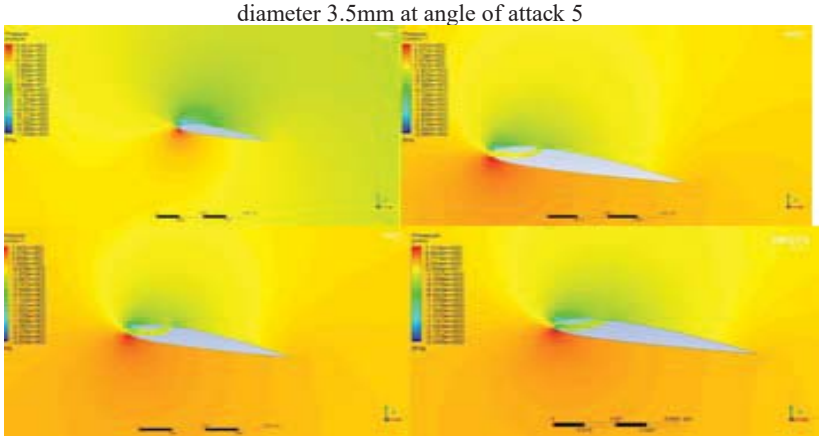

FIGURE 4. Pressure contours of NACA 2412 without bleed hole, with bleed hole exit diameters 2mm, 3.5mm, 6mm and inlet diameter 3.5mm at angle of attack 10.

The flow is allowed through the leading edge and is induced at an arbitrary point. This process reduced the stagnation pressure in front of the airfoil thereby reducing the differential pressure. Moreover, adding the energy

reduced the pressure and created a favorable pressure gradient which has increased the lift along with decreasing the drag. Unlike turbulators and slats, boundary layer suction does not contribute to drag while increasing the lift.

CONCLUSION

The computational study showed promising results increasing the lift over the airfoil section and reducing the drag. The force reports are tabulated from the analysis.

TABLE 3. Force report for angle of attack 0

ANGLE OF ATTACK – 0		
conditions	**Lift**	**Drag**
No bleed hole	0.228N	0.058N
Bleed hole with exit diameter- 2mm	0.266N	0.046N
Bleed hole with exit diameter- 3.5mm	0.261N	0.0473N
Bleed hole with exit diameter- 6mm	0.253N	0.048N

The tabulated results for an angle of attack of 0o showed an increase in lift of 14.3%, 12.7%,.10% for converging, uniform and diverging ducts respectively. The reduction in drag is 20.33%, 18.83%, 17.1% for converging, uniform and diverging ducts respectively.

TABLE 4. Force report for angle of attack 5

ANGLE OF ATTACK – 5		
conditions	**Lift**	**Drag**
No bleed hole	0.8829N	0.0810N
Bleed hole with exit diameter- 2mm	1.9162N	0.0588N
Bleed hole with exit diameter- 3.5mm	1.1828N	0.0591N
Bleed hole with exit diameter- 6mm	1.166N	0.0635 N

The tabulated results for an angle of attack of 5o showed an increase in lift of 53.92%, 25.35% ,24.31% for converging, uniform and diverging ducts respectively. The reduction in drag is 27.4%, 27.03%, 21.5% for converging, uniform and diverging ducts respectively.

TABLE 5. Force report for angle of attack 10

ANGLE OF ATTACK – 10		
Conditions	**Lift**	**Drag**
No bleed hole	1.7377N	0.1389N
Bleed hole with exit diameter- 2mm	1.9472N	0.1051N
Bleed hole with exit diameter- 3.5mm	1.93046N	0.107182N
Bleed hole with exit diameter- 6mm	1.9163N	0.1081N

The tabulated results for an angle of attack of 10o showed an increase in lift of 10.76%, 9.98% ,9.32% for converging, uniform and diverging ducts respectively. The reduction in drag is 24.33%, 22.83%, 21.1% for converging, uniform and diverging ducts respectively. There has been an extensive reduction in the drag with the increase in the lift improving the aerodynamic performance.

The analysis provided vital data to elucidate the improved aerodynamic performances of the wing sections.

- The convergent sections provide the best efficiencies since the flow is accelerated at subsonic speeds in the convergent section. This improved the velocity added and increased momentum in the boundary layer.
- It produced a low-pressure at the arbitrary point chosen resulting in a favorable pressure gradient. This addition of energy resulted in the delay of the flow separation.
- Reduction of pressure drag is witnessed due to reduction of pressure difference between the stagnation pressure at leading edge and the empty wake region.

FUTURE SCOPE

In the current work, the bleed hole is only limited to subsonic low Reynolds number speeds which can be further worked on. This concept of bleed holes with varying duct areas can be further applied to supersonic speeds with a proper design of the C-D duct. This can be applied into the turbine and compressor blades however pressure losses must be considered. This work can be applied to low-speed aircrafts to add energy to the boundary layer and delay

the flow separation at subsonic speeds. It can pave the way for longer ranges and longer endurance fixed wing aircrafts

REFERENCES

1. Eppakayala Naresh, Pinnamaneni Dileep Kumar, Anil Kumar.N, B. Nagaraj goud, "Drag reduction over A circular cylinder", *International Journal of Civil Engineering and Technology* (IJCIET) ISSN Print: 0976-6308 and ISSN Online: 0976-6316, Volume 8, Issue 8, August 2017, pp. 1334–1345.
2. Suddala Abhishek , B.Nagaraj Goud, "Compressor Design optimization for a High speed Jetengine", *IOP Conference Series: Materials Science and Engineering*, 2018, 455(1), 012036.
3. Sreelakshmi, K., Niharika, B., " Design and analysis of mini-UAV", *International Journal of Mechanical and Production Engineering Research and Development* (IJMPERD) ISSN (P): 2249-6890; ISSN (E): 2249-8001 Vol. 8, Issue 1, Feb 2018, 1-8, 2018.
4. Genc, M.S., Kaynak U , 2009. "Control of laminar separation bubble over a NACA 2415 aerofoil at low Transitional flow using blowing/suction", Proceedings of the 13th International Conference on Aerospace Sciences & Aviation Technology, Military Technical College, Cairo, Egypt.
5. Huang L, Huang, P.G., LeBeau, R. P., 2004. "Numerical study of blowing and suction control mechanism on NACA0012 Airfoil", *AIAA Journal* 41 (1), 1-10.
6. Jalil, J.M., Yousif, A.H., Mahmood, Y.A., 2010. "Control of separation for NACA 2412 airfoil at different angles of attack using air blowing", Engineering and Technology Journal 28 (16), 5138-5150.
7. McLachlan, B. G., 1989. "Study of a circulation control airfoil with leading/trailing edge blowing", *Journal of Aircraft* 26 (9), 817-819.
8. McCullough, G.B., Gault, D.E., 1948. "An experimental investigation of an NACA 632-012 airfoil section with leading-edge suction slots", *NACA Technical* Note No. I683.
9. Menter, F. R., 1994. "Two-equation eddy viscosity turbulence models for engineering applications", *AIAA Journal* 32 (8), 1598- 1605.
10. Tuck, A., Soria, J., 2004. "Active flow control over a NACA 0015 airfoil using a ZNMF jet", Proceedings of the 15th *Australasian Fluid Mechanics Conference*, Sydney, Australia.
11. Zha, G.C., Careoll, B.F., Paxton, C. Conley, C.A., Wells, A., 2005. "High performance airfoil using co-flow jet flow control", Proceedings of 43rd *AIAA Aerospace Sciences Meeting and Exhibit Conference*, Reno, Nevada, AIAA Paper No. 2005-1260.
12. D., Moin, P., 2006. "Large-eddy simulation of flow separation over an airfoil with synthetic jet control", *Center for Turbulence Research, Annual Research* Briefs, 337-346.
13. Walters, D.K., Cokljat, D., 2008. "A three equation eddy-viscosity model for Reynolds- averaged Navier-Stokes simulations of transitional flows", *ASME Journal of Fluids Engineering* 130 (12), 1-14.
14. John D Anderson, "Introduction to flight", Fifth Edition, *Tata Mc Graw* Hill, 2007.
15. John D Anderson, "Aircraft Performance and design", Fifth Edition, *Tata Mc Graw Hill.*
16. David F Anderson, "Understanding flight", Second Edition. *Tata Mc Graw Hill.*

Buckling analysis of thin walled C-section

Cite as: AIP Conference Proceedings **2446**, 180032 (2022); https://doi.org/10.1063/5.0110214
Published Online: 29 November 2022

N. Madhavi, D. Mahesh, G. Sravanthil, et al.

Buckling Analysis of Thin Walled C-Section

N. Madhavi[1,a)], D. Mahesh[1], G. Sravanthil[1] and M. Selvambikai[2]

[1]*Department of Aeronautical Engineering, MLR Institute of Technology, Hyderabad, India.*
[2]*Department of Physics, Kumaraguru College of Technology, Tamil Nadu, India.*

Corresponding author email: [a)]madhunagireddy@gmail.com

Abstract. Buckling analysis is done on a thin walled C-sectional beam which is unsymmetrical. Different loads are applied on this section to predict the natural frequencies at a critical loading conditions and also for the different thickness of the beam the maximum critical moment is also calculated and plotted. A constant load is applied on the beam and the impact of the load in the frequencies are also calculated. A general theory of coupling flexure and straight beam torsion is considered to calculate the axial load in different boundary conditions.

Keywords: Critical Moment, Axial Load, Vibrations

INTRODUCTION

The Blended wing Body (BWB) is basically a flying wing with a delta-shaped wing/fuselage in the center, large enough for a passenger cabin [1]. BWB is a hybrid of flying-wing aircraft and the conventional aircraft where the body is designed to have a shape of an airfoil and carefully streamlined with the wing to have a desired plan form [2].The advantages of using a Blended wing are reduced wetted area and improved structural efficiency. The major problem with this configuration is pitch stability.

The objective of present work is to design and fabrication of a Blended Wing Body aircraft which can carry maximum payload with highest payload fraction. The design shall be an initial approach to develop a commercial Blended wing aircraft in future. Hence, to replicate the passengers,5 footballs are considered as payload. Along with these footballs a payload which is the cargo that has to be carried by the aircraft is also considered. The aircraft must fly with full control for the specified range with endurance. The detailed requirements are given in further sections [3-19].

BUCKLING OF THIN WALLED C-SECTION BEAM

When a beam undergoes axial load, the sudden change in shape of the structure component is called buckling. A tensile loading is acting on the column then the column tends to buckle. The continuous load is applied to determine the Eigen values.

FORMULA

Thin walled structures range from aircraft, bridges and warehouses to a large and growing proportion of engineering works. A thin wall C sectional beam is very useful type of beam. The thin walled beams consist of thin panels linked to each other to create parts of a beam (structure) that are closed or open. The cross-section of thin walled c sectional beams consists of thin panels. Which are connected to each other and created closed and open cross-sections. The bending stiffens of the beams are given by bending stiffness is less per unit cross-sectional area.

International Conference on Materials Research in Science and Engineering
AIP Conf. Proc. 2446, 180032-1–180032-6; https://doi.org/10.1063/5.0110214
Published by AIP Publishing. 978-0-7354-4208-5/$30.00

The bending stiffness is less than that of solid cross-sections. Finally, we can archived minimum weight for the rigid beams

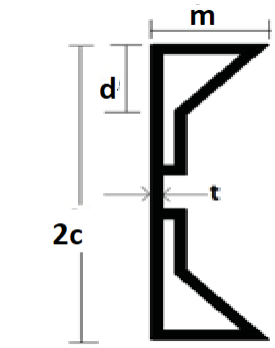

FIGURE 1. Thin wall C-section

Consider the C-section as shown in Figure. The C-section is symmetric about the x axis i.e; I_{xy}=0 and the moment of area I_{xx} is given by

$$I_{xx} = 2\left[\frac{(m + t/2)t^3}{12} + \left(m + \frac{t}{2}\right)th^2\right] + t\frac{[2(h - t/2)]^3}{12}$$

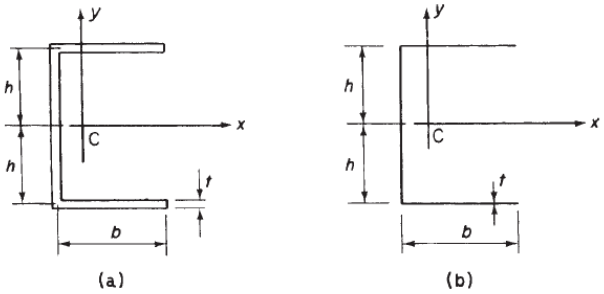

FIGURE 2. Design process (a) Thin-walled C-section (b) approximate diagrammatic representation of C-section.

Expanding the equation, we get

$$I_{xx} = 2\left[\frac{(m + t/2)t^3}{12} + \left(m + \frac{t}{2}\right)th^2\right] + \frac{t}{12}\left[(2)^3\left(h^3 - 3h^2\frac{t}{2} + 3h\frac{t^2}{4} - \frac{t^3}{8}\right)\right]$$

Finally the equation reduces to t^2 and upwards are ignored, to

$$I_{xx} = 2mth^2 + t\frac{(2h)^3}{12}$$

Area of the C-section about C_y is obtained in the same procedure. Therefore, the properties are calculated for the C section beam is represented by straight line.

DESIGN SPECIFICATIONS

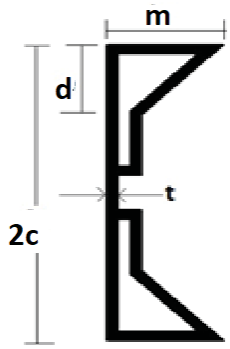

FIGURE 3. Design specifications of Thin walled C-section

TABLE 1. λ and Mcr values for different thicknesses at Young's modulus =10e-3

S.NO	λ = l/h	T_1= 0.6	T_2=1.10	T_3=2	T_4= 3.14
1	7.5	502.68	2320.4	4730.1	8164.5
2	10	502.29	1631.3	3359	5858.3
3	12.5	502.07	1281.3	2632	4610.3
4	15	498.52	1065.1	2176.6	3820.6
5	17.5	434.14	915.83	1861.9	3271.9
6	20	386.17	805.1	1629.9	2866.3

RESULTS

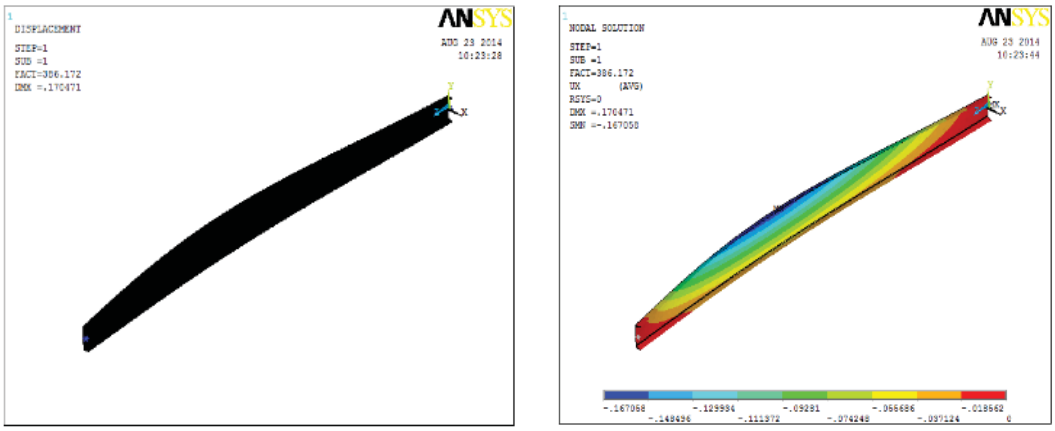

FIGURE 4. Youngs modules =10e-3, thickness =0.6

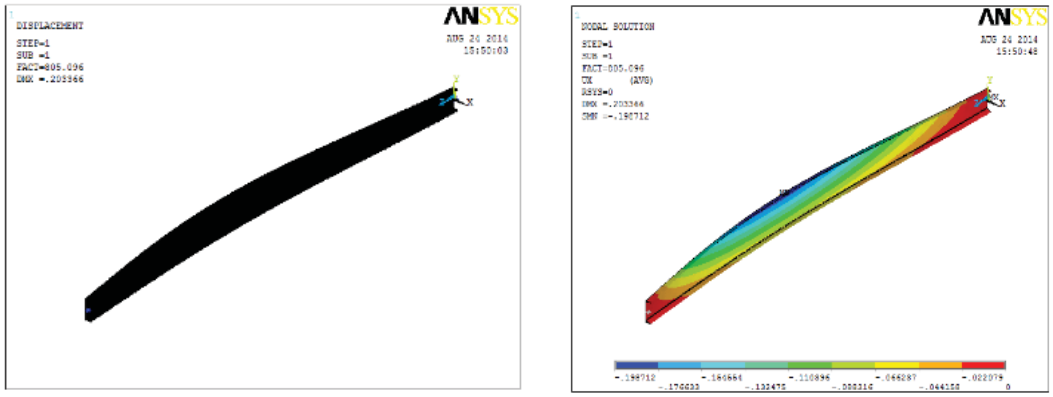

FIGURE 5. Youngs modules =10e-3, thickness =1.10

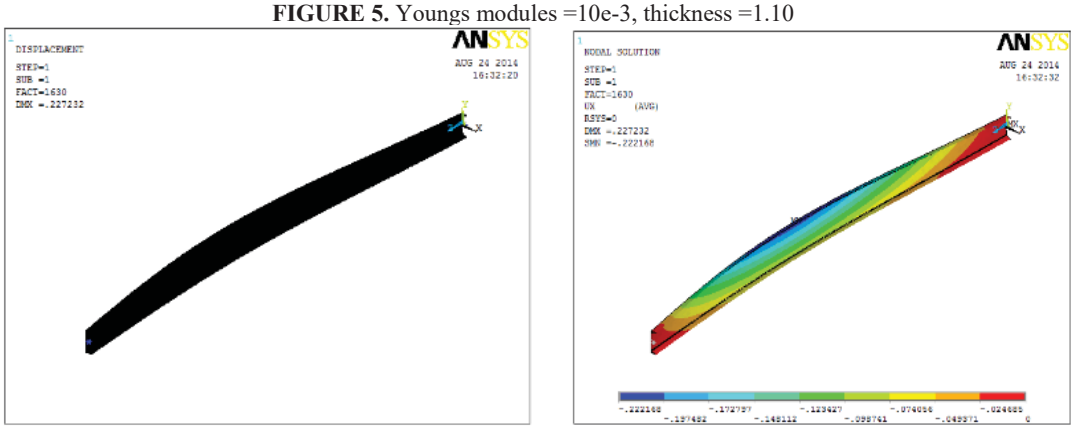

FIGURE 6. Young's modules =10e-3, thickness = 2.0

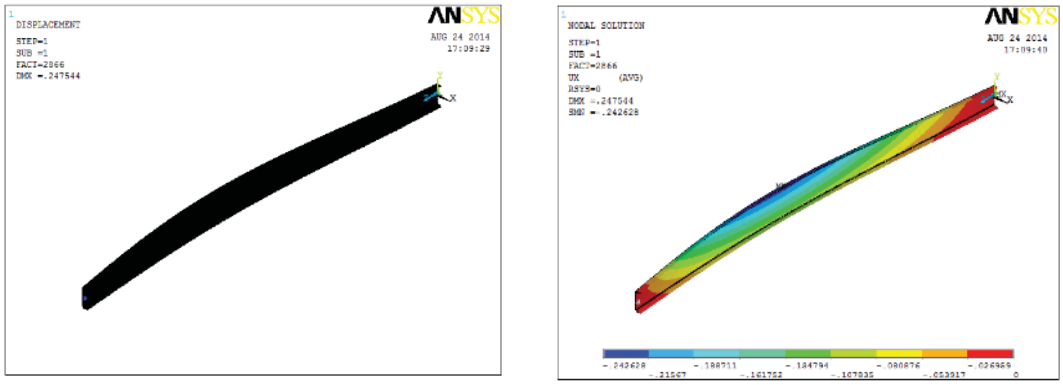

FIGURE 7. Young's modules =10e-3, thickness =3.14

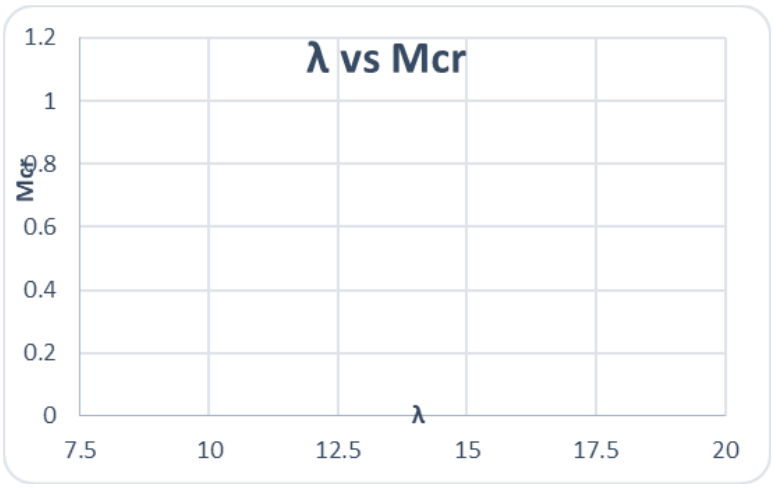

FIGURE 8. Critical Moment Vs λ

CONCLUSION

The critical moment for the unsymmetrical thin wall C-section which is having length of 80mm, breadth of the flange is 37.81e-3, for different thickness 0.6,1.10,2,3.14 . From the above graph we can understand that as the thickness of the flange increases the maximum critical moment increases. As the thickness increases Mcr increases. M_{cr} is directly proportional to its thickness. Therefore the M_{cr} increasing every time.

REFERENCES

1. M.Satyanarayana Gupta, B.Balunaik, KGK Murthi, "finite element modeling and analysis of rotating tool used for friction stir welding of Al/Cu bimetallic lap joints", Proceedings of national conference on resent advancements in engineering and management, 10th April 13, 2012, pp: 146-148.
2. Alka, Gunji Suresh, Simhachalam Naidu, "Modeling and Analysis on 20Gas Turbine Rotar Blade" International Journal of Engineering and Innovative Technology (IJEIT) Volume 4, Issue 12, pp: 99-104,June 2015.
3. Mr. Sreekanth Sura, Alka Sawale, M Satyanarayana Gupta "Dynamic Analysis of Cantilever Beam" International Journal of Mechanical Engineering And Technology (Ijmet), Date: 05-05-2017, Volume No:8, pp:1167-1173(2017).
4. B. Nagaraj Goud, K. Shiva Shankar, B. Manideep, K. Veeranjaneyulu, "Experimental Test on Glare Composite of an Aircraft Structure Under Tensile Strength Failure", International Journal of Engineering and Advanced Technology (IJEAT) ISSN: 2249 – 8958, Volume-9 Issue-2, pp:674-677, December, 2019.
5. Muttangi Sushma, D.Mahesh Kumar, N.Madhavi, "Vibration Analysis on a Thin Walled Structure, International Journal of Innovative Technology and Exploring Engineering(IJITEE) ISSN:1787-1789,Volume-9,pp:1787-1789, Jan2020.
6. D. Mahesh Kumar, N.Madhavi, Muttangi Sushma , "Thin walled C-Sectional Beam under Axial Load", International Journal of Innovative Technology and Exploring Engineering (IJITEE) ISSN:2278-3075, Volume-9 issue-3,pp:498-499, jan 2020.
7. Madhavi, Y.B.SudhirSastry, R.Budarapu Pattabhi N ,"Buckling analysis of thin wall stiffened composite panels", Volume 96, Issue 5,pp: 459-471(2015).
8. Piovan M, CortinezV, "Mechanics of Thin-walled curved beams made of composite materials, allowing for shear deformability", Volume 45, Issue 9, September 2007, Pages 759-789(2007).
9. Daniel Ambrosini "On free vibration of non symmetrical thin-walled beams", Volume 47, Issues 6–7, June–July 2009, PP: 629-636(2008).
10. Yoon KY, Kang YJ, Choi YJ, Park NH, "Free vibration analysis of horizontally curved steel I-girder bridges" Volume 43, Issue 4,pp: 4 679-699 (2005).

11. N Madhavi,K.Sreelakshmi,Sudhakar Atchyutuni, “Buckling Analysis Of Stiffened Composite Panels For Different Ply Orientations”, International Journal of Mechanical and Production,Engineering Research and Development (IJMPERD), ISSN (P): 2249-6890; ISSN (E): 2249-8001,Vol. 8, Issue 1, Feb 2018, PP:745-752.
12. Vamsi V, K Veeranjaneyulu,M S N Gupta,Dhanajayan , “Damage Analysis of Low Speed Impact on Composite Materials”, International Journal of Civil Engineering and Technology (IJCIET),Volume 8, Issue 5, May 2017, pp. 717–727.
13. N Madhavi, B Niharika M Satyanarayana Gupta “Evaluation of ply orientation on failure of Kevlar Epoxy149” IJCIET, ISSN Print: 0976-6308 and ISSN Online: 0976-6316,Volume 8, PP: 457-465,May2017.
14. B. Niharika , N. Madhavi & M. Sai Krishna,” Structural Analysis On Composite Laminate With Different Orientation, IJMPERD, ISSN (P): 2249-6890; ISSN (E): 2249-8001, Volume 8, Issue 1,PP: 551-556,Jan 12, 2018.
15. Madhavi, K Sreelakshmi , M. Satyanarayana Gupta, “Evaluation of Ply Orientation on Failure of Composites”, IJCIET, ISSN Print: 0976-6308 and ISSN Online: 0976-6316, Volume 8, pp. 409–417 May2017.
16. K. Sreelakshmi, N Madhavi, M Satyanarayana Gupta, “Analysis of Interlaminar Stresses in a Composite Material with A Circular Hole by Using Finite Element Method”, IJCIET, ISSN Print: 0976-6308 and ISSN Online: 0976-6316, Volume 8, pp. 500–508, May2017.
17. K. Sai Priyanka, Babitha Kodavanla, A. Barai and N. Madhavi, “ Thermo-Mechanical Analysis of High Temperature Insulating Composites”, International Journal of Mechanical and Production Engineering Research and Development, Vol. 8, Issue 3, (ISSN (P): 2249-6890; ISSN (E): 2249-8001, pp. 915-920, 2018.
18. G. Dhanajayan, Veeranjaneyulu Kalavagunta, V.Vamshi And M.Satyanarana Gupta,2017. Environmental Study On Gfrp Composite Laminates, International Journal Of Civil Engineering & Technology (Ijciet) - Scopus Indexed. Volume:8,Issue:6, Pages:480 – 493.
19. Veeranjaneyulu K, Khannan T Structural Modeling And Analysis Of Composite Wing Rib Using Finite Element Method ‘publication date 2015/10 Journal International Journal & Magazine of Engineering, Technology, Management and Research Volume 2 Issue 5 Pages 20 Publisher IJMETMR

Elastic flexural buckling of thin walled zig-zag flanged section

Cite as: AIP Conference Proceedings **2446**, 180034 (2022); https://doi.org/10.1063/5.0110159
Published Online: 29 November 2022

D. Mahesh Kumar, N. Madhavi, N. Uday Ranjan Goud, et al.

Elastic Flexural Buckling of Thin Walled Zig-Zag Flanged Section

D. Mahesh kumar[1,a)], N. Madhavi[1], N. Uday Ranjan Goud[1], G. Sravanthi[1] and R. Kannan[2]

[1]*Department of Aeronautical Engineering, MLR Institute of Technology, Hyderabad, India – 500043*
[2]*Department of Physics, School of Foundational Sciences, Kumaraguru College of Technology, Coimbatore – 641 049, Tamil Nadu, India.*

Corresponding author: [a)] maheshmaya707@gmail.com

Abstract. The total potential theory and Lu's theory for cantilever beam to calculate critical loads considering various beam length and various cross sections of mono symmetric structures by above buckling theories and also predicting the critical loads of doubly symmetrical cantilevers and comparing with existing critical results from existing solutions and finite element analysis. Based on above buckling theories, am applying these theories to calculate critical loads for simply supported beams with two torsional loads and one torsional load on fixed beam of mono symmetric beam with dropped flanges. Explicit solutions, capable of considering various lengths and cross sections under various kinds of loads are predicting the critical loads of doubly symmetric simply supported beam and fixed beam. The obtained solutions are exploited through the comparisons of critical results with those from existing solutions and finite element analysis.

Keywords: Critical loads, Torsional Load, FEA, Buckling, Elastic.

INTRODUCTION

An aircraft's wings are designed to lift it into the air. Their specification for any given aircraft is determined by a variety of factors, including the aircraft's size, weight, intended use, desired speed in flight and at landing, and desired rate of climb. The left and right sides of an aircraft's wings correspond to the operator's left and right sides when sitting in the cockpit. Fuel is often borne within a stressed-skin aircraft's wings. Fuel can be stored directly within the frame by sealing the joints in the wing with a special fuel resistant sealant. Wet wing design is the term for this. A fuel-carrying bladder or tank may also be mounted within a wing [1-17].

THIN WALLED STRUCTURES

In this section we will consider the stresses and strains generated in thin-walled sections due to various loads. In general the wall thickness of the section is assumed to be very much less than the other dimensions of the structure and this allow us to make a number of assumptions about the nature of the stresses:

1. Through-thickness stresses are zero
2. The stress state is uniform through the section

Real thin walled structures, such as the box girder bridge below or the airbus A321 in the structural design case study have additional stiffeners:

- To prevent local buckling of the walls
- To carry locally concentrated loads
- As a fail-safe device

International Conference on Materials Research in Science and Engineering
AIP Conf. Proc. 2446, 180034-1–180034-7; https://doi.org/10.1063/5.0110159
Published by AIP Publishing. 978-0-7354-4208-5/$30.00

FORMULA

Consider the C-section as shown in Figure. The C-section is symmetric about the x axis i.e; I_{xy}=0 and the moment of area I_{xx} is given by

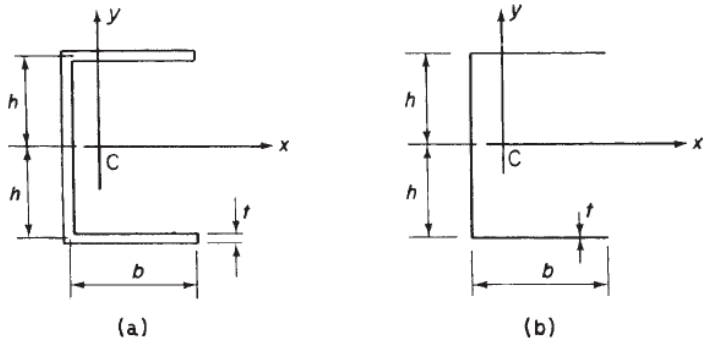

FIGURE 1. a) Thin-walled C-section (b) approximate diagrammatic representation of C-section.

Expanding the equation, we get

$$I_{xx} = 2\left[\frac{(m+t/2)t^3}{12} + \left(m+\frac{t}{2}\right)th^2\right] + \frac{t}{12}\left[(2)^3\left(h^3 - 3h^2\frac{t}{2} + 3h\frac{t^2}{4} - \frac{t^3}{8}\right)\right]$$

Finally the equation reduces to t^2 and upwards are ignored, to

$$I_{xx} = 2mth^2 + t\frac{(2h)^3}{12}$$

Area of the C-section about C_y is obtained in the same procedure. Therefore, the properties are calculated for the C section beam is represented by straight line.

DESIGN SPECIFICATIONS

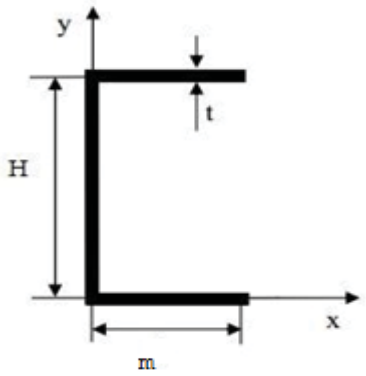

FIGURE 2. C-Section Dimensions

Problem dimensions (initial):

- Height of the C-Section (H=2 X a)
- Initial thickness (t)
- Length of the C-Section(L)
- Length of the Flange (m) Specification:
- Material : Al
- Young's Modulus (E)=7.2e10
- Poison's ratio (μ)=0.3
- Density ρ=2800kg/m^3

The critical load (P_{cr})

$$P_{cr} = \frac{\pi^2 E(\frac{th^2(6b+h)}{12}}{4l^2}$$

The Moment of Inertia (I)

$$I = \frac{th^2}{120}(6b + h)$$

C-section is constrained at both ends as simply supported beam and applied buckling loads

ANALYSIS

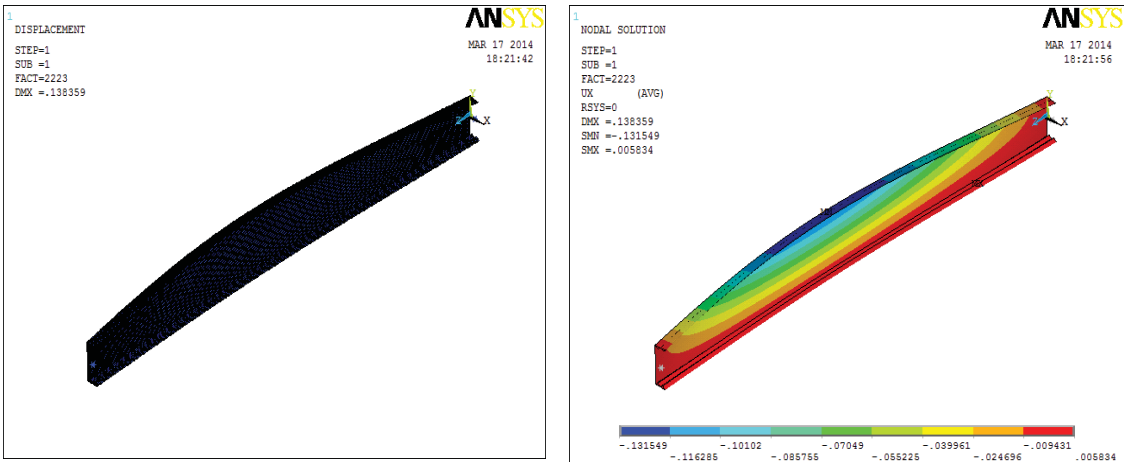

FIGURE 3. Youngs modules =10e-3, thickness =0.6e-3, *λ=12.6(h=2.0)*

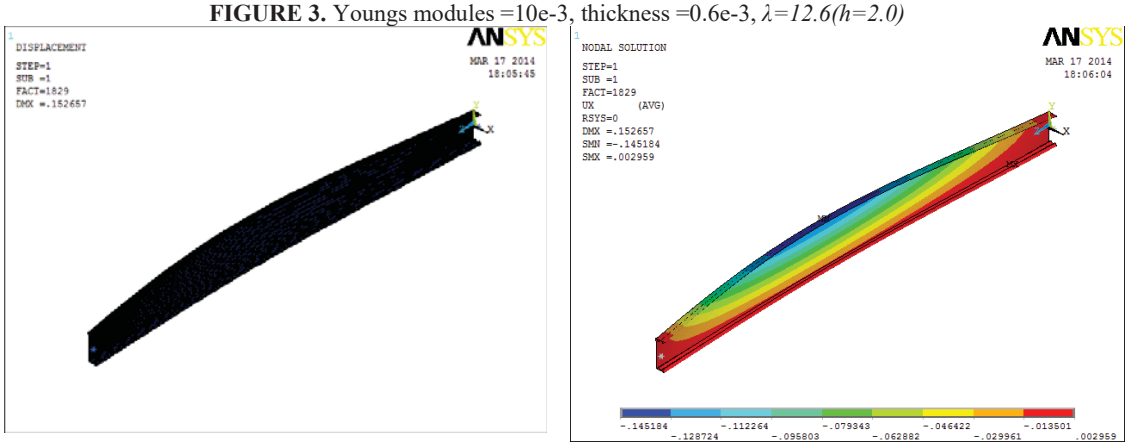

FIGURE 4. Youngs modules =10e-3, thickness =0.6e-3, *λ=17.6(h=2.8)*

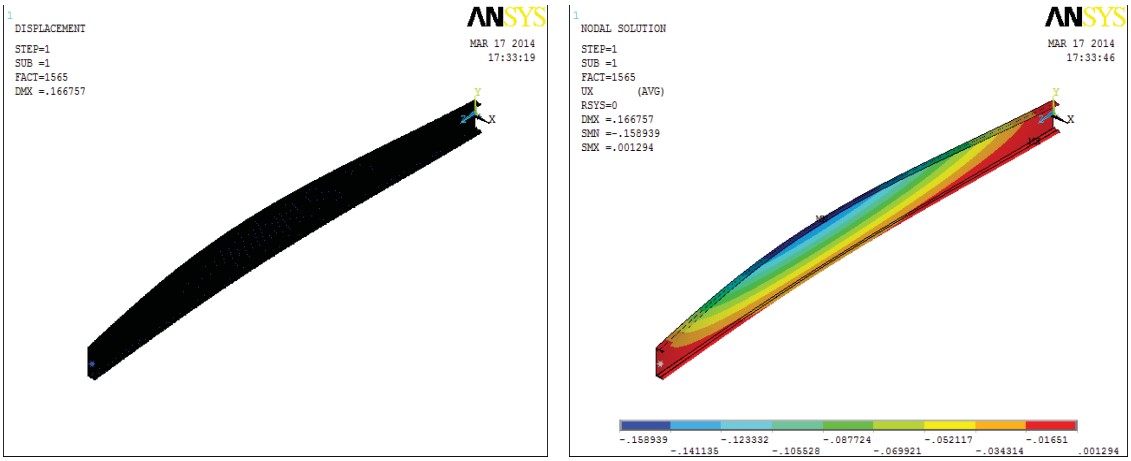

FIGURE 5. Youngs modules =10e-3, thickness = 0.6e-3, *λ=17.6(h=2.8)*

TABLE 1. Values for Mcr and λ for t=0.6e^{-3}

λ=L/H	Mcr
7.56	418.67
10.1	417.69
12.6	416.74
15.1	415.92
17.6	415.27

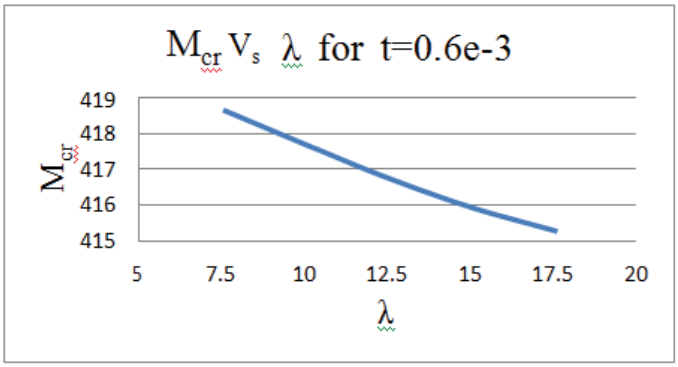

CASE I: Graph For thickness t=0.6e-3

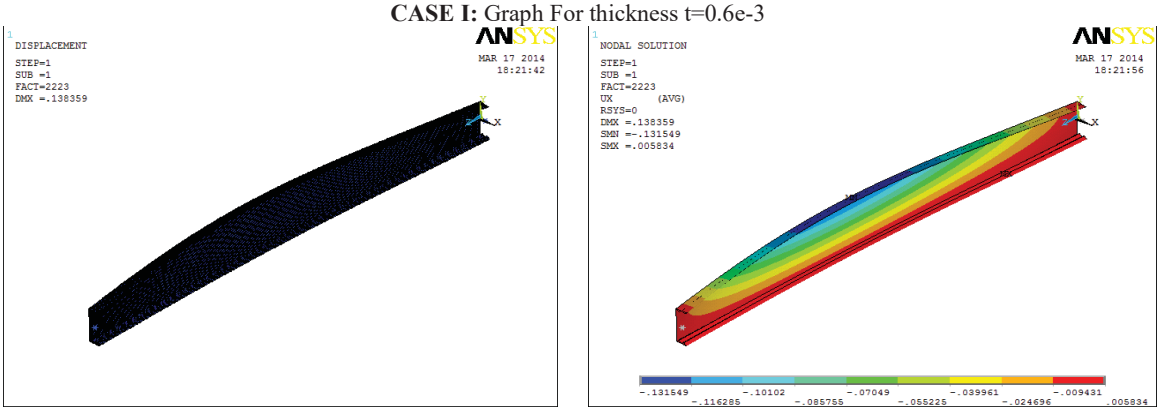

FIGURE 6. Youngs modules =10e-3, thickness =1, *λ=12.6(h=2.4)*

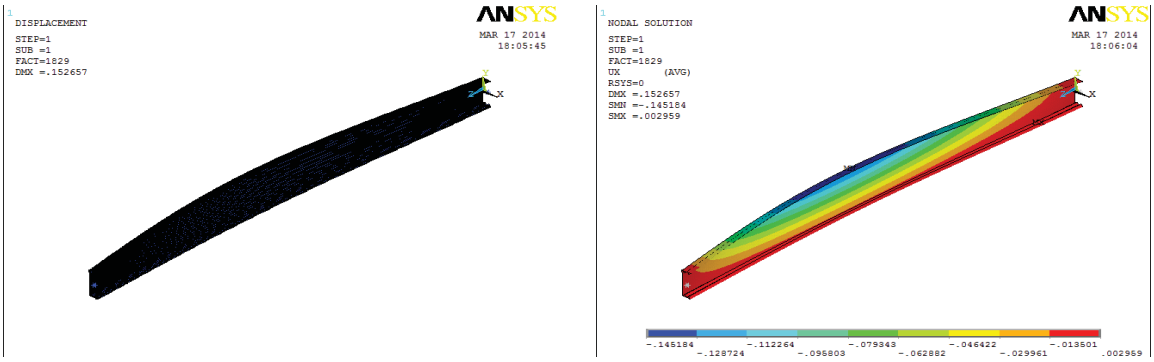

FIGURE 7. Youngs modules =10e-3, thickness =1.10, *λ=17.6(h=2.8)*

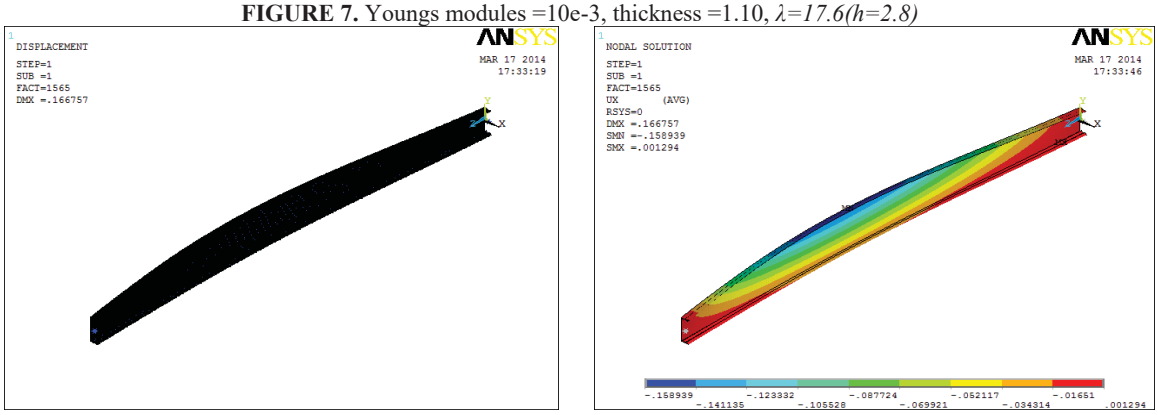

FIGURE 8. Youngs modules =10e-3, thickness = 1.10, *λ=17.6(h=2.8)*

TABLE 2. Values for Mcr and λ for t=1.10e^{-3}

λ=L/H	M_{cr} (Nm)
7.56	2550
10.1	2551.4
12.6	2223.4
15.1	1828.6
17.6	1565.4

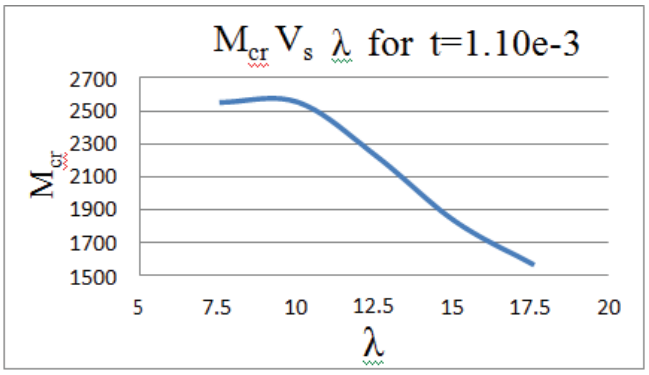

CASE II: Graph For thickness t=1.10e-3

RESULT

TABLE 3. Values for Mcr and λ for different thickness

λ=L/H	Mcr (Nm) for t=0.6	Mcr(Nm) for t=1.1	Mcr(Nm) for t=2.0	Mcr(Nm) for t=3.14
7.56	418.67	2550	8666.8	14841
10.1	417.69	2551.4	6013.8	10465
12.6	416.74	2223.4	4652.2	8145.8
15.1	415.92	1828.6	3818.9	6702.8
17.6	415.27	1565.4	3251.1	5710.4

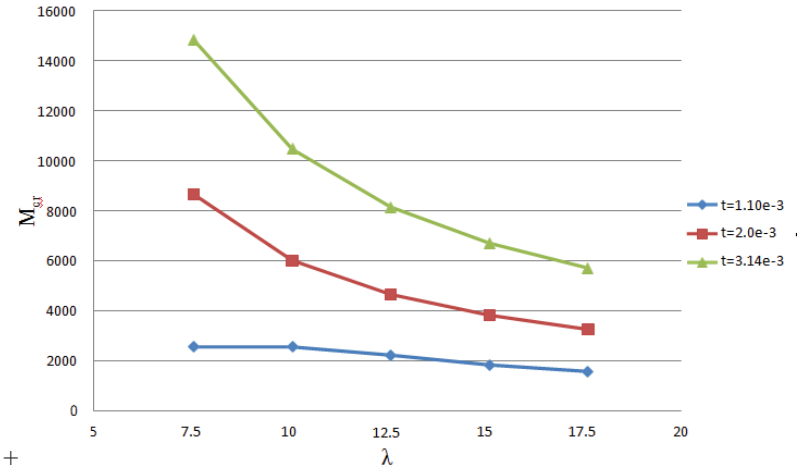

FIGURE 9. Graph for all thicknesses

CONCLUSION

Thin-walled beams (Channel section) analysis has been considered in this project. For the case when *E=10e-3,* we can observe that, the graph between critical moment Mcr and L/H ratio (denoted by **λ)**. Here, we find that for thicknesses t=1.10e-3 and t=2.0 e-3, as **λ** is increased Mcr decreases whereas for thickness t=3.14e-3 Mcr approximately remains the same for different values of **λ**

REFERENCES

1. Vivek Anand A, Gollakota S, Hariprasad V, Shunmugavelu N, Ahifkhan & Arumugam V, "Role of Micropatterns on Wettability and Corrosion Characteristics of SS304 Steel Surfaces", International Conference on Materials, Manufacturing and Machining (ICMMM - 2019), 8 & 9 March 2019, BIT Sathy, India.
2. Vivek Anand A, Venkatesh G & Anand P, 2014, "Noval method for fabrication of 3-D spacer fabric composite and investigation of mechanical property", Int. J. Modern Engineering Research, Vol. 1, No. 4, pp. 27-30.
3. Mr. Sreekanth Sura, Alka Sawale, M Satyanarayana Gupta "Dynamic Analysis of Cantilever Beam" International Journal of Mechanical Engineering And Technology (Ijmet), Date: 05-05-2017, Volume No:8, pp:1167-1173(2017).
4. B. Nagaraj Goud, K. Shiva Shankar, B. Manideep, K. Veeranjaneyulu, "Experimental Test on Glare Composite of an Aircraft Structure Under Tensile Strength Failure", International Journal of Engineering and Advanced Technology (IJEAT) ISSN: 2249 – 8958, Volume-9 Issue-2, pp:674-677, December, 2019.
5. Muttangi Sushma, D.Mahesh Kumar, N.Madhavi, "Vibration Analysis on a Thin Walled Structure, International Journal of Innovative Technology and Exploring Engineering(IJITEE) ISSN:1787-1789,Volume-9, pp:1787-1789, Jan2020.

6. D. Mahesh Kumar, N.Madhavi, Muttangi Sushma , “Thin walled C-Sectional Beam under Axial Load”, , International Journal of Innovative Technology and Exploring Engineering (IJITEE) ISSN:2278-3075, Volume-9 issue-3,pp:498-499, jan 2020.
7. Madhavi, Y.B.SudhirSastry, R.Budarapu Pattabhi N ,“Buckling analysis of thin wall stiffened composite panels”, Volume 96, Issue 5,pp: 459-471(2015).
8. Piovan M, CortinezV, “Mechanics of Thin-walled curved beams made of composite materials, allowing for shear deformability”, Volume 45, Issue 9, September 2007, Pages 759-789(2007).
9. Daniel Ambrosini “On free vibration of non symmetrical thin-walled beams”, Volume 47, Issues 6–7, June–July 2009, PP: 629-636(2008).
10. Yoon KY, Kang YJ, Choi YJ, Park NH, “Free vibration analysis of horizontally curved steel I-girder bridges” Volume 43, Issue 4,pp: 4 679-699 (2005).
11. N Madhavi, K. Sreelakshmi, Sudhakar Atchyutuni, “Buckling Analysis Of Stiffened Composite Panels For Different Ply Orientations”, International Journal of Mechanical and Production,Engineering Research and Development (IJMPERD), ISSN (P): 2249-6890; ISSN (E): 2249-8001,Vol. 8, Issue 1, Feb 2018, PP:745-752.
12. Vamsi V, K Veeranjaneyulu,M S N Gupta,Dhanajayan , “Damage Analysis of Low Speed Impact on Composite Materials”, International Journal of Civil Engineering and Technology (IJCIET),Volume 8, Issue 5, May 2017, pp. 717–727.
13. N Madhavi, B Niharika M Satyanarayana Gupta “Evaluation of ply orientation on failure of Kevlar Epoxy149” IJCIET, ISSN Print: 0976-6308 and ISSN Online: 0976-6316,Volume 8, PP: 457-465,May2017.
14. B. Niharika , N. Madhavi & M. Sai Krishna,” Structural Analysis On Composite Laminate With Different Orientation, IJMPERD, ISSN (P): 2249-6890; ISSN (E): 2249-8001, Volume 8, Issue 1,PP: 551-556,Jan 12, 2018.
15. Madhavi, K Sreelakshmi , M. Satyanarayana Gupta, “Evaluation of Ply Orientation on Failure of Composites”, IJCIET, ISSN Print: 0976-6308 and ISSN Online: 0976-6316, Volume 8, pp. 409–417 May2017.
16. K. Sreelakshmi, N Madhavi, M Satyanarayana Gupta, “Analysis of Interlaminar Stresses in a Composite Material with A Circular Hole by Using Finite Element Method”, IJCIET, ISSN Print: 0976-6308 and ISSN Online: 0976-6316, Volume 8, pp. 500–508, May2017.
17. K. Sai Priyanka, Babitha Kodavanla, A. Barai and N. Madhavi, “ Thermo-Mechanical Analysis of High Temperature Insulating Composites”, International Journal of Mechanical and Production Engineering Research and Development, Vol. 8, Issue 3, (ISSN (P): 2249-6890; ISSN (E): 2249-8001, Scopus Indexed), pp. 915-920,June 2018.

Design and fabrication of composite shaft using stir casting technique (MMC)

Cite as: AIP Conference Proceedings **2446**, 040014 (2022); https://doi.org/10.1063/5.0109227
Published Online: 29 November 2022

Sreekanth Sura, B. Nagaraj Goud, B. Manideep, et al.

Design and Fabrication of Composite Shaft using Stir Casting Technique (MMC)

Sreekanth Sura[1,a)], B. Nagaraj Goud[1,b)], B. Manideep[1,c)] and G. Raj Kumar[2,d)]

[1]*Department of Aeronautical Engineering, MLR Institute of Technology, Hyderabad, India*
[2]*Department of Aeronautical Engineering, Kumaraguru College of Technology, Coimbatore, Tamil Nadu, India.*

Corresponding author: [a)]sreekanthsuramlrit@gmail.com,
[b)] nagaraj2107@gmail.com
[c)] manideepbalusani.9@gmail.com
[d)] rajkumar.g.aeu@kct.ac.in

Abstract. In this paper most of the work deals with the design and fabrication of composite shaft using stir casting technique (MMC). In this we are using composite materials due to their advantages of higher specific strength and stiffness. In this work we are fabricating composite shaft using the Aluminium Alloy 2024 by adding the reinforcement materials such as silicon carbide (Sic) and boron carbide (B4C) by trying out different weight fractions in order to increase the higher specific strength and stiffness of the composite shaft.

Keywords: Stir Casting, Composite Shaft, Hardness, tensile, MMC.

INTRODUCTION

These days, the composite materials have been used in large volume of applications with varying engineering structures specially most of the applications including the spacecrafts industry technology, airplanes technology, automobiles technology, marine technology, light weight sports related equipment's with satisfying quality requirements, long life bridges and buildings with high strength and stiffness. Now a days the composite materials are widely using in research industry is due to the most useful excellent required characteristics are there such as, like high specific required strength and high specific required hardness with required strength to weight ratio and high hardness to weight ratio.

If we see the most of the shafts are generally prefer to make of solid or hollow circular tube of materials like steel or aluminium. The composite material like metal matrix composite (MMC) is with minimum two composition constituent parts, one is being a metal necessarily included, the other side material may be have a different selection of metal or another selection of material, such as like a ceramic material or organic related compound included. Metal matrix composites (MMC's) are mostly made by the distributing of a reinforcing material into the metal matrix, the matrix is generally a light weight metal such as like aluminium (al), magnesium (mg) or titanium (Ti) and the reinforcement of materials are generally behaves high strength to the composite such as silicon carbide metal (SiC), boron carbide metal (B4C), aluminium oxide, graphite, granite etc.

A composite shaft provides behaves with the excellent high strength, high stiffness and high hardness compared to generally used normal shafts. The composites shaft was developed and designed as a direct response to industry required demands for greater satisfied performance and with good efficiency in aerospace industry and the high-performance automobiles industry. The MMC were fabricated using common three main processes namely the solid metal state processing, liquid metal state processing and in-situ processing are generally used [1-15].

International Conference on Materials Research in Science and Engineering
AIP Conf. Proc. 2446, 040014-1–040014-8; https://doi.org/10.1063/5.0109227
Published by AIP Publishing. 978-0-7354-4208-5/$30.00

In this paper we preferred the process to fabricating composite shaft using liquid metal state process namely with the help of stir casting technique approach. The MMC's are definitely having required high strength and required high stiffness compared to aluminium and steel materials in use so that finally the composite shaft has lot of benefits such as like reduced weight and to overcome the problems like high noise and huge vibrations.

DESIGN SPECIFICATIONS

The efficient design process of composite drive shaft depends upon in section of proper variables then it could be achieved. The design of shaft variables mainly includes the outer radius and then the length of the composite shaft. But the present work is made to put effort make the design AA 2024/SiC-B4C of high strength and stiffness composite shaft which the composite shaft for aerospace industry applications was designed and analyzed successfully using ANSYS software tool.

Design parameters of the composite shaft
Length of the composite shaft = 150 mm.
Diameter of the composite shaft = 25 mm.
The young's modulus of the composite shaft = 75 Gpa.
The poisson's ratio of composite shaft = 0.33.
Density of the composite shaft = 2.78 g/cc.
Moment applied on the Composite shaft = 670 Nm.

STRUCTURAL ANALYSIS

The Pre Processing Stage

The number of steps followed in preferences select structural from which is in main menu toolbar, than select h-method than press ok.Go to pre processor in main menu tool bar select element type and add element from add, edit, delete than select solid Tet 10 node 187 press ok and close.

Than go to material properties select material models in that structural, liner, elastic and isotropic and give values. Young's modulus = 0.75e11, Passions ratio= 0.33, Density of aluminium = 2780 than press ok and close. Than from the menu select pre processor go to modelling create volume of cylinder, solid cylinder by giving the values than press ok. Give radius 12.5mm, depth 150mm

Next go to meshing the geometry which is created select meshing from menu go to mesh tool give smart size, fine mesh 3 than close. Next in meshing select mesh volumes select free mesh, pick all and press ok. From fig 1, we can see the meshed model of composite shaft.

Next Phase Applying Loads and Solve

Select defining loads go to apply structural, displacement, select areas, than select the first edge than press ok and give all degree of freedom select ok than all degree of freedom arrested. Again select define loads, apply, structural, force and moment on key points, by using box select the second edge than press ok give force value 670Nm, equivalent to 3500rpm.Than from menu go to solving the solution select solve in current ls. You can see in fig 2, that one side of the composite shaft is fixed and the other side is rotated about 3500 rpm.

The General Post Processing Stage

For plots from menu select general post processing go to plot results, deformed shape select deformed undeformed option than click ok to view both the deformation and the un deformation of shaft. From the fig 3, we can see the deformed and undeformed shape of the composite shaft. Select Plot results in menu go to contour plot, nodal solution, select all degree of freedom solution, select displacement vector sum than press ok. From the fig 4, we can see that the maximum twisting takes place at the centre of the composite shaft.

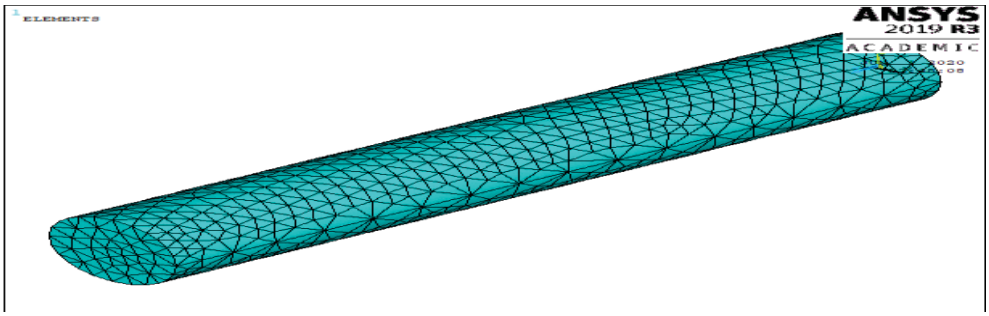

FIGURE 1. The mesh configuration of composite shaft

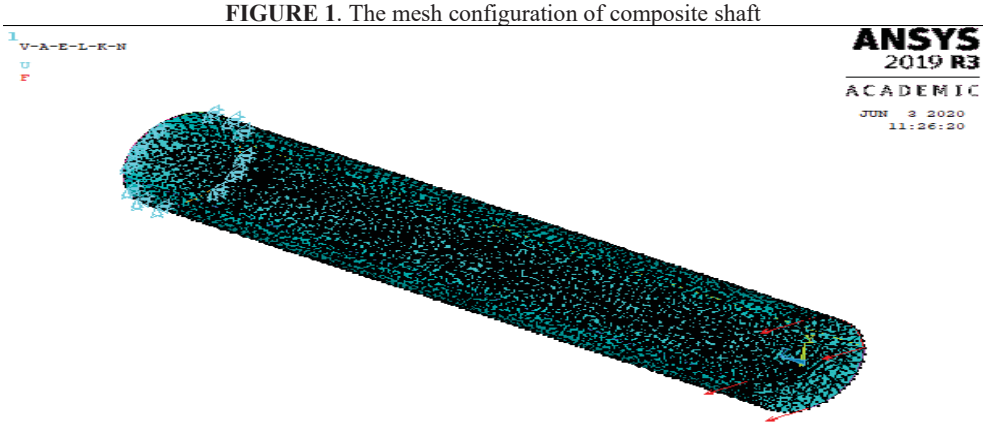

FIGURE 2. Moment applied on the shaft

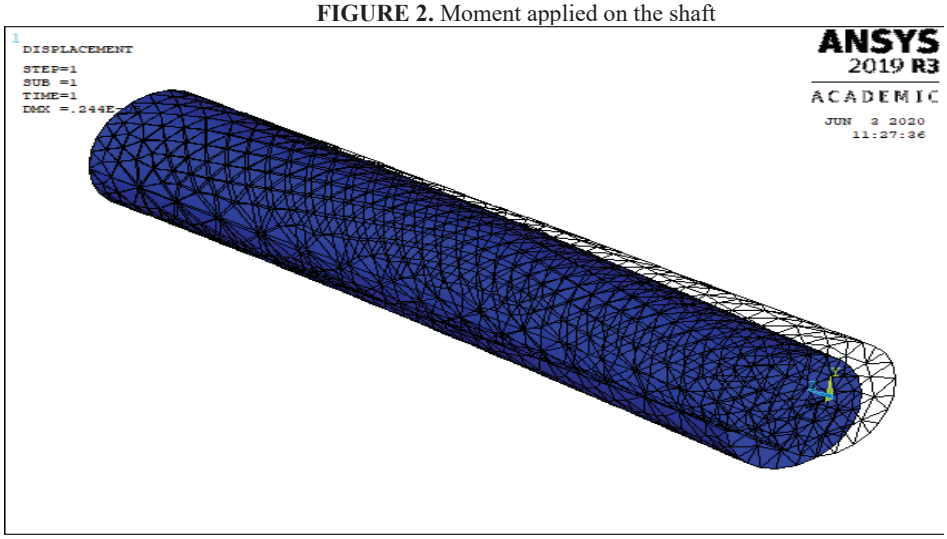

FIGURE 3. The deformation form of composite shaft at first mode

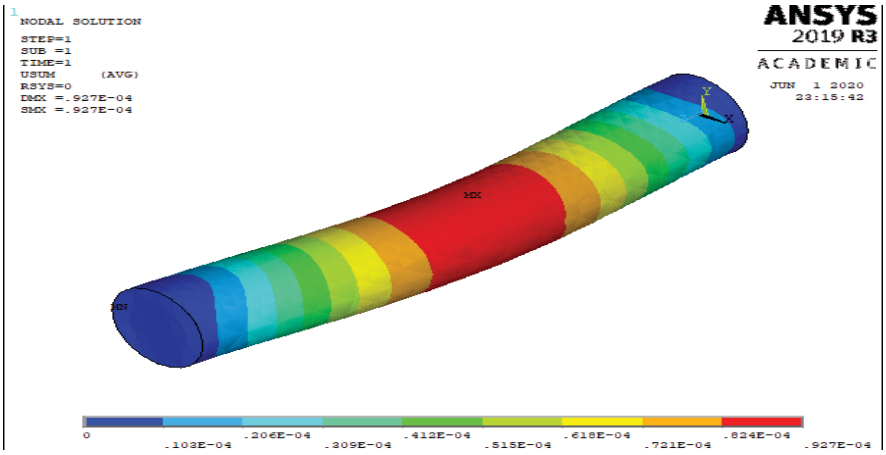

FIGURE 4. The total displacement of composite shaft.

FABRICATION TECHNIQUE

In the present project we are using stir casting technique for the fabrication of AA 2024 with silicon carbide (SiC) and boron carbide (B4C) using bottom pour stir casting machine. In this process we have to apply graphene paste thoroughly into the mould cavity so that molten material will not stick to the mould cavity and then preheat the furnace, reinforcement chamber and mould cavity at 100°C. When the furnace reaches above 100°C we have to add the required weight percentage fraction of AA 2024 into the furnace and when it reaches above 650°C the materials gets melted so that the reinforcements materials such as silicon carbide and boron carbide are added as per the weight percentage fraction to know the tensile strength and hardness of shaft specimen and the results were compared. Then the stirrer is made to rotate at 1500 rpm will mix the composite material thoroughly about 2 minutes. After that the composite material is sent into mould cavity and allows it to cool for some-time and then remove the composite material.

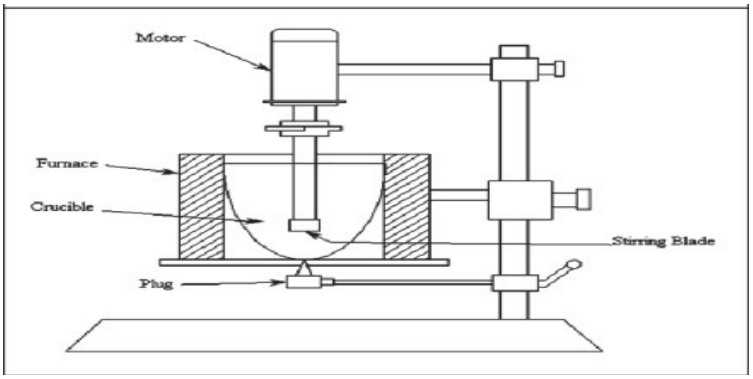

FIGURE 5. Line diagram of Stir Casting Machine

TABLE 1. Specimen-1 Composition.

Material	AA 2024	B4C	SiC
1. Material (%)	97%	2%	1%
2. Weight(grams)	600 grams	12.37 grams	6.18 grams

TABLE 2. Specimen-2 Composition.

Material	AA 2024	B4C	SiC
1. Material (%)	97%	1.5%	1.5%
2. Weight(grams)	600 grams	9.27 grams	9.27 grams

FIGURE 6. Fabrication of AA 2024 with Sic/ B4C

RESULTS AND DISCUSSION

Tensile Test

A universal testing machine (UTM) is used to test the Tensile strength and Compressive strength of materials.

FIGURE 7. Specimen prepared for tensile test

FIGURE 8. Specimen after undergoing tensile load

SPECIMEN 1

TABLE 3. Specimen1 tensile test results

Maximum force(Fm)	8780.000N
Disp.at Fm	7.880mm
Max.Disp	6.910mm
c/s Area(So)	80.643mm2
Tensile strength(Rm)	506.532N/mm2
Elongation	15.083%

SPECIMEN 2

TABLE 4. Specimen2 tensile test results

Maximum force(Fm)	6730.000N
Disp.at Fm	4.580mm
Max.Disp	3.820mm
c/s Area(So)	68.532mm2
Tensile strength(Rm)	432.415N/mm2
Elongation	10.314%

From the tensile test values we known that the tensile strength is high in specimen one compare both specimen 1& 2 due to the difference in the weight fraction of reinforcements which we used in the fabrication of the both the specimen.

Brinell's Hardness Test

The hardness of the materials is determined by Brinell's hardness test. Structure high course or high rough surfaces are tested. In this method the load is applied on specimen to find hardness number, the fixed diameter carbide ball is used to test and particular predetermined time the force is applied than removed. The impression is resulted is measured with brinell microscope which is specifically designed optical system of brinell microscope across at least two diameter.

$$\mathbf{BHN} = \frac{2L}{\pi D(D-\sqrt{(D^2-d^2)})}$$

Hardness Test Results

TABLE 5. Hardness test results of specimen1.

S No	Material	Applied load (kgf)	Indenter diameter 'D' (mm)	Indentation diameter 'd' (mm)	BHN (kg/mm2)
1.	AA2024/Sic-B4C	100	6.35	0.5	4988.435
2.	AA2024/Sic-B4C	100	6.35	0.8	1943.862
3.	AA2024/Sic-B4C	100	6.35	1	1241.255

TABLE 6. Hardness test results of specimen2.

S No	Material	Applied load (kgf)	Indenter diameter 'D' (mm)	Indentation diameter 'd' (mm)	BHN (kg/mm2)
1.	AA2024/Sic-B4C	100	6.35	1.5	547.277
2.	AA2024/Sic-B4C	100	6.35	1.2	859.579
3.	AA2024/Sic-B4C	100	6.35	1.3	731.254

FIGURE 9. Hardness test on the first specimen

FIGURE 10. Hardness test on the second specimen

From the hardness test results we known that the specimen 1 have high hardness compared to specimen 2 due to the difference in the weight fraction of reinforcements which we used in the fabrication of both the specimens.

RESULTS

In this project work we are comparing the two fabricated models by changing the Wt% of Sic and B4C and the results are shown below,

Tensile Strength of first model = 506.532N/mm^2.

Tensile strength of second model = 332.415N/mm2.

BHN of first model = 4988.435 kg/mm2; BHN of second model = 859.579kg/mm2.

From the tensile test results of the both models we have conclude that the model 1 having more tensile strength, Elongation percentage and maximum yield strength compared to the model 2 because of the change in the weight percentage of the reinforcement materials that are SiC and B4C. Due to the addition of more percentage of SiC the model 2 gone through brittle nature which will reduces the strength of the model 2.

TABLE 7. Hardness test results.

S.No	Tensile Strength(N/mm2)	Hardness(kg/mm2)
1.Model 1	506.532	4988.435
2.Model 2	332.415	859.579

From the Brinell's hardness test results of the both models we have conclude that the model 1 having more Brinell's hardness number (BHN) compared to the model 2 because of the change in the weight percentage of the reinforcement materials that are SiC and B4C. Due to the addition of more percentage of SiC the model 2 gone through brittle nature which is the reason for the reduction of hardness in the model 2.

CONCLUSION

In this project we have replaced the normal shaft with the composite shaft with the increase of strength and hardness. Static analysis was done specimen to obtain the maximum deflection of the composite shaft and the replacement of composite shaft has results in increase in strength and hardness compared to convectional steel shaft. Hence from the tested results we have finally concluded that the high strength and hardness are in specimen 1 compared to specimen 2 due to the addition of more percentage of reinforced material B4C.

REFERENCES

1. Parshuram D, Sunil Mangsetty, "Design and Analysis of Composite/Hybrid Drive Shaft For Automotives", The IJES, 2, 01, 160-171, 2013.
2. Srinivasa Moorthy.R, Yonas Mitiku and K. Sridhar 2013 "Design of Automobile Driveshaft using Carbon/Epoxy and Kevlar/Epoxy Composites", AJER, 02, 10, 173-179, 2013.
3. Ashwin Russelle, N. Naganambi "Numerical investigation of Bonded Repair for TDS of Helicopter and Characterization of Kevlar/Epoxy Composite Patch", Elsevier Procedia
4. Materials Science, 5, 204 – 211, 2014.
5. Chaitanya G Rothe, A.S.Bombatkar "Design and Analysis composite Material Drive Shaft" IJIERE, 2, 2015.
6. Kumar Rompicharla.R.P "Design and Optimization of Drive Shaft with Composite Material", IJMER, 1, 7, 2012.
7. B. Nagaraj Goud, K. Shiva Shankar, B. Manideep, K. Veeranjaneyulu "Experimental Test on Glare Composite of an Aircraft Structure under Tensile Strength Failure", IJEAT, 9, 2, 2019.
8. N Madhavi, B Niharika M Satyanarayana Gupta "Evaluation of ply orientation on failure of Kevlar Epoxy"149, IJCIET, 8, 2017.
9. M. Ganesh ,G Hima Bindu,A. Sai Kumar "Modeling And Analysis Of a Composite Wing For Missile Structure " (IJMET), 8, 6, 2017.
10. K. Venkatesan et al., Advanced structural analysis of various composite materials with carbon nano-tubes for property enhancement, AIP Conference Proceedings 2270, 030005 (2020), pp. 030005-1 to 030005-6, https://doi.org/10.1063/5.0019367
11. P. Mirrudula et al., Comparative structural analysis of the sandwich composite using advanced numerical simulation, AIP Conference Proceedings, 2270, pp. 040005-1 to 040005-5, 2020, https://doi.org/10.1063/5.0019370
12. S. Indira Prasanth et al., Advanced structural analysis on E-glass fiber reinforced with polymer for enhancing the mechanical properties by optimizing the orientation of fiber, AIP Conference Proceedings 2270, pp. 040006-1 to 040006-5, 2020, https://doi.org/10.1063/5.0019378
13. S. Bhagavathiyappan et al., Comparative computational impact analysis of multi-layer composite materials, AIP Conference Proceedings, 2270, pp. 040007-1 to 040007-5, 2020, https://doi.org/10.1063/5.0019380.
14. K. Venkatesan, K. Ramanathan, R. Vijayanandh et al., Comparative structural analysis of advanced multi-layer composite materials, Materials Today: Proceedings, Volume 27, Part 3, 2020, Pages 2673-2687, https://doi.org/10.1016/j.matpr.2019.11.247.
15. Vijayanandh R, Venkatesan K, Ramesh M, Raj Kumar G, Senthil Kumar M, Optimization of Orientation Of Carbon Fiber Reinforced Polymer Based On Structural Analysis, International Journal of Scientific & Technology Research, ISSN 2277-8616, Volume 8 - Issue 11, pp. 3020 – 3029, 2019.